NON-LINEAR STATIC ANALYSIS OF AIRCRAFT TIRE SUBJECTED TO INFLATION PRESSURE AND GROUND CONTACT LOADS USING FINITE ELEMENT ANALYSIS

A Thesis

Submitted to the Graduate Faculty of the

University of New Orleans

in partial fulfillment of the

requirements for the degree of

Master of Science

in

The Department of Mechanical Engineering

by

Indrajith Kizhakkethara

B.S., University of Calicut, India, 1991

June, 1995

DTIC COULD NOT GET MISSING

PAGES FROM CONTRIBUTOR

ACKNOWLEDGMENTS

I would like to express my sincere gratitude to Dr. Arnold H. Mayer and Dr. David Hui for the support and guidance provided to me during the completion of my thesis work. I acknowledge receipt of support for this work through a grant AFOSR #F49620-94-1-0213 from the Air Force Office of Scientific Research Mathematics Directorate AFOSR/MA to the University of New Orleans, LA.

ABSTRACT

The pneumatic tire has been an integral part of transportation almost since its inception, yet it remains a product whose characteristics are not easily predictable or comprehensible by conventional engineering techniques. This thesis is an attempt to provide a numerical model for predicting the ground contact pressure pattern between an aircraft tire and road under static condition.

TABLE OF CONTENTS

LIST OF FIGURES:

CHAPTER 1

INTRODUCTION

1.1. Introduction:

Pneumatic tires usually contain a variety of rubber compositions, each designed to contribute some particular factor to overall performance. Rubber compounds designed for a specific function will usually be similar but not identical in composition and properties, although in some cases there can be significant differences between compounds of tires in various types. The guiding principle in development of rubber compositions for tires is to achieve the best balance of properties for a particular type of tire service. Since a tire is a mechanical structure, a rubber compound should be judged on how it functions in the system rather than on its individual properties or performance capabilities. Thus a rubber compound which did not adhere well to other tire components, or which required vastly different vulcanization conditions than other parts of the tire, could be useless in the tire even though it had excellent strength and other mechanical properties. Tire performance is the result of skill and experience in producing a mechanically harmonious structure of rubber compounds, fabric and adhesive, beads and other components which work together to give optimum service.

The principal functions of the rubber compositions in a tire are fairly obvious. The tread compound must provide wear resistance and be tough and resilient to minimize cuts, tears, and cracks, as well as to protect the tire body from bruising impacts. Low mechanical hysteriesis loss in the tread is desirable since lower tire operating temperatures are advantageous. Good friction properties of the tire tread for all driving

conditions are, of course very important. In some cases optimum tread properties are obtained by using a cushioning compound between tread and tire body as an additional protection against fabric bruises, thus making a "double layer" tread. This cushion can also serve, especially in retreading, as a bonding or transition layer between tread and body compounds. Intermediate hardness properties between those of tread and body are usually used in the cushion or breaker under the tread.

Tire body or carcass rubber compounds must form strong bonds to the adhesive-coated fabric. Their strength and durability should be adequate to insulate the cords and hold them in their paths. The rubber must however, be soft enough to permit a slight change of cord angles when the tire is flexed. The body rubber serves as insulation between the fabric plies. Outstanding fatigue resistance is required of body compounds in order to withstand cyclic deformation. It is essential that they retain adequate physical properties and durability at the internal tire temperatures generated in service. Hence, low mechanical energy losses are needed for body compounds. There may be gradations in the properties of body compounds, if the hardness usually diminishing somewhat from tread to cushion to top plies to inner plies.

In tubeless tires, a liner or coating on the inside ply retards diffusion of inflating air into the fabric, and protects against ensuing ply seperations. Rubber compositions around the wire bead are called bead insulation, and give it geometric stability, shape it to fit the rim, and provide firm anchorage for the cords.

1.2 Tire Inflation

The conventional aircraft tire possesses three distinct structural components: the rubber matrix which contains the air and provides abrasion resistance and road grip; the cords (textile, steel, or glass) which provide tensile reinforcement for the rubber and carry most of the load applied to the tire in service; and the steel beads which circumferentially connect the tire to the wheel of a car or aircraft. These three components, with air under pressure, form a thin-walled composite toroidal shell which is both highly flexible and relatively inextensible. The purpose of this chapter is to discuss those methods of stress analysis which are applicable for the calculation or measurement of the stresses and strains developed in the three structural components of the present day automobile or aircraft tire.

Stress analysis is that branch of mechanics which is concerned with the quantitative determination of internal stresses and strains produced in a body as the result of external loads and deformation. Its methods are both theoretical and experimental. The complete stress analysis of the tire should establish the magnitude and direction as well as the type of stress at all points in the tire under each loading condition of interest. This information defines the so called state of stress. Such knowledge, when combined with the material properties of the rubber, cord, and steel can be used to predict or explain the behavior of the tire in service.

The material properties of the three structural components of the tire are widely different. For example, the Young's moduli obtained at room temperature from statically

conducted tests are approximately: 300-3000 psi for the rubber, 100,000-800,000 psi for the textile cords, and 30,000,000 psi for the steel bead wire. In addition, the final geometries into which these components can be combined are diverse. Presently, there are three distinct cord arrangements in aircraft tire construction: bias, belted-bias and radial. These material and geometric factors, coupled with the fact that the tire as a whole is an anisotropic body subjected to finite deformations which are rate and temperature dependent, have made the theoretical and experimental stress analysis of the tire more difficult than that associated with the majority of engineering structures.

1.3 Ground Contact Analysis

The tire casing takes up its equilibrium shape, which is determined primarily by the cord paths, perhaps modified somewhat in local regions by the presence of extra rubber, ply turn-ups, flippers, filler, etc. For clarity and ease of discussion we will ignore these features and their effects and start from the simple theoretical equilibrium shape.

As the tire is pressed against a flat roadway the tread rubber is compressed and at the same time the tire casing locally loses its axial symmetry and takes on a substantially flattened contact patch. If there were no tread rubber on the tire , the casing would be flat over of the casing in actual contact with the ground will also lie in a flat plane parallel to the ground plane, the line of the cord is straight. It follows that the tension in the cord bears no relation to the internal inflating gas pressure, in this particular region of the tire. To make this point emphatically clear it will be noted that the basic law determinig the relation between tension in the casing cords and the internal gas pressure which it resists

is based on the simple laws of statical force resolution, and in such cases a path of infinite radius of curvature results in zero resultant force opposing the gas pressure. The tension in the cords across the flat part on the contact patch is therefore determined primarily by the cord tension transmitted from the adjacent free wall of the tire, modified by the effects of the transition curvature around the perimeter of the flat contact patch. It also follows that the contact pressure between the tire casing and the ground will be equal to the inflation pressure, modified around the edges of the contact patch by the extra pressures set up by the bending stresses within the transition zone.

In the case of practical tire designs the presence of tread rubber of differing thickness, of tread pattern design, and such factors as the bending stiffness caused by the multiple layers of cord cause the actual tire contact pressure to be locally greater than the inflation pressure, and in fact to differ in different parts of the contact patch. The contact pressure at the sides of the contact patch, under the shoulders of the tire tread, is often higher than the general contact pressure because of the reaction necessary to develop the bending stresses in the transition zone around the contact area. An analysis of the problem will require the application of numerical methods, based on finite element analysis.

1.4 Objective:

The main objective of this analysis is to determine the displacement and stresses in an aircraft tire subjected to inflation pressure and ground contact loading and thereby determining the contact pressure pattern between the tire and road. The objective was to develop an inexpensive analysis of tire deflection and ground contact loads by utilizing

two 2-D analysis of the tire cross section and a tread band ring - on - foundation model of the tire respectively to replace a full 3-D finite element analysis.

center on page

CHAPTER 2

LITERATURE REVIEW

2.1Composition of Tire Compounds

Ingredients [1] in tire compounds can be classified as :(1) the rubber which may be a single polymer or a blend of polymers [2,3] and, with high molecular weight polymers, may include an extending oil; fillers, principally various types of highly-developed carbon blacks; (3) relatively small additions of softeners, plasticizers, or reclaim rubber which serve principally as processing aids; (4) the chemical vulcanization system, which is likely to include two accelerators, sulfur, and a small amount of zinc oxide; (5) chemical protective agents, known as antioxidants and antiozonants.

With such a wide variety of ingredients, the important mechanical properties for a given tire compound can usually be obtained from a number of different compositions. For example, modulus and hardness can be controlled by varying either the amount of carbon black, the amount of extender-oil or softener, the fineness and structure of the carbon black, or the number of molecular crosslinks introduced during vulcanization. Thus even small advantages in cost, performance, and processing, which may only become apparent with extensive testing or service experience, become important factors in compound selection.

2.2 Physical Properties of Tire Compounds

The physical properties of any rubber compound depend upon the state of cure[4], that is, upon how far the chemical vulcanization reactions have been carried. Vulcanization introduces chemical crosslinks or bonds between the long chain polymer molecules. This

crosslinked network is decisive for the physical properties and is determined, for a given rubber compound, by vulcanization time and temperature. The traditional rule of thumb is that the vulcanizing time to reach a given level of a property, such as static modulus, is halved if vulcanization temperature is raised by 18F, and vice versa. Although this rule is still often adequate, a more precise description of the time-temperature dependence of vulcanization requires determination of the activation energy of vulcanization for each rubber compound.

The effect of cure on the physical properties of a rubber compound is usually determined by vulcanizing a series of test sheets for different times at the same temperature. This may, of course, also be done at several temperatures if more thorough tests are required. Dumbbell shaped test specimens are cut from the sheets and static stress-strain curves are taken[5].

Rubber stress-strain curves under static conditions are concave toward the axis, i.e., strain hardening, except for a short portion near the origin. The concavity is accentuated by the occurrence of stress-induced crystallization in natural rubber at higher elongations[6,7]. There is no yield point before failure, as is usual with metals. The curves in figure 2.1 represent approximately the effect of cure time on static stress-strain properties for a range of cures of a tread-type compound. Stress and tensile strength are calculated using the original cross-section area. In rubber technology, this stress is called modulus and is designated for a specific elongation, so that 300 percent modulus for a rubber compound

is the stress required to extend a strip to four times its original length. Volume changes are negilgible [8], when rubber is trained so that Poisson's ratio is assumed to be one-half.

Static modulus provides a convenient parameter to assess the temperature range in which elastomeric properties are exhibited. While this varies somewhat with individual polymers, in general the modulus of an elastomer varies with temperature as shown in figure 2.2. At low temperatures a hard or glassy character is evident. As temperature is raised the rubber passes through a transition region in which properties change rapidly. Rubber properties prevail over a range of temperatures above the transition temperature, and finally at yet higher temperatures above the transition temperatures viscoelastic or flow properties become important and predominate.

At high temperatures and for long times, the flow properties of rubber are marked. Stress relaxation in this region can often be attributed to oxidative degradation. In the elastomeric region there is relatively little stress relaxation, and in this state molecular network comes into equilibrium with applied stress, so that here the concept of modulus is valuable.

As shown in figure 2.1, modulus or stress at a given elongation increases, and breaking elongation decreases, as cure advances. Tensile strength usually goes through a maximum, although this is not always observed in a range of test cures. In some

compounds a phenomenon known as reversion occurs and modulus, tensile strength, and breaking elongation all decrease with overcuring. For tire tread compounds the usual tensile strength will be in the range 2500 to 4000 psi, 300 percent modulus in the range of 1000 to 1700 psi, and breaking elongation in the range of 400 to 600 percent.

2.3 Aging tests

Physical properties of tire compounds, especially stress-strain properties, are also routinely examined in rubber laboratories after the rubber has been exposed to one or more accelerated aging test [9]. These are usually run at elevated temperatures in order to simulate deterioration in service over a long period of time. Several of the tests are over-aging tests under carefully controlled conditions, while others use a bomb filled with air or oxygen under pressure to further accelerate degradation.

Figure 2.4 gives an example of the effect of oven aging on the stress-strain curve of a tread compound. Although such results do not correlate perfectly with aging deterioration in service, they can be very helpful, especially with a background of experience, in anticipating whether or not a compound will be satisfactory in this respect. These aging effects are quite complicated [10,11] as they depend on oxidative chemical reactions on the polymer [12,13]. Hence they are very depenedent both on the chemical nature of the polymer and on antioxidants in the compound recipes. In general, SBR is less sensitive to aging than natural rubber. The basic mechanism of degradation in these two rubbers appears to be quite different, SBR tending to harden on aging and natural rubber to

soften, reflecting, respectively, predominance of additional molecular crosslinks and chain scission, i.e., cutting of chain molecules into smaller molecules.

2.4 Tear tests

Rubber tear tests [14] are designed to cause a high stress gradient at the end of a cut or notch in an angle or crescent shaped testpiece, which is pulled in a testing machine. Figure 2.5 illustrates various types of tear test specimens. Although tearing phenomena with rubber most important and revealing in regard to mechanisms of rubber failure [15,16], technical tear tests have very limited practical significance, probably because the notch effect is so complicated and difficult to control for rubber. Tear test values are reported as load per unit of specimen thickness. An SBR tread compound with tensile strength about 3000 psi might reasonably show a crescent tear stength of about 250 lb/in.

2.5 Hardness

Rubber hardness is an important quality control parameter. It is conveniently measured with a Shore A Durometer, a pocket instrument which has been standardized [16] but use of whih often leaves much to be desired in the way of precision. The durometer uses a small, spring loaded indenter with a truncated conical point protruding from a flat base. When indenter and base are pressed against the rubber, the resulting spring deflection, which dpeends upon rubber hardness, is indicated by a pointer with a scale graduated from 0 (no hardness) to 100 (no indentation). Shore A hardness for rubber tread

compounds is typically in the range of 50 to 65 units and for unfilled vulcanizated about 25 to 30.

There are a variety of other hardness test instruments for rubber and a well-developed International Rubber Hardness Degree (IRHD) scale which agrees approximately with the Dhore A Durometer scale [17,18]. Indentation of thick rubber obeys the classical elasticity analysis of Hertz very well [19], and this gives a mechanism to relate elastic modulus to hardness mesurements.

2.6 Dynamic test

Many different test procedures are available to measure rubber stiffness and energy loss for relatively small cyclic deformations, often over ranges of temperature and frequency. These evaluations are especially pertinent for tire compounds because heat generation and temperaure rise from rubber hysteresis losses are important factors in tire durability [20].

One of the oldest and still most widely used types of test for this purpose is a pendulum rebound test, in which a pendulum is released from a fixed height to strike a rubber block and then rebound [21]. Superiority of natural rubber or synthetic cis 1,4-polyisoprene in this test is pronounced. Percent rebound for SBR tread compounds will usually be in the range of 52 to 62 percent while that for comparable natural rubber compounds may be more than 70 percent. A falling ball instead of a pendulum is often used in a rebound test.

Free vibration tests [22] and forced nonresonant and resonant vibration test are also found in great variety [23,24]. These are used to measure dynamic modulus, internal friction, and resilience of rubber compounds.

2.7 Rubber Elasticity:

2.7.1 Thermodynamic aspects

Distinctive features of rubber elasticity are easy deformability or low modulus, enormous deformations, and rapid recovery when deforming forces are released. There is also more sensitivity to temperature than for many elastic materials. Figure 2.7 shows the dramatic effect of low temperatures on relative modulus of unfilled vulcanizates of several polymers. For any elastomer there is a range of temperatures over which transition occurs from a rubbery to a glassy state, as shown in figure 2.2. This transition temperature range for SBR is from -60 C to -40 C, which is about as high as can be tolerated for a general purpose tire rubber. The curve forcis-polybutadiene in figure 2.7 is complicated by crytallization, which starts to affect the warming curve at about -95 C.

In the transition range from the glassy to the rubber state modulus falls rapidly with increasing temperature, but further temperature increase results in a slowly rising modulus. This rise first observed in experiments by Gough, published in 1805, as a contraction when a rubber specimen by Gough, published in 1805,as a contraction when a rubber specimen stretched by a weight was heated. Joule, about 50 years later, studied thermoelastic phenomena exhibited by rubber and interpreted them in terms of the new

science of thermodynamics then being developed by Kelvin. Treolar [29] gives a very good review of the thermodynamic fundamentals of rubber elasticity. For a reversible process, the first and second laws of thermodynamics provide,

$$dE = TdS + dW \tag{2.1}$$

in which E is internal energy of a system, T is absolute temperature, S is entropy, and W is work done on the system. At once there is a difficulty here because ordinary rubber deformations are not completely reversible. It is necessary to take special measures with any test specimen, such as solvent vapor treatments or prestretching them at an elevated temperature, in order to secure reversible deformations.

If the tensile force on a rubber strip is *f,* then the work done during an isothermal displacement *dl* is, neglecting small volume changes,

$$dW = f\,dl \tag{2.2}$$

and, with eq (2.1)

$$f = (\delta W/ \delta l)_T = (\delta E/ \delta l)_T - T(\delta S/ \delta l)_T \tag{2.3}$$

Equation (2.3) resolves the force into two terms. The first arises from changes in internal energy and the second from entropy changes with changes in length.

By differentiation of eq. (2.3) can be written

$$(\delta f / \delta T)_l = -(\delta S / \delta l)_T \qquad (2.4)$$

$$f = (\delta E / \delta l)_T + T(\delta f / \delta T)_l \qquad (2.5)$$

Equation (2.5) , in conjunction with eq (2.4), has been very important for understanding rubber elasticity because it allows experimental evaluation of internal energy and entropy changes upon deformation. If the equilibrium force exerted by a stretched rubber strip held at constant length is measured and plotted as a function of temperature, the slope at any value of T is $(\delta f / \delta T)_l$,which eq (2.4) shows to be the entropy change per unit change in length for isothermal expansion at T. The corresponding internal energy change $(\delta E / - \delta l)_T$ is given by the intercept of the tangent with the zero T axis.

Careful experimental work of this type by Meyer and Ferri [25], Anthony, Caston, and Guth [26], Wood and Roth [27], Gee [28] and many others showed that over a considerable temperature range stress was closely proprtional to absolute temperature, and this led to the conclusion that rubber elasticity resides principally in the entropy terms of eq (2.5). There is an entropy decrease on extension and an increase on retraction, except at very low elongations, below about 10 percent where a so-called thermoelastic inversion is observed due to thermal expansion obscuring the entropy effect.

a. at large elongations, where high orientations and crystallization may occur.

b. Voume changes and internal energy effects, however, appear never to be entirely absent. This entropy basis indicates that rubber elasticity must have had an entirely different moecular origin or mechanism than ordinary elasticity, where stresses increase the internal energy by increasing molecular or atomic spacings.

2.7.2 Molecular picture: elasticity of a rubber molecule

The unique thermoelastic behavior of rubber is elated to molecular structure by the kinetic or statistical theory of rubber elasticity. The theory provides a very satisfactory explanation of what might be called the mainspring of rubber elasticity, but it involves idealizations which have restricted its quantitative application to very carefully controlled equilibrium experiments with suitable rubber compounds and limited elongations and temperatures. It can only be regarded as semiquantitative for rubber in real applications. Reasons for these deviations from the theory, however, are quite comprehensible in light of what is known from many sources concerning the molecular geometry and forces.

There is extensive evidence that a rubber is composed of long chain molecules as shown in figure 2.8. The monomer repeating unit in the chain molecule of cis-polyisoprene or natural rubber is

```
          CH3
           |
----CH2----C====CH------CH2-------
```

while in cis-polybutadiene it is ---CH2---CH==CH---CH2-----. In SBR, styrene units amounting to about 23 percent by weight occur at random in the polybutadiene chain.

Such molecules are flexible by virtue of rotation around the single bonds, except at low temperatures where packing becomes too close or crystallization may occur for the first two rubbers. They tend to assume haphazard or chance configurations because of thermal agitation of their segements. Most of these configurations will be very crumpled, so that a chain molecule can be extended by an external tensile force provided that interaction with its neighbors is not too strong. As temperature is lowered, this interaction increases until the typical low modulus and rubber elasticity are no longer present this temperature influence is shown in figure 2.7.

A single, long chain rubber molecule assumes random statistical configurations to the extent permitted by hindered bond rotations, fixed valence-bond angles, excluded volumes (since no two atoms can occupy the same space simultaneously), and intermolecular forces. Some of these effects can be accomodated in the theory, but in the first mathematical model the molecule is assumed to undergo random thermal fluctuations among all possible configurations of its *n* links, each of length , just as if they were freely orienting. Thus the problem of describing the configurations is the random walk problem, and the configurations have analogies to the Brownian motion of a particle.

The distance between the ends of a chain, *r,* is called the displacement length, end-to-end distance, or simply the chain length. The distance measured along the chain is the chain contour length.

The distribution of chain lengths is Gaussian provided they are not extended more than about one-third of their fully extended length, *nl*.

This distribution is given by

$$P(r)dr = (4b^3 / \Pi^{1/2})r^2 \exp(-b^2 r^2)\, dr \qquad (2.6)$$

In eq (2.1.6) P(r) is the probability function for r and

$$b^2 = (3/2)/(nl^2) \qquad (2.7)$$

The root mean square value of *r* is

$$(r^2)^{1/2} = ln^{1/2} \qquad (2.8)$$

This shows at once that *n* must be large to account for rubber elongations, since the ratio of the average unstretched chain end seperation to the fully extended chain length is *n* . Higher molecular weights thus favor greater extensibility.

According to the familiar Boltzmann relation the entropy of a system is proportional to the logarithm of the number of possible configurations. Hence from eq (2.6) the entropy S of a single chain molecule is

$$S = c - k \cdot b^2 \cdot r^2 \qquad (2.9)$$

in which *c* is an arbitrary constant and *k* is Boltzmann's constant. It is apparent from eq(2.9) that the entropy decreases as *r* becomes larger, that is, as the molecule is stretched. The work required to increase *r* to *r+dr* is

$$f dr = -T\, dS/dr \qquad (2.10)$$

in which f is the stretching force on the molecule. From eq (2.9)

$dS/dr = -2kb^2 r$ so that

$$f=2kTb^2 r \qquad (2.11)$$

That is the average fluctuating statistical force exerted at the end of a stretched molecule. It is proportional to absolute temperature and to the value of r, the end-to-end distance, and it acts along the line of r.

2.7.3 Elasticity of the molecular network:

A chain molecule reaching from one crosslink to another is called a network chain. The gaussian distribution of eq(2.6) is assumed to apply to each network chain so that the entropy change for deformation of the network can be calculated by summing the entropy changes for all the chains in the network. In doing this the assumption is made that the deformation is affine, that is, the vector components of length of each chain are changed in the same ratio as the corresponding dimensions of the rubber specimen. Treolar[29] gives the entroy change ΔS of the network due to deformation as

$$\Delta S = -\frac{1}{2} Nk (\lambda_1^2 + \lambda_2^2 + \lambda_3^2 - 3) \qquad (2.12)$$

in which N is the number of network chains per unit volume and λ_1 , λ_2 , and λ_3 are the principal extension ratios along the three mutually perpendicular axes of strain for a pure homogenous strain. The extension ratio is defined as the ratio of the deformed to the undeformed length.

If the deformation is not accompanied by any change in internal energy the work of deformation, W, is --T Δ S, so that

$$W = 1/2NkT (\quad \lambda_1^{\,2} + \lambda_2^{\,2} + \lambda_3^{\,2} \text{ ---3)} = 1/2G(\quad \lambda_1^{\,2} + \lambda_2^{\,2} + \lambda_3^{\,2} \text{ ---3)} \qquad (2.13)$$

W is the elastically stored free energy per unit voulme and is known as the stored energy function.

In eq (2.13) G is the modulus of rigidity which in this simpler version of the theory depends uniquely on chain molecular weight through the relation

$$G = NkT = \rho RT/M_c \qquad (2.14)$$

Here ρ is the density of the rubber, R is the gas constant and M_c is the number-average network chain molecular weight. The theory thus provides a single elastic constant which is proprtional to the degree of crosslinking.

To calculate the principal stresses from eq(2.13) it is assumed that volume changes can be neglected so that

$$\lambda_1 \,.\, \lambda_2 \,.\, \lambda_3 \quad = 1 \qquad (2.15)$$

Work done by the applied forces is

$$dW = f_1\, d\lambda_1 \; + f_2 \; d\lambda_2 \; + f_3 \; d\lambda_3 \qquad (2.16)$$

in which f_1, f_2, and f_3 are forces per unit initial unstrained area and act along the principal axes. Comparing dW obtained by differentiating eq (2.13) with dW in eq (2.16), after eliminating λ_3 from both by use of eq (2.15) and equating the coefficients of $d\lambda_1$ and $d\lambda_2$ gives the general stress-strain relations:

$$\lambda_1 f_1 \; - \; \lambda_3 f_3 \; - \; G\,(\lambda_1^{\,2} \; - \; \lambda_3^{\,2}\;) \qquad (2.17)$$

$$\lambda_2 F_2 \; - \; \lambda_3 f_3 \; = G\,(\lambda_1^{\,2} \; - \; \lambda_3^{\,2}\;) \qquad (2.18)$$

Eqations (2.17) and (2.18) can be written in terms of principal stresses t_1, t_2, t_3 defined as forces per unit area after straining, by use of relations such as $f_1 = t_1 \; \lambda_2 \; \lambda_3$, in the form

$$t_1 \; - \; t_3 = G\,(\lambda_1^{\,2} \; - \; \lambda_3^{\,2}\;) \qquad (2.19)$$

$$t_2 \; - \; t_3 = G\,(\lambda_2^{\,2} \; - \; \lambda_3^{\,2}\;) \qquad (2.20)$$

These equations give only the difference between two principal stresses, since eq (2.15) has introduced the indeterminancy of an arbitrary hydrostatic stress. This may be recognized by writing the principal stresses [29] as

$$t = G\lambda_1^{\,2} + p;\; t = G\lambda_2^{\,2} + p;\; t = G\lambda_3^{\,2} + p \qquad (2.21)$$

However, if one or more of the principal stresses is given, a unique solution can be obtained for the other two stresses provided that the extension ratios λ_1 , λ_2 , λ_3 are known.

For uniaxial extensions f_2 and f_3 both vanish, and $\lambda_2 = \lambda_3 = \lambda_1^{-1/2}$ so that from eqs (2.17) and (2.18), the rubber stress-strain relation is

$$f = G(\lambda_3 - \lambda_1^{-2}) \qquad (2.22)$$

Treolar carried out experiments to verify eqs (2.19) and (2.20) using simple extension, uniaxial compression, uniform two dimensional extension and shear deformation on natural rubber gum vulcanizates. He found that these equations using the single physical constant G provided a fairly satisfactory first approximation to experimental results. However, deviations were observed both at moderate strains, where measured stresses tended to be lower than predicted, and at very high strains where they were larger than predicted. The effects at large strains are caused by failure of the Gaussian distribution, eq (2.6) to apply for large extensions of the chain molecules. This can be explained by non-Gaussian statistics [29].

Deviations at moderate strains have been attributed to inadequacy of the stored energy function using only a single constant. Krigbaum and Roe [30] analyze such deviations from the kinetic theory in detail, summarize the evidence that there are, in fact, appreciable energy changes in rubber deformations, and describe more recent attempts to test and refine this theory.

2.7.4 Strain-energy representation of rubber elasticity:

The preceding sections have shown how thermoelastic phenomena, along with rubber and thermodynamic analysis, led to the kinetic or statistical theory of rubber elasticity. In turn, this leads to a description of rubber elasticity in terms of a stored energy function using a single elastic constant, called G in eq (2.13).

The stored energy approach has been developed for rubber in an entirely phenomenological way, independent of any molecular theory, both by Mooney [31] and by Rivlin [32]. In applying the general elasticity theory for large deformations of incompressible, isotropic elastic materials, Mooney assumed a linear shear stress law consistent with kinetic theory. Rivlin showed that it was unnecessary, for many purposes, to assume any particular elastic law and that the elastic law could be determined experimentally through relations derived from the theory.

The strain energy per unit unstressed volume stored in a material is a function of the general components of strain at any point [33]. The stored-energy function is unaffected by coordinate transformations. The form of this function is as characteristic of the material as the stress strain relation, with which, of course, it is closely connected. The nature of the stored energy for a pure homogenous strain completely determines the elastic properties of the material. The assumption of incompressibility simplifies the function, and is justified for rubber in practical terms because stresses required for changing the volume are so much larger than those required to change the shape.

It follows from this general theory for large elastic deformations of rubber [29,33-35] that the stored energy W is a symmetric function of the three principal extension ratios λ_1, λ_2 and λ_3, can be expressed in terms of the three following strain invariants:

$$I_1 = \lambda_1^2 + \lambda_2^2 + \lambda_3^2 \qquad (2.23)$$

$$I_2 = \lambda_1^2 . \lambda_2^2 + \lambda_2^2 . \lambda_3^2 + \lambda_3^2 . \lambda_1^2 \qquad (2.24)$$

$$I_3 = \lambda_1^2 . \lambda_2^2 . \lambda_3^2 \qquad (2.25)$$

Assuming incompressibility, $I_3 = 1$, and λ_3 can be eliminated from eqs (2.23) and (2.24) so that W can be expressed in terms of two independent variables I_1 and I_2, which in turn contain only λ_1 and λ_2 This means, of course, that only two of the extension ratios can be varied independently.

The most general form of this stored energy function can be written [29]

$$W = \sum_{i=0}^{\infty} \sum_{j=0}^{\infty} C_{ij} (I_1 - 3)^i (I_2 - 3)^j \qquad (2.26)$$

$(I_1 - 3)$ and $(I_2 - 3)$ are used in eq (2.26) instead of I_1 and I_2 so that W will be zero for zero strain.

The first term of the series, i =1, j =0, gives for W the form derived from the kinetic theory, eq (2.13) which gives a reasonably good first approximation to the rubber stress-strain realtions.

Retention of the first two terms, i=1, j=0 and i=0, j=1 gives

$$W = C_1 (I_1 - 3) + C_2 (I_2 - 3) \qquad (2.27)$$

This was the form derived by Mooney which, having two constants, provides better agreement with experimental data than eq (2.13).

From eq (2.27) for simple extension, the force f per unit initial cross section is derived as

$$f = 2\left(\lambda - 1/\lambda^2\right)\left(C_1 + C_2/\lambda\right) \qquad (2.28)$$

Equation (1.1.28) is known as the Mooney-Rivlin equation. For simple shear,

$$t_\sigma = 2(C_1 + C_2)\sigma \qquad (2.29)$$

in which t_σ is shear stress, σ shear strain and hence $2(C_1 + C_2)$ is the modulus of rigidity.

2.8 Elastic Properties of Cord Reinforced Rubber

The increased use of more sophisticated structural configurations in pneumatic tires during the last few years has resulted in a greater interest in the elastic properties of cord-rubber lainates. The role of material properties in pneumatic tire design and analysis has been approached in three distinct ways:

a) First, the anisotropic nature of such materials may be completely ignored, and all tire structures treated as membranes whose stresses are determined entirely from membrane equilibrium considerations. This is a statically determinate shell approach, and in some regions tire stresses, and cord loads, may be found rather accurately by this technique when loadings are simple, such as in the case of inflation of a tire. However, proper elastic properties are necessary for adequate stress determinations near edges or boundaries in all shell problems, and in the case of a pneumatic tire it is necessary to know the material characteristics in order to find stresses near the bead and in the sidewall.

In more complex loadings where bending is an important factor, such as in deflecting a tire against a flat surface, the elastic properties of the material are needed for estimation of cord loads, and an isotropic approximation is not adequate.

Quite apart from stress analysis problems, which are always governed by force and moment equilibrium and hence can sometimes be less dependent on material properties, all deformation characteristics of cord-rubber structures are entirely determined by their elastic constants so that an isotropic approximation might be characterized as a very crude one in most c\ases.

b) An interesting and unique attempt to calculate cord loads in a cord rubber structure has been provided by Rivlin and his co-workers [36-37] and by Adkins [38-43]. They both utilize the concept of an inextensible net made up of the reinforcing textile cords in a normal cord-rubber structure, with the assumption that in such a net the cross-over points between cords in adjacent lamina act as knots which do not slip. This analysis has much to recommend it. Basically, in most situations, the reinforcing textile cords do indeed carry a major share of the tire structural loads. Thus neglect of the sorrounding rubber matrix is not generally serious, although situations exist when the sorrounding rubber can contribute substantially to the load carrying ability of the composite, as has recently been discussed by Clark and Dodge [44].

c) A third and somewhat later general approach to the elastic properties of cord-rubber laminates utilizes the overall elastic stiffnesses of both the cords and rubber treated as a two-dimensional orthotropic material. This requires that the concentrated cords and distributed rubber be viewed over dimensions much greater than cord spacing, so that the

average elastic modulus of a single lamina may be obtained, as opposed to the local or microscopic modulus which varies widely with position. The primary reason for this is that it is difficult to mathematically describe the large variations which exist in elastic stiffness of a cord-rubber laminate. It is much more convenient to work with an average property.

The main objective of this analysis is to determine the displacement and stresses in an aircraft tire subjected to inflation pressure only.

CHAPTER 3

THEORY OF RUBBER ELASTICITY

3. Theory

3.1 Tire Inflation

The simplest stress analysis problem to consider from a theoretical standpoint is the calculation of the shape taken by and the stresses developed in an inflated but otherwise unloaded bias tire. A portion of a pressurized but otherwise unloaded toroidal shell is shown in figure 3.1. The axial coordinate z is an axis of revolution. Because of the very small bending stiffness of the tire walls and rotational symmetry of both the applied loads and shell geometry, in-plane internal reactions develop which are constant through the shell thickness.

These internal reactions denoted by N_θ and N_ψ are usually called membrane stress resultants and they act in the meriodional and circumferential directions, respectively. Physically, the stress resultants represent forces per unit length.

The applied load (inflation pressure p) is just balanced by the internal reactions N_θ and N_ψ that is , force equilibrium exist so that summing forces normal to the shell surface leads to the well known equilibrium equation

$$N_\psi / r_\psi + N_\theta / r_\theta = p \qquad (3.1)$$

where r_θ and r_ψ are principal radii of curvature for the doubly curved toroidal surface. Both the stress resultants and the radii of curvature are functions of the radial distance r. A second equation of equilibrium can be obtained from figure 1 by summing forces along the axis of revolution to obtain:

$$N_\psi = p\, r_\theta\, (r^2 - r_\psi^2)/ 2r^2 \qquad (3.2)$$

Equations 3.1 and 3.2 are two equations for the two unknown stress resultants and they can be immediately solved when the meridional geometry of the toroidal shell is given.

3.2 Strain energy potentials

There are two forms of strain energy potentials used in ABAQUS for modeling approximately incompressible isotropic elastomers the polynomial form and Ogden form.

The form of the polynomial strain energy potential is

$$U = \sum_{i+j=1}^{N} C_{ij} (I_1 - 3)^i (I_2 - 3)^j + \sum_{i=1}^{N} (1/ D_i) (J_{el} - 1)^{2 i} \qquad (3.3)$$

where U is the strain energy per unit of reference volume, N is a material parameter, C_{ij} and D_i are temperature dependent material parameters, I_1 and I_2 are the first and second deviatoric strain invariants defined as

$$I_1 = \lambda_1^2 + \lambda_2^2 + \lambda_3^2 \qquad (3.4)$$

$$I_1 = \lambda_1^{-2} + \lambda_2^{-2} + \lambda_3^{-2}$$

with the deviatoric stretches $\lambda_i = J^{-1/3} \lambda_i$, J is the volume ratio, λ_i are the principal stretches, and J_{el} is the mechanical elastic volume ratio. J_{el} does not include thermal expansion effects.

3.3 Particular cases of the strain energy potentials

If all of the D_i are zero, the material is fully incompressible. If D_i is equal to zero, all of the D_i is equal to zero.

For cases where the nominal strains are small or only moderately large (<100%), the first terms in the polynomial series usually provide a sufficiently accurate model. The

simplest form of the polynomial function is the incompressible form with N =1, which is the classical Mooney-Rivlin form:

$$U = C_{10} (I_1 - 3) + C_{01} (I_2 - 3) \qquad (3.5)$$

When $C_{01} = 0$ the strain energy function corresponds to the neo-Hookean form.

The initial shear modulus and bulk modulus are given by

$$\mu_0 = 2 (C_{10} + C_{01}) \ , \ K_0 = 2 / D_1 \qquad (3.6)$$

The neo-Hookean form is obtained with N =1 and $\alpha = 2$ and can be made equivalent to the polynomial form through the relation .

The Mooney-Rivlin form is obtained when N =2, $\alpha_1 = 1$ and $\alpha_2 = -2$ and is equivalent to the polynomial form when

$$\mu_1 = 2 C_{10} \text{ and } \mu_2 = 2 C_{01}$$

$$U = \mu_1 /2 (\lambda_1^{-2} + \lambda_2^{-2} + \lambda_3^{-2} - 3) + \mu_2/2 (\lambda_1^{-2} + \lambda_2^{-2} + \lambda_3^{-2} - 3) \qquad (3.7)$$

We will develop the stress-strain relationships for the different tests for the incompressible version of the material model using derivatives of the strain energy function with respect to the strain invariants. We define these relations in terms of the nominal stress (the force divided by the original, undeformed area) and the nominal, or engineering strain defined below.

The deformation gradient, expressed in the principal directions of stretch, is

$$F = \begin{bmatrix} \lambda_1 & 0 & 0 \\ 0 & \lambda_2 & 0 \\ 0 & 0 & \lambda_3 \end{bmatrix} \qquad (3.8)$$

where λ_1 , λ_2 and λ_3 are the principal stretches, which are the ratios of current length to

length in the original configuration in the principal directions. The principal stretches, λ_i are related to the principal nominal strains, ε_i , by

$$\lambda_i = 1 + \varepsilon_i \qquad (3.9)$$

Because we assume incompressibilty and isothermal response, J = det(F) = 1, and, hence, $\lambda_1 \lambda_2 \lambda_3 = 1$. The deviatoric strain invariants in terms of the principal stretches are then

$$I_1 = \lambda_1^2 + \lambda_2^2 + \lambda_3^2 \quad \text{and}$$

$$I_1 = \lambda_1^{-2} + \lambda_2^{-2} + \lambda_3^{-2} \qquad (3.10)$$

3.4 Uniaxial Tests

The uniaxial deformations mode is characterized in terms of the principal stretches, λ_i , as

$$\lambda_1 = \lambda_u, \qquad \lambda_1 = \lambda_2 = 1/\sqrt{\lambda_u} \qquad (3.11)$$

where λ_u is the stretch in the direction of loading.

The uniaxial tension test is the most common of all the tests and is usually performed by pulling a "dog-bone" specimen. The uniaxial compression test is performed by loading a compression button between lubricated surfaces. The loading surfaces are lubricated to prevent any barreling effect in the button that would cause deviations from a homogenous uniaxial compression stress-strain state.

To derive the uniaxial nominal stress, T_u, we invoke the principle of virtual work,

$$\delta U = T_u \delta\lambda_u$$

so that the

$$T_u = \partial U / \partial \lambda_U = 2(1 - \lambda_U^{-3})(\lambda_U \partial U/\partial I_1 + \partial U/\partial I_2) \qquad (3.12)$$

To start with the only experimental data I had was from a stress strain curve of +/_ 38 nylon rubber composite coupons.

A curve fit was performed on the stress vs elongation graph to determine the value of constants C_{01} and C_{10}.

3.5 Finite Elements: Basic Concepts For Solid Mechanics Problems

This represents a reasonably general basis for the finite element approximation of nonlinear dynamic problems in solid mechanics. The development is applicable to situations involving large deformations, material nonlinearities, and frictionless surface contact. The resulting semi-discrete system may be discretized in time to obtain the governing equations for implicit, explicit, or steady-state dynamic solutions, or specialized to obtain finite element formulations for linear and nonlinear static problems. For the field equations, we adopt a spatial (Eulerian) frame of reference, in which the current configuration of the system is the reference configuration. However, the finite element mesh will be Lagrangian (that is, moving and deforming with the material); this approach is common in solid mechanics problems, where the system of interest often consists of a fixed collection of material. We will use the velocity components v_i as fundamental unknowns, to obtain a discrete problem in which velocity (or displacement) variables are the primary variables.

3.5.1 Field Equations

At any instant of time, let the region occupied by the system of interest be denoted by V, and its boundary by ∂ V. Within region V, we assume that a constitutive relationship

$$\sigma_{ij} = \chi_{ij} [d_{mn}, \int d_{mn}\, dt, ...] \qquad (3.13)$$

which defines the stress σ_{ij} in terms of the velocity and related quantities is satisfied at all times. Here **d** is the *rate of deformation* tensor, defined as the symmetric part of the velocity gradient:

$$d_{ij} = 1/2 \, [\partial v_i / \partial x_j + \partial v_j / \partial x_i \,] \qquad (3.14)$$

If the history of the velocity and the velocity gradient are known at a material point, we assume that the stress history can be evaluated directly. In the interior of the region the field equation whose solution will be approximated in the finite element solution, is the momentum balance

$$\partial \sigma_{ij} / \partial x_i + \rho \, b_i = \rho \, a_i \qquad (3.15)$$

Here ρ is the mass density, b_i are components of the body force per unit mass, and a_i are the components of acceleration.

The condition of conservation of mass will be satisfied through the use of a Langrangian mesh. During the solution, we will let the mesh deform with the material, so that material never crosses the element boundaries. Consequently, the region V is "updated" automaticallt to reflect the deformation of the system. The density ρ, which may be needed for stress, force, or energy calculations, may be obtained by integrating in time using the continuity equation

$$d\rho/dt = -\rho \, \partial v_i / \partial x_i \qquad (3.16)$$

3.5.2 Boundary Conditions

At each point of the boundary ∂V, in each of three linearly independent directions, a boundary condition is required to specify a velocity, a traction (force) component, or some relationship between the two. we denote the portion of the boundary on which

velocity components are prescribed by ∂V_u, and that on which forces are specified by ∂V_σ; in what follows, this notation is used chiefly to specify limits of integration. Notice that at one physical location of the boundary we may have the velocity prescribed in one direction, and forces in the remaining directions. For this reason, an expression which is said to hold "on ∂V_σ" may in fact apply only to certain components of the velocity, traction, or stress. The boundary conditions for the velocity and stress are:

$$v_i = \bar{v}_i \quad \text{on } \partial V_u$$

$$n_j \sigma_{ij} = \bar{t}_i \quad \text{on } \partial V_\sigma \tag{3.17}$$

Here n is a unit vector along the outward normal direction to the boundary at a point. An overbar indicates the prescribed quantity.

To accommodate the contact problem, we will introduce two additional boundary regions denoted by ∂V^A and ∂V^B. These two surfaces represent opposing faces of a contact surface; for each point belonging to ∂V^A, a corresponding point exists which belong to ∂V^B. Since the opposing surfaces are in contact, we have $n^A = - n^B$. The complete boundary ∂V therefore consists of the union of four mutually exclusive point sets:

$$\partial V = \partial V_u \cup \partial V_\sigma \cup \partial V^A \cup \partial V^B \tag{3.18}$$

Here we restrict attention to frictionless contact problems. Then, of the three directions at a point on either contact surface, only the direction normal to the surface belongs to ∂V^A or ∂V^B. The force condiotion for the contact interface requires normal traction components which are equal and opposite:

$$n_i{}^A [\, \sigma^A{}_{ji}\, n_j{}^A + \sigma^B{}_{ji}\, n_j{}^B \,] = 0 \tag{3.19}$$

The remaining two directions are stress-free (since the mutual tangential forces vanish) and therefore belong to ∂V_σ.

3.5.3 Principle of Virtual Work

The basis of our finite element approximation is a weak form of the momentum equations and the force-related boundary conditions. We assume that the kinematic boundary conditions on ∂V_u are satisfied *a priori,* since this is easily accomplished in terms of the nodal variables. Letting the test functions be δv_i , we can write

$$\int_V [-\partial \sigma_{ij} / \partial x_i - \rho b_i + \rho a_i] \delta v_i \, dV + \int_{\partial V\sigma} [\sigma_{ji} n_j - t_i] \delta v_i \, dA$$

$$+ \int_{\partial V^A \cup \partial V^B} (\sigma^A{}_{ji} n_j{}^A + \sigma^B{}_{ji} n_j{}^B) \delta v_i \, dA = 0 \qquad (3.20)$$

The use of a common test function for the opposing contact surfaces ∂V^A and ∂V^B reflects the requirement that the normal veloities of the two surfaces be equal, so the test functions cannot be independent.

The equality above may be interpreted in several ways. As a weak formulation of the boundary value problem, it states that the velocity field history **v(x,t)** which satisfies the initial conditions and which makes the weak form zero for any arbitrary choice of the test functions δv_i is the solution of the boundary value problem. This interpretation follows the same essential reasoning as Galerkin's method. A physical interpretation is provided by the *principle of virtual work*; each of the integrals in the weak form represents a rate of work performed by a sytsem of "generalized forces" (the quantities in parentheses), during the occurrence of a *virtual velocity field* δv_i. If these generalized forces (which actually are the residulas of the momentum equation and the boundary conditions) vanish, then the resulting integrals should vanish regardless of the choice of virtual velocities.

Notice that the virtual velocities (or test functions) δv_i vanish on ∂V_u, where the kinematic boundary conditions must be satisfied a priori.

In applying the principle of virtual work to the formulation of finite elements, it is useful to shift the derivative from the stress to the virtual velocities using the divergence theorem. In particular,

$$- \int_V \partial \sigma_{ij} / \partial x_i \ \delta v_i \ dV = \int_V \ \sigma_{ij} \ \ \delta v_{i,j} \, dV - \int \partial_V n_j \ \sigma_{ij} \ \delta v_i \ dA \qquad (3.21)$$

Notice that the boundary integral vanishes on ∂V_u (where $\delta v_i = 0$). The resulting virtual work expression is

$$\int_V \rho \, a_i \, \delta v_i \ dV + \int_V \ \sigma_{ij} \ \ \delta v_{i,j} \, dV - \int_V \rho \, b_i \, \delta v_i \ dV - \int \partial_{V\sigma} \ t_{ji} \ \delta v_i \ dA = 0 \quad (3.22)$$

3.5.4 Finite Element Approximation

An admissible finite element approximation of the virtual work principle requires continuity of the virtual velocities δv_i. Normally we adopt a continuous approximation for the actual velocity field v_i as well, by using the same shape functions for both variables. For most elements in common use, the stress field is discontinuous between adjacent elements.

Below, we develop the discrete equations for the finite element system in a form of indicial notation, with upper-case indices referring to nodes of the finite element model. This notation is useful for manipulating the equations for nonlinear systems, which do not lend themselves to matrix notation.

Let the finite element shape functions be $N_K(x)$. The approximations for the velocity and the virtual velocities are then:

$$v_i\ (x,t) = N_K(x)\ V_{K\,I}(t) \qquad (3.23)$$

$$\delta v_i\ (x,t) = N_K(x)\ \delta V_{K\,I}(t) \qquad (3.24)$$

The nodal velocities $V_{K\,I}$ are unknown, while the virtual nodal velocities $\delta V_{K\,I}$ each are arbitrary and independent. Note that each meaningful combination of indices (K,i) refers to a unique degree of freedom of the model.

If we introduce the finite element approximation into the virtual work expression, we obtain:

$$\delta V_{K\,I}[\ \int_V \rho\ N_K\ N_L\ V_{Li}\ dV + \int_V\ \sigma_{ij}\ \ N_{K,j}\ dV - \int_V \rho\ b_i\ N_K\ dV - \int \partial_{V\sigma}\ t_i\ \ N_K\ \ dA\ ] = 0 \qquad (3.25)$$

in which $\delta V_{K\,I}$ are arbitrary and independent of one another. Therefore the quantity in brackets must vanish for each degree of freedom. The resulting conditions, one for each unconstrained degree of freedom $V_{K\,I}$, are the semi-discrete governing equations for the finite element model:

$$\int_V \rho\ N_K\ N_L\ V_{Li}\ dV + \int_V\ \sigma_{ij}\ \ N_{K,j}\ dV - \int_V \rho\ b_i\ N_K\ dV - \int \partial_{V\sigma}\ t_i\ \ N_K\ \ dA = 0 \qquad (3.26)$$

If we define the mass coefficients

$$M_{KL} = \int_V \rho\ N_K\ N_L\ dV \qquad (3.27)$$

the external force vector

$$F^{ext}_{Ki} = \int_V \rho\ b_i\ N_K\ dV + \int \partial_{V\sigma}\ t_i\ \ N_K\ \ dA \qquad (3.28)$$

and the internal force vector

$$F^{ext}_{Ki} = \int_V\ \sigma_{ij}\ \ N_{K,j}\ dV \qquad (3.29)$$

then the system of ordinary differential equations describing the motion of the finite element model can be written as:

$$M_{KL}\, V_{L\,I} = F^{ext}{}_{Ki} - F^{int}{}_{Ki} \qquad (3.30)$$

The range of index I is normally 1 - 3 (for three-dimensional problems); K varies from 1 to the number of nodes in the finite element model. This coupled, nonlinear system of ordinary differential equations may be integrated versus time once the initial conditions (on position and velocity) are specified.

In practice, the method used for solving the finite element system depends upon the type of solution to be performed (transient, steady-state, or static), the time frame of interest, and whether or not the system is indeed nonlinear. The semi-discrete system formulated above provides a suitable starting point for all of these problem types.

3.5.5 The Finite Element System in Matrix Form

Often it is more convenient to express the finite element equations in matrix form. Let the shape functions for all components of the displacement or velocity be assembled in a matrix [N] such that

$$\begin{bmatrix} v_1 \\ v_2 \\ v_3 \end{bmatrix} = [N] \begin{bmatrix} V_{11} \\ V_{21} \\ \vdots \\ \vdots \\ V_{n3} \end{bmatrix} = [N]\{V\} \qquad (3.31)$$

Here n is the number of nodes in an element (or the system). {V} is the column vector of nodal velocity degrees of freedom. Also define the *linear strain-displacement matrix:*

$$[B] = \begin{bmatrix} N_{1,x} & N_{2,x} & \dots & N_{n,x} & 0 & 0 & \dots & 0 & 0 & 0 & \dots & 0 \\ 0 & 0 & \dots & 0 & N_{1,y} & N_{2,y} & \dots & N_{n,y} & 0 & 0 & \dots & 0 \\ 0 & 0 & \dots & 0 & 0 & 0 & \dots & 0 & N_{1,z} & N_{2,z} & \dots & N_{n,z} \\ 0 & 0 & \dots & 0 & N_{1,z} & N_{2,z} & \dots & N_{n,z} & N_{1,y} & N_{2,y} & \dots & N_{n,y} \\ N_{1,z} & N_{2,z} & \dots & N_{n,z} & 0 & 0 & \dots & 0 & N_{1,x} & N_{2,x} & \dots & N_{n,x} \\ N_{1,y} & N_{2,y} & \dots & N_{n,y} & N_{1,x} & N_{2,x} & \dots & N_{n,x} & 0 & 0 & \dots & 0 \end{bmatrix} \quad (3.32)$$

Arrange the unique rate of deformation components in a vector {d} such that

$$\{d\} = \{ d_{11}, d_{22}, d_{33}, 2\,d_{23}, 2\,d_{13}, 2\,d_{12} \}^T = [B]\,\{V\} \quad (3.33)$$

Similarly, define a column vector containing the unique stress components:

$$\{\sigma\} = \{ \sigma_{11}, \sigma_{22}, \sigma_{33}, \sigma_{23}, \sigma_{13}, \sigma_{12} \}^T \quad (3.34)$$

With the definition above, the semi-discrete finite element system becomes

$$[M]\,\{V\} = \{F\}^{ext} - \{F\}^{int} \quad (3.35)$$

Here the mass matrix [M] is defined by:

$$[M] = \int_V \rho\,[N]\,[N]^T\,dV \quad (3.36)$$

The vector of external forces is:

$$\{F\}^{ext} = \int_V \rho\,[N]^T\,\{b\}\,dV + \int_{\partial V_\sigma} \rho\,[N]^T\,\{t\}\,dV \quad (3.37)$$

Using the symmetry of the stress components, it is possible to arrange the internal force vector in the form:

$$\{F\}^{int} = \int_V [B]^T\,\{\sigma\}\,dV \quad (3.38)$$

In linear problems, the displacement gradient terms are small and the stress-strain relation is linear, so that

$$\{\varepsilon\} = [B]\,\{U\} \quad (3.39)$$

and

$$\{\sigma\} = [D]\{\varepsilon\} = [D][B]\}\{U\} \qquad (3.40)$$

For such problems, the internal forces may be written in the more familiar form

$$\{F\}^{int} = \int_V [B]^T [D][B]\, dV\, \{U\} = [K]\{U\} \qquad (3.41)$$

Matrix [K] is the linear stiffness matrix, and {U} is the vector of displacement degress freedom corresponding to {V}.

3.6 Formulation for two-dimensional small-sliding rigid contact

The formulation for two-dimensional small-sliding rigid contact follows from its deformable counterpart by exploiting the fact that the evolution of the contcat plane is fully determined by the motion of the rigid body's reference node. Figure 3.4 shows how the undeformed coordinates X_o of the contact plane's anchor point are related vectorially to the undeformed coordinates of the rigid refrence node, X_{rs}, and the relative position vector R. We can express this relationship as

$$X_o = X_{rs} + R \qquad (3.42)$$

Suppose the rigid reference node undergoes a motion described by the displacement vector u_{rs} and the rotation vector $\phi_{rs}\, e_z$, then the current coordinates of the contact plane's anchor point are given by

$$x_o = X_{rs} + u_{rs} + C(\phi_{rs}\, e_z)\,.\, R$$

$$= x_{rs} + r \qquad (3.43)$$

CHAPTER 4

EXPERIMENTAL METHODOLOGY

4.0 Experimental Techniques

4.1 Approach and Experimental Strategy

Since the theoretical methods are not sufficiently developed to allow the tire engineers to predict the stresses generated in the cord, rubber, and steel components of a tire under service conditions, a great deal of effort has been expended developing experimental procedures for this purpose. These stress and strain measurements are important since they may suggest changes in tire design which will make efficient use of tire construction materials and/ or improve performance materials especially with regard to tire cord fatigue performance phenomena.

Additionally, experimental data can be used to validate analytical predictions. Experimental results are often valuable in that they provide guidance in the development of an accurate mathematical model governing tire loaded in some particular manner.

Inorder to determine the value of Young's Modulus of the nylon-rubber composite used in the construction of the aircraft tire being analyzed, an experiment was conducted to determine the stress vs elongation of the same till failure occurred.

Apparatus:

1. Nylon rubber composite coupons of size 4"*0.75"*0.18" approximately so that the unsupported or gage length = 2".

2. All coupons were made of four plies, (+38/-38)s.

Procedure:

1. The room temperature was recorded once during each test.

2. Strain rate of 0.001 inch/sec was applied. This corresponds to elongation rate of 0.002 inch/sec.

3. From the start of test time, coupon temperature, load, elongation, specimen width and specimen thickness were measured as the test specimen is being stretched.

4. Strain rates of 0.0005 inch/sec and 0.01 inch/sec were applied and steps 1,2 & 3 repeated.

5.Stress vs elongation was plotted for each strain rate. Stress plotted is the actual stress computed by dividing the actual load by the true cross section area.

Figure 1 shows the stress vs elongation for various strain rates of (+38/-38) coupons.

4.2 Theory Of Operation Of 3D Digitizer

The building of the tire cross-sectional geometry was achieved using a 3 dimensional digitizing software and associated electronic equipment named GP-12-3D. The 3 dimensional equipment essentially uses the principle of ultrasonic soundwaves to determine the location of a point in space with respect to a set of reference coordinates. The basic system comprises of

a) an Offset Probe, which generates ultrasonic sound waves

b) a pre-calibrated microphone triangle (essentially it consists of three microphones located in an equilaterally shaped frame)

c) a Control box and a Pilot Bar

The GP-12 is conveniently designed to sit between the typical personal computer/color monitor combination found on most office desks today. The basic system comprises the

Control Box, an offset micro probe a pre-calibrated microphone triangle and optionally a pilot bar.

In the one meter (active cubic volume) Mode the GP-12 has a counter frequency of 39.3216 Mhz, yielding a resolution of approximately 114 cnts/mm at 21 C (0.0087mm). Due to the large number of possible configurations, both physically and mathematically, and the superior number crunching ability of the anticipated host CPU, this digitizer transmits slant range data - defined as the distance from the given emitter to the selected receiver.

Cartesian coordinates (X,Y,Z) resolution is a function the counter frequency and the actual speed of sound of the given digitized line-of-sight path.

Sonic digitizers take advantage of the fact that sound travels between two points (a sound emitter & a sound receiver) at a speed which can be calibrated (known). If a sound wave travels from a single emitter to three or more receivers of known orientation, and the speed of this sound wave and time duration between the emitter and each receiver are known, then it is possible to calculate the location of that emitter in three dimensional space.

While sonic digitizers offer the advantages of being able to digitize any material, including

metals, there are some practical limitations which need to be observed. Every emitter/ receiver combination being used requires a direct line of sight., i.e any object directly between an emitter and any receivers listening to the emitter will disrupt the digitizing

process. The probe emitters should face the detector array.

Because sound bounces (echoes) off hard objects, it sometimes happens that an echo, or reflection, from a previous emitter can interfere with the current emitter. The 3D digitizer has a feature called delay. The exact value required depends on your setup and its surroundings. The default value of 10ms was set in the experiment.

The higher the degree to which the speed-of-sound is calibrated, the higher the level of digitized accuracy is.

4.3 Procedure

The initial difficulty encountered mainly was in orienting the cut section of the tire and wheel axis together. The reason being the object has to be oriented in such a way that the transmitting sound beams are not in any way obstructed in its path to the receivers. After several attempts, it was found the best way to orient the object was to keep it on a level ground facing the three set of microphones (receivers).

The digitization of the sidewall, and the cord area was done without much difficulty. But since the crown part of the tire consisted of several depressions, it was extremely difficult to obtain good results out of the digitization. Hence another modification was made, namely to trace the cross section of the tire to be digitized on a graph paper. The digitization of the crown region of the tire was then carried out without much difficulty. After the readings were obtained the the readings were directly fed into the software PATRAN3, which is a pre and post processor for several finite element analysis packages. The geometry of the tire cross-section was generated using the software

without much difficulty except for the fact that some regions of the tire cross section had to be redigitized later on.

Due to the symmetry of the cross section about the y-axis it was decided to analyze only one half of the cross section. The geometry of the tire cross section is highly irregular. Therefore it is not advisable to do automatic mesh generation (the reason being it might produce irregular elements). The small group of lines which made up the tire cross section were first made to join together to form a group of curves. By making use of these curves, surfaces were generated. The surfaces were generated in such a way that cord areas had different surfaces from the pure rubber regions. Upon these surfaces four noded quadrilateral elements were created. The material and element properties were then assigned. The material properties were assigned for both rubber and nylon-rubber composite.

The first analysis was performed using axisymmetric hybrid reduced integration elements (CAX4RH is the notation used in ABAQUS for this particular element.). A second analysis was performed on the same mesh with axisymmetric , incompatible hybrid elements (CAX4IH) and the two results were compared. The analysis package used for this purpose was ABAQUS.

Similarly a finite element mesh consisting of eight elements was created for the rectangular coupon. The material and element properties were then assigned. The nylon rubber composite coupon was assumed to be hyperelastic. The element properties assigned were plane stress, reduced integration elements (CPS4R).

CHAPTER 5

STRUCTURAL ANALYSIS

OF

TIRE CROSS-SECTONS

AND

TREAD BAND RING-ON-FOUNDATION

TIRE MODEL

5.0 Static Structural Anaysis of Tire Cross Sections and Tread Band Ring on Foundation Tire Models.

5.1 Assumptions

The tire model can be considered axisymmetric for the purposes of analyzing inflation and determining the contribution of the sidewalls to the resistance of deflection within a reasonable range of accuracy. The elements used were hybrid reduced in order to give better results since we were using a very coarse mesh.

Hyperelastic Behavior:

Both the rubber as well as the nylon rubber composite were assumed to be made of hyperelastic material. Hyperelastic models are used to describe the behavior of materials that exhibit elastic response up to large strains, such as rubber. These materials are described in terms of a "strain energy potential", U, which defines the strain energy stored in the material per unit of volume in the initial configuration as a function of the strain at that point in the material.

Incompressibility assumption:

Most solid rubberlike materials are almost incompressible: their bulk modulus is several orders of magnitude larger than their shear modulus. For applications where the material is not highly confined, the assumption that the material is fully incompressible is a good approximation. Hence in this material model both the nylon rubber composite and rubber are assumed to be incompressible.

In either case the use of "hybrid" (mixed formulation) elements is recommended for this material in all but plane stress cases, because the bulk modulus is usually very large compared to the shear modulus (it is infinite if incompressibility is assumed).

Isotropy assumption:

The initial orientation of the long-chain molecules of rubber is random, hence the material is initially isotropic. As the material is stretched, the molecules orient themselves, giving rise to anisotropy. The same cannot be said of cord reinforced nylon rubber composite plies, as it is initially anisotropic. But due to the balanced layup of the plies it was treated as isotropic. The strain energy potential can be formulated as a function of the strain invariants.

5.2 Material Properties

Isotropic Elastic properties:

Nylon Rubber Composite

Average Young's Modulus = 15.24E02 N/cm^2

Rubber

Average Young's Modulus = 55.16E01 N/cm^2

Hyperelastic properties:

Nylon Rubber composite

$C_{01} = -472.81$

$C_{10} = 732.0$

Rubber

$C_{10} = 850.0$

5.3 Load and Boundary Condtions

5.3.1Coupon Analysis

The rectangular coupon was rigidly fixed on one side and tensile load was applied on the other end at three different strain rates of 0.001 , 0.0005 and 0.01 inch/sec respectively. The load was applied till the failure occurred in each case.

For the finite element analysis, a pressure load of 3.E+6 N/m^2 (435.10 psi) was used as the input load, to compare with the experimental results.

Two types of loading were applied:

1) Concentrated loading

2)Distributed loading

5.3.2 Tire Analysis

The tire was assumed to be rigidly fixed to the wheel taking into account the iron bead which goes through the tire cross section which firmly fixes the tire to the wheel. Hence in the finite element model the nodes which formed part of the fixed end was assumed to have no translation as well rotation.

The part of the tire where it was cut to account for the symmetry about the y-axis, symmetric boundary conditions were applied. The load was assumed to be pressure load acting on the inner surface of the tire. The applied pressure load was about 310 psi.

5.4.1 Analysis

The first step in the finite element analysis was to curve fit the stress-elongation curve of the +/-38 coupons. Since the polynomial form with N=1 is very commonly used for cases

where the nominal strain is not too large, an alternative method of finding the material constants, assuming incompressibility, is to use the uniaxial test data as follows.

The nominal strain in the direction of loading in the uniaxial test is $\epsilon_U = \lambda_U - 1$.

For equibiaxial tests, we have the following relations,

$$\delta U = 2\, T_B\, \delta\, \lambda_B$$

$$T_B = 1/2\, (\partial U/\partial \lambda_B) = 2(\lambda_B - \lambda_B^{-5})\, (\partial U/\partial I_1 + \lambda_B^2\, \partial U/\partial I_2) \quad (5.1)$$

where T_B is the nominal equibiaxial stress.

Expanding the above equation in terms of ϵ_U, using the Mooney-Rivlin form (Equation 5.1),and neglecting terms of higher than second-order in ϵ_U ,gives

$$Tu = 6\, \epsilon_U\, (C_{10} + C_{01} - (C_{10}+2\, C_{01})\, \epsilon_U) \quad (5.2)$$

This is a parabola; the slope of this curve at the origin (effective Young's modulus at zero strain) is $6(C_{10}+C_{01})$: the slope of this curve at the origin (effective Young's modulus at zero strain) is $6(C_{10}+C_{01})$: this slope, together with second-order term $-6\, (C_{10} + 2\, C_{01})\, \epsilon_U^2$, defines the constants C_{10} and C_{01}.

Substituting,

$$6(C_{10} + C_{01}) = A$$

$$-6(C_{10} + 2\, C_{01}) = B, \text{ we obtain}$$

$$Tu = A\epsilon_U + B\, \epsilon_U^2 \quad (5.3)$$

Using the above set of equations to curve fit the data we obtain,

$$C_{01} = -472.81, \qquad C_{10} = 732.0$$

don't use "I" in a formal report

But since I did not have the sress vs strain curve for the rubber, a neo-Hookean formulation was assumed by setting C_{01} equal to zero. The value of C_{10} was set to 850, which is approximately the average value of Young's modulus for rubber.

The analysis was done using ABAQUS. The model was initially assumed to be made of isotropic elastic material, with the rubber and nylon rubber composite having average Young's modulus as given in the materials table above. Then a non linear static analysis of the inflation was performed with a maximum of hundred incrementations. The method being used for the geometric non linearity was Newton Raphson method. But it was found that halfway through the analysis the elements were distorting inside out. Hence the convergence parameters were relaxed slightly to account for the large strains developed. The result proved to be the same as earlier and hence it was decided to model the tire as made of hyperelastic material.

The validity of the above assumption was then verified on the+/-38 coupons, with rigidly fixed boundary conditions on one side of the coupon and pressure load on the other side of the coupon. The type of elements used were four noded quadrilateral elements. The element properties used were hyperelastic, plane stress and reduced integration (CPS4R is the notation used for the particular element in ABAQUS).

Non linear static analysis was then performed with concentrated loading initially and distributed loading later on. In the former case convergence was obtained in six increments and in the latter convergence was obtained in thirty three increments.

The same finite element mesh was used in both the cases. The result proved to be more or less the same.

A linear static analysis was also performed on the same to compare the behavior of two different results.

The method used for the non linear static analysis is the Newton Raphson method in ABAQUS. In some cases it uses an exact implementation of Newton's method, in the sense that the Jacobian of the system is defined exactly, and quadratic convergence is obtained when the estimate of the solution is within the radius of convergence of the algorithm. In other cases the Jacobian is approximated, so that the iterative method is a modified Newton Method. For example, some material and surface interfaces models (such as nonassociated flow plasticity models, or Coulomb friction) create a nonsymmetric Jacobian matrix, but the user may choose to approximate this matrix by its symmetric part.

5.5 Analysis of Tire Cross-Section to determine Contact length and Sidewall Contribution

As mentioned earlier the purpose of analyzing the two dimensional model of the cross-section was to chracterize the spring force effect of the sidewalls resulting from the local deflection. The force-displacement relationship thus obtained will be used in defining the non-linear spring in the ring model. The total force-displacement curve is obtained and is shown in figure 5.2.

The analysis was performed in three steps. The ground was given a rigid body displacement by means of the rigid surface node. The different steps involved in the analysis were:

1) First the internal pressure load and boundary conditions were applied, namely:

a) The tire sidewall is assumed to be rigidly fixed to the wheel taking into account the iron bead which passes through the cross-section. Hence, in the finite element model the nodes labelled "0" (see figure 6.1.1 - 6.1.4) which form the fixed end of the sidewall are assumed to be rigidly fixed i.e. $U_i=0$ and $R_i=0$, i=1,2. Where U_i and R_i are the displacements and the rotations with reference to the reference rectangular coordinate system.

b. Due to bilateral symmetry of the tire cross-section only half of it is analyzed. Therefore we assume symmetric boundary condition for the nodes, labelled 0x (see figure 6.1.1) lying on the line of the symmetry, i.e. $U_i = 0$, i=2,3.

c. The load was assumed to be pressure load acting on the inner surface of the tire. The applied pressure was 150 N/ cm^2.

2. The second step the rigid surface node was given a translation in the horizontal direction till the ground came into contact ith the tire, the boundary conditions remaining still active from the first step.

3. The third step, the rigid surface node was given different displacements by activating a degree of freedom in the horizontal direction, boundary conditions remaining still active from the first step.

The analysis was conducted under the assumption that the cross-sections remain lane during deflection and deformation, and requires that the cross-sections be analyzed as an axisymmteric cross-section. The finite-element model of the tire was made of CAX4RH elements(4 noded axisymmetric reduced hybrid integration elements). The possible contact region was paved with IRS21A elements(one dimensional rigid surface elements). A rigid reference node was created to impart necessary ground displacement conditions. The ground was modeled by one dimensional rigid bar elements. Utilization of axisymmteric cross-section is equivalent to treatment of the ground contact as occuring from the effect of progressively shrinking a right circular cylinder with axis held parallel to the tire axis down around the tread of the tire. This will produce an upper bound to the resistance of the tire cross-section to deflection and deformation. The figure 6.2.1 shows a typical cross-section under inflation.

5.5.1 Ground Contact Analysis

At the interface between the tire and the roadway an element of the tire surface area is acted upon by a force vector which can be expressed as two components, one perpendicular to the contact surface, called the normal component, and one tangential to the contact surface. This latter component may be further decomposed into two components, each lying in the contact plane, but one parallel to the central plane of the tire and the other perpendicular to it. These components in the contact plane are commonly called as the shear components. In this particular analysis attention is directed first to the normal pressure distribution components caused by contact of the tire with some other surface.

As a basic primary concept one might state that

$$p = p_0 + f(\text{Tire structural characteristics, tire side forces, tire driving or braking, torque, tire velocity, etc.}) \qquad (5.4)$$

where 'p' is the vertical presssure component at any point, p_0 is the inflation pressure of the tire and 'f' is some general functional relationship which insofar as is now known is extremely complicated, and can be best described in a qualitative sense.

5.5.2 Definition of a Non-Linear Spring to Model Sidewall Elasticity for Use in Tread Band Models of the Tire

The non-linear spring defined above includes the resistance to deflection from internal pressure, the sidewall and the tread band.The tread band width is defined to be the maximum contact length obtained, when the cross-section is subjected to 34 percent ground deflection. This assumption is justified by Figure 6.2.13 where it is seen that the contact length remains firmly constant beyond a sidewall deflection of 30% and so bounds the tread band width. The tread band was assumed to posess constant thickness equal to thickness of the unloaded cross-section at the crown.

This model was used to get the total forces normal to the plane of the cross-section which includes the tire axis, and also the forces normal to the plane which bisects the tread and is perpendicular to the tire axis. These forces represent respectively the total radial force and axial force acting over the thickness of the tread. In order to determine the sidewall force which is nothing but the spring force in the ring model, we must subtract from the total ground contact force for a given deflection the radial force, the radial component of the internal pressure force.

The total ground contact pressure force needed is obtaind by integrating the contact pressure over the contact length. The internal pressure force is computed to be the internal pressure multiplied by the inner radius of the tire for a particular value of ground deflection by the maximum contact length i.e. the tread band width.

The radial force is taken to be the force normal to cross-section computed over the tread thickness along a radial line perpendicular to the tire axis and intersecting the crown corresponding to a particular value of ground deflection. Tread width is again the maximum contact length.

Symbolically, the recipes for these forces may be expressed as follows: The forces in order of appearance are the ground contact force per radian 'P_i (d)', the radial pressure force 'F_p(d)', the radial force acting on the edges of the tread band parallel to the tread axis 'F_r(d)', and axial orce over the ends of the tread band model per radian of circumferential wedge element 'F_z(d)'. With reference to the figure(3.2) 'd' is the ground deflection, 'p' is the tire pressure,'s' is the width of the tread band, 'r_o(d)' and 'r_i(d)' are the outer and inner radius, 'ϕ' is the circumferential angle, 'θ' represents the direction normal to a plane through the axis, 'z' is the axial direction, 'p_g(d)' is the pressure distribution over the contact length 'l(d)'.

$$Pi = P(d) = {}_0\int^{l(d)} p_g(d)\, dl \qquad (5.5)$$

$$F_p(d) = - p r_i(d)\, s\, d\phi \qquad (5.6)$$

$$F_R(d) = s\, d\phi\, {}_{ri(d)}\int^{ro(d)} f_\theta(r,d)\, dr \qquad (5.7)$$

$$F_z(d) = d\phi\, {}_{ri(d)}\int^{ro(d)} f_z(r,d)\, dr \qquad (5.8)$$

The various forces ~~talked about~~ above are in terms of force per unit radians. The maximum contact length is taken to be the contact length at a deflection equal to 34 percent of the wheel to crown height. The various forces are plotted as function of percentage of crown to wheel height ground deflection and is seen in the figure(3.4). The ground contact pressure distributions corresponding to these sections are also shown in the figure(3.5) for varying ground deflection. The above equations were derived making use of the formulations given in [45].

5.6 The Tread-Band on Non-Linear Foundation Representing the Tire Sidewall Model of the Tire

The tread band or the ring finite-element model of the tire incorporating the non-linear spring forces due to the sidewalls is shown in figure 5.3. This figure also depicts the ring model in the state of inflation. Note that the springs determined previously are connected within the tread band model by pin-joints to the points on the inner radius of the tread as well as on the hub of the wheel. These springs may therefore are free to rotate, but must remain straight and therefore deform along their instantaneous lengths.

From figure 6.2.4 we infer that the relative importance of sidewall compared with the tread-band with respect to their resistance to deflection is about equal and thus deserving to be accounted for in the ring model. This also shows that the axisymmetric model is stiff as assumed earlier.

The finite-element ring model was made up of CPE4RH (4 noded plane strain reduced hybrid integration elements) elements to model the rubber and carcus part of the tire. The sidewall was modeled making use of SPRINGA elements. The expected contact region

was paved with IRS21 elements. The elements were assumed to be under plane strain condition.

5.7 Load and Displacement Boundary Conditions

1. As mentioned above the nodes at locations correspoding to spring attachments to the hub are assumed to be pin joints such that, i.e. $U_i = 0$ for i=1,2 . Where U_i represents the displacements and rotations with reference to the cylindrical coordinate system.
2. The nodes at locations corresponding to spring attachments to the tread are free to move in radial and tangential direction and also free to rotate in the plane of the cross-section.
3. The pressure load is the same as for the cross-section and is assumed to be acting normal to the inner edges of the tread.

The above ring model is then subjected to a particular single maximum, value of ground deflection in a similar maximum to that applied to the cross-section, and the corresponding contact length and the ground contact pressure distribution is then obtained. The corresponding pressure distribution in the rolling direction integrated across the width of the tread is shown in figure 6.2.6 for various values of sidewall deflection . The figure 6.2.7 depicts the inflated ring model and the deformation of the ring tread band model due to ground contact in 6.2.8.

5.8 Determination of Shape and Pressure Distribution Over the Ground Contact Patch

From the plane symmetric deflection analyses of the meridional tire cross-sections under ground contact conditions we had previously obtained the lateral pressure distribution and lateral extent of the contact zone as well as the sidewall forces for

a practical range of sidewall deflections. For later use we create a set of normalized pressure distributions from the computed ones. The full two dimensional shape of the contact patch and the distribution of normal pressures within it however are not defined until after the tread-band ring-on-foundation model of the tire has been exercized and analyzed to determine the extent of the contact patch measured along the tread centerline and the distribution of the net ground contact force over the local patch width as it varies along the tread centerline in the rolling direction corresponding to a given maximum value of sidewall deflection. To determine the local contact patch width and lateral distribution pressure at each point of the tread centerline, we interrogate the nodes at the extremities of the distributed springs which represent the resistance to deflection of the tire sidewalls in order to compute their change in length. If the data do not already exist , we then compute the ground contact lengths and normalized pressure distributions for the cross-section corresponding to these deflections. The local lateral width of the contact patch is taken to equal the ground contact lengths of the cross-sections. The true lateral pressure distribution in a direction perpendicular to the tread centerline is taken to be the local normalized lateral pressure distribution multiplied by the local net force at the particular point along the tread fore-aft centerline as determined from the tread band on foundation model of the tire. Figures 6.2.9 and 6.2.10 show the shape of the contact patch corresponding respectively to 20 and 34 percent sidewall deflections. For these same values of sidewall deflections, Figures 6.2.11 and

6.2.12 show the distributions of ground normal pressure distributions over the contact patch.

CHAPTER 6

RESULTS

6.1 Coupon Analysis

The results show that convergence is approached much easier if concentrated load is applied instead of pressure load.

1) Non linear static analysis:

Distributed load = 3.E+6 N/m^2

Deflection = 10.71 mm

Concentrated load = 270 N

Deflection = 9.71 mm

2)Experimental result:

Load applied = 3.E+6 N/m^2

Deflection = 10mm (approximately)

Error using concentrated load = 2.9% (approximately)

Error using distributed load = 7.1% (approximately)

Figure 6.1 shows the stress vs elongation of the (+38/-38)S coupons with different strain rates. The results show that a non linear analysis performed with concentrated load produces much better accuracy than the one done using distributed load.

We can also note that as the distributed load increases the end point deflection of the particular node being monitored decreases and then increases again.

6.2 Tire Analysis (Inflation)

We have two different results in the case of tire analysis. The first one is performed using hybrid reduced integration elements (CAX4RH) and the second one is performed using hybrid incompatible elements (CAX4IH).

1) Axisymmetric Hybrid Reduced Integration Elements (CAX4RH):

The following results are obtained from the analysis:

Pressure ?

Load applied = 206.9 N/sq.cm

Node at which maximum deflection occurs in the x-direction = 56

Maximum deflection in the x-axis direction = 1.678 cm

Node at which maximum deflection occurs in the y-direction = 6

Maximum deflection in the y-axis direction = 5.186 cm

Maximum stress in the x-axis direction = 1679.0 N/sq.cm

Maximum stress in the y-axis direction = 2869.0 N/sq.cm

Maximum stress in the z-direction = 1602.0 N/sq.cm

Maximum stress in the xy direction = 1089.0 N/sq.cm

Maximum strain in the x-axis direction = 0.1279

Maximum strain in the y-axis direction = 0.3763

Maximum strain in the z-axis direction = 0.2068

Maximum strain in the xy direction = 0.6266

2) Axisymmetric Incompatible Hybrid Elements (CAX4IH):

The following results are obtained from the analysis:

Load applied = 206.9 N/sq.cm

Node at which maximum deflection occurs in the x-direction = 56

Maximum deflection in the x-axis direction = 1.192 cm

Node at which maximum deflection occurs in the y-direction = 1

Maximum deflection in the y-axis direction = 4.619 cm

Maximum stress in the x-axis direction = 1823.0 N/sq.cm

Maximum stress in the y-axis direction = 2875.0 N/sq.cm

Maximum stress in the z-axis direction = 2108.0 N/sq.cm

Maximum stress in the xy direction = 1153.0 N/sq.cm

Maximum strain in the x-axis direction = 0.2664

Maximum strain in the y-axis direction =0.3849

Maximum strain in the z-axis direction = 0.1976

Maximum strain in the xy direction = 0.6323

From the results we can see that the maximum deflection both in the horizontal and vertical directions are more in the case of axisymmetric hybrid reduced integration elements than with axisymmetric incompatible hybrid elements. But the maximum stresses in the x, y, z and xy directions are more in the case of latter than former. From the experimental curves we can note that the results obtained analytically by applying concentrated load gives more accurate results.

6.3 Ground Contact Analysis

The various results obtained from the above 2-dimensional analysis are discussed below. The various ground pressure distributions over the contact length were plotted and are shown in figure 6.2.5. It is clear from the figure that the double peaking of the pressure occurs at 30 percent deflection which signifies the initiation of bifurcation. It is also clear from the figure 6.2.5 that the pressure over the contact length is fairly uniform and equal to the internal pressure at small ground deflections. But as the deflection is progressively

increased the contact length increases and the pressure tends to concentrate towards the edges. The variation of ground contact length with sidewall deflection is shown in figure6.2.13. The beginning of a plateau at 30 percent deflection marks the beginning of bifurcation. The bifurcation is also seen in figure 6.2.6 for 50 percent sidewall deflection. Another interesting feature which is conspicuous in this figure is the decrease in the fore-aft contact length at bifurcation which is easily explained by the fact that as the tread deflects inwards it pulls the sidewalls together.

Figure 6.2.14 and figure 6.2.15 show us the contact pressure distribution variation with fore-aft distance from midpoint of contact patch centerline for 20 percent and 34 percent sidewall deflections. It is seen that the pressure is uniformly distributed over the contact length for 20 percent case with no double peaking of the presssure.

The contact patch for 20 percent and 34 percent sidewall deflections were obtained and are shown in figure 6.2.9 and figure 6.2.10 respectively. The 3-D pressure distribution over the contact patch were obtained and are shown in figure 6.2.11 and figure 6.2.12 for 20 and 3 percent cases respectively. From these plots the pressure is clearly seen to peak at the edges of the foot-print.

CHAPTER 7

CONCLUSIONS

7.0 Conclusions

7.1 Coupon Analysis

We can conclude from the coupon analysis that the value of the Mooney-Rivlin constants calculated from the stress vs elongation curve of the nylon rubber composite was quite accurate in modelling the behavior of the hyperelastic material at moderate strains.

7.2 Tire Analysis (Inflation)

Based on the fact that value of the hyperelastic material constant for rubber used in the analysis is approximate due to the lack of experimental data, we can conclude that the value of stresses and displacements obtained are approximate.

The result obtained is approximate also due to the fact that in the coupon analysis only one mode of deformation is excited, whereas in the tire model more than one mode of deformation is excited. Hence to model the tire accurately more tests have to be conducted inorder to evaluate the hyperelastic material constants.

The tests to be conducted are :

1) Biaxial test:

This is achieved by stretching a square sheet in a biaxial testing machine. The state can also be obtained by inflation of a circular membrane into a spheroidal shape (like blowing a balloon). The stress field in the middle of the membrane then closely approximates

equibiaxial tension, provided the thickness of the membrane is very much smaller than the radius of curvature at this point.

2)Planar test:

The experiment is usually done with a thin, short and wide rectangular strip of material fixed on its wide edges to rigid loading clamps which are moved apart.

3)Volumetric test:

If it is necessary to allow some compressibility in the material model, the bulk modulus must also be determined. An approximate way of conducting a volumetric test consists of using a cylindrical rubber specimen which fits snugly inside a rigid container and whose top surface is compressed by a rigid piston. In this test we make use of the fact that the bulk modulus is much higher than the shear modulus.

7.3 Ground Contact Analysis

The following conclusions were drawn from the above work:

1. Demonstrated a low cost extension of the tire tread band ring model to handle non-linear features of ground contact by employing two 2-D models.
2. Elucidated features of the tire ground contact load bifurcation phenomenon.
3. Elucidated the significance of the 30 percent sidewall deflection limitation rule for tire operation.
4. The obtained results were compared with the experimental studies carried out by the Materials Command at WPAFB and was found that the results were qualitatively comparable.

CHAPTER 8

REFERENCES

8.0 References

[1]Walker, Richard, ed., Materials and Compounding Ingredients for Rubber and Plastics (Rubber World, New York, N.Y. 1965).

[2]Brown,R.J., et al., Rubber World 145(2), 70(1961); Rubber Chem. Tech. 3592), 546(1962).

[3]Sarbach,D.V.,Hallman,R.W., and Cavicchia,M.A., Rubber Age 98(11), 67(1966).

[4]Alliger,G., and Sjothun,I.J.,eds., Vulcanization of Elastomers (Reinhold Publishing Corp., New York, N.Y., 1964).

[5]1967 Annual Book of ASTM Standards, Part 28. Method D412-66, Tensile testing of vulcanized rubber, p.200.

[6]Gehman,S.D., Chem. Revs. 26(2), 203(1940).

[7]Mandelkern,L., Crystallization of Polymers (McGraw-Hill Book Co., New York, N.Y., 1964).

[8] Mullins,I., and Tobin,N.R., Trans, Inst. Rubber Ind. 33(1),2 (1957): Rubber Chem, Tech. 31, 505 (1958).

[9] 1967 Annual Book of ASTM Standards, Part 28. Method D454-53, D572-67, D573-53, D865-62.

[10]Barnhart,R.R., and Newby,T.H., Antioxidants and antiozonants, chap. 6, p. 130, Introduction to Rubber Technology, Morton, M., ed., p.172 (Reinhold Publishing Corp., New York, N.Y., 1959).

[11]Buist, J.M., Aging and Weathering of Rubber (W. Heffer & Sons, Cambridge, England, 1956).

[12]Shelton,J.R., Rubber Chem. Tech. 30(5), 1251(1957).

[13]Norling,P.M., Lee,T.C.P., and Tobolsky,A.V., Rubber Chem. Tech. 38(5), 1198(1965).

[14] 1967 Annual Book of ASTM Standards, Part 28. Method D624-54, Tear resistance of vulcanized rubber,p.342.

[15]Kainradl,P., and Handler,F., Kautschuk Gummi 12, 239 (1959); Rubber Chem. Tech. 33, 1438(1960).

[16]Gehman,S.D., Mechanism of tearing and abrasion of reinforced elastomers, chap 2, Reinforcement of Elastomers, G.Kraus, ed., p.23 (Interscience Publishers, Inc., New York, N.Y., 1965).

[17] 1967 Annual Book of ASTM Standards, Part 28. Method D2240-64-T, Indentation hardness of vulcanized natural and synthetic rubbers, p.642.

[18]Payne,A.R., and Scott, J.R., Engineering Design with Rubber, p.122 (Interscience Publishers, New York, N.Y., 1960).

[19] Waters,N.E., Brit. J. Appl. Phys. 16, 557 & 1387 (1965); J. Inst. Rubber Ind. 1(1), 51(1967).

[20]Coddington, D.M., Marsh, W.D., and Hodges, H.C., Rubber Chem. Tech, 38(4), 741(1965).

[21] 1967 Annual Book of ASTM Standards, Part 28. Method D1054-66. Impact resilience and penetration of rubber by the rebound pendulum, p. 509.

[22] 1967 Annual Book of ASTM Standards, Part 28. Method D945-59, Mechanical properties of elastomeric vulcanizates under compressive or shear strains by the mechanical oscillograph.

[23]Gehman,S.D., Rubber Chem. Tech. 30(5), 1202 (1957).

[24] 1967 Annual Book of ASTM Standards, Part 28. Method D2231-66, Forced vibration testing of vulcanizates, p. 1003.

[25]Meyer, K.H., and Ferri,C., Helv. Chim. Acta 18, 570(1935).

[26] Anthony, R.I., Caston,R.H., and Guth,E..,J.Phys. Chem. 46, 826(1942).

[27]Wood.L.A., and Roth,F.L.,J.Appl.Phys. 15, 781(1944).

[28] Gee,G., Trans. Faraday Soc. 42, 585 (1946).

[29] Treolar,L.R.G., The Physics of Rubber Elasticity, second edition (Oxford University Press, 1958).

[30] Krigbaurn, W.R., and Roe,R.J., Rubber Chem. Tech. 38, 1039 (1965).

[31] Mooney, M., J.Appl. Phys. 11, 582 (1940).

[32] Rivlin, R.S., Chap. 10, vol. 1, Rheology: Theory and Application (5 vols.), F.R. Eirich, ed., p.351 (Academic Press, New York, N.Y., 1956).

[33] Varga, O.H., Stress-Strain Behavior of Elastic Materials; Selected Problems of Large Deformations (Interscience Publishers, New York, N.Y., 1956).

[34] Rivlin,R.S., Phil. Trans. Ry. Soc. (london) A241, 379(1948).

[35] Blatz, P.J., Rubber Chem. Tech. 36(5), 1450(1963).

[36] Rivlin,R.S., Plane strain of a net formed by inextensible cords, J. Ratl. Mech. Anal. 4, 951 (1955).

[37] Rivlin, R. S., Networks of inextensible cords, Nonlinear Problems of Engineering, W.F. Ames, ed. (Academic Press, New York, 1964).

[38] Genensky,S.M., and Rivlin, R.S., Infinitesimal plane strain in a network of elastic cords, Arch. Ratl. Mech. Anal. 4, 30-34 (1959).

[39] Adkins, J.E., Large elastic deformations, Progress in Solid Mechanics, Vol. II, I. N. Sneddon and R. Hill, eds. (North Holland Publishing Co., Amsterdam, 1961).

[40] Adkins,J.E., Cylidrically symmetrical deformations of incompressible elastic materials reinforced with inextensible cords, J. Ratl. Mech. Anal. 5, 189 (1956).

[41] Adkins, J.E., Finite deformation of materials exhibiting curvilinear aeolotropy, Proc. Roy. Soc. A229, 119 (1955).

[42] Adkins, J.E., Finite plane deformation in thin elastic sheets reinforced with inextensible cords, Phil. Trans. Roy. Soc. (London) A249, 125 (1956).

[43] Adkins, J.E., and Rivlin, R.S., Large elastic deformations of isotropic materials, X: reinforcement by inextensible cords, Phil. Trans. Roy. Soc. (London) A248, 201 (1955).

[44] Clark, S.K., and Dodge, R.N., A comparison of net and continuum theory for cord reinforced laminates, Textiles Res. J. 38(9), 931 (Sept. 1968).

[45] Timoshenko, Theory of Plates and Shells.

and consistent
Use standard ref-tech. for all references

LIST OF FIGURES:

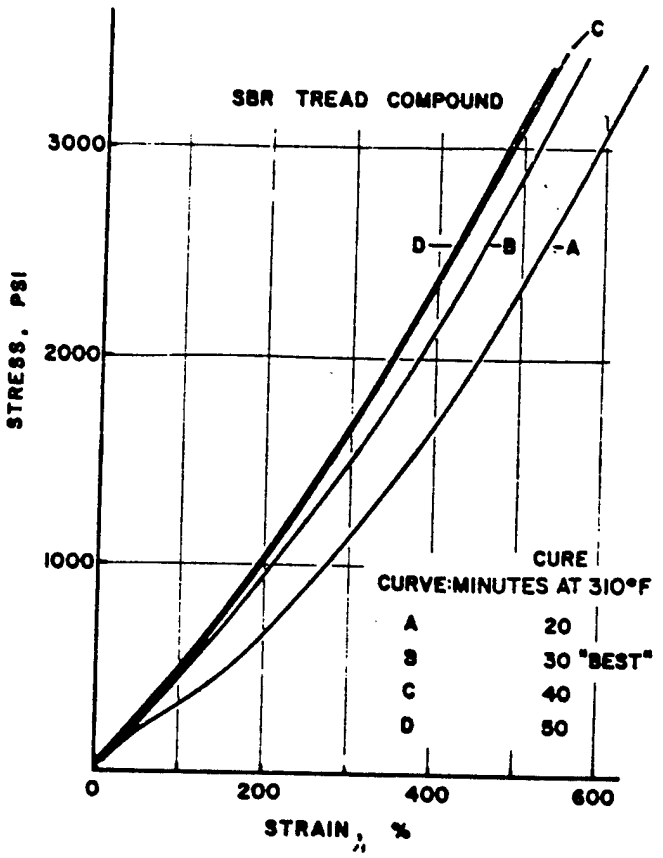

Figure 2.1 Variation of stress-strain curves with cure.

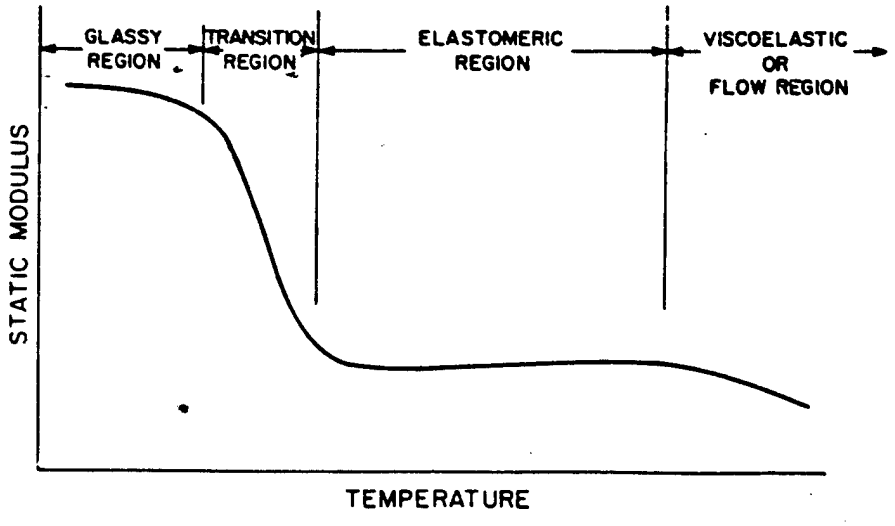

Figure 2.2 General variation of rubber modulus with temperature.

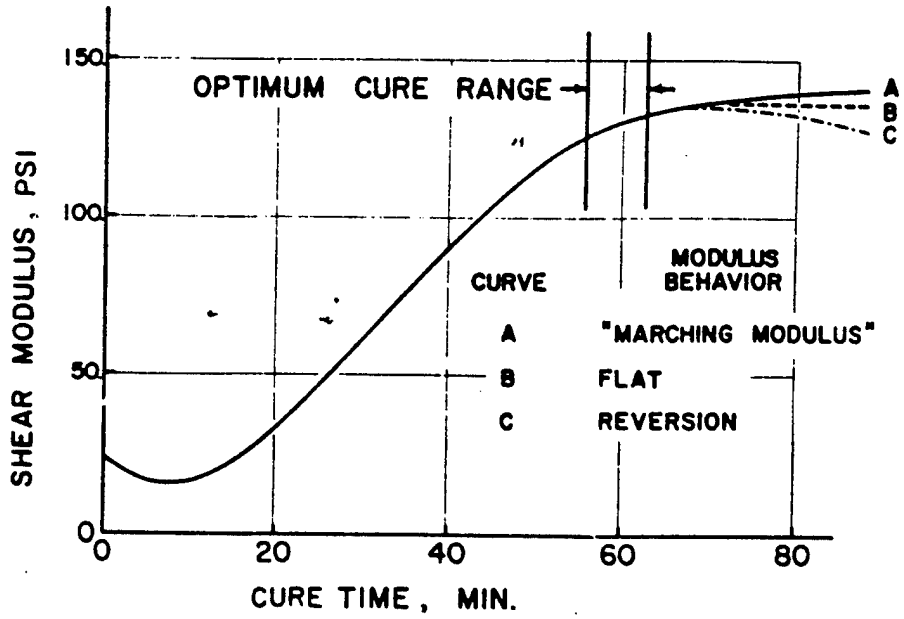

Figure 2.3 Diagram of continuous cure curves.

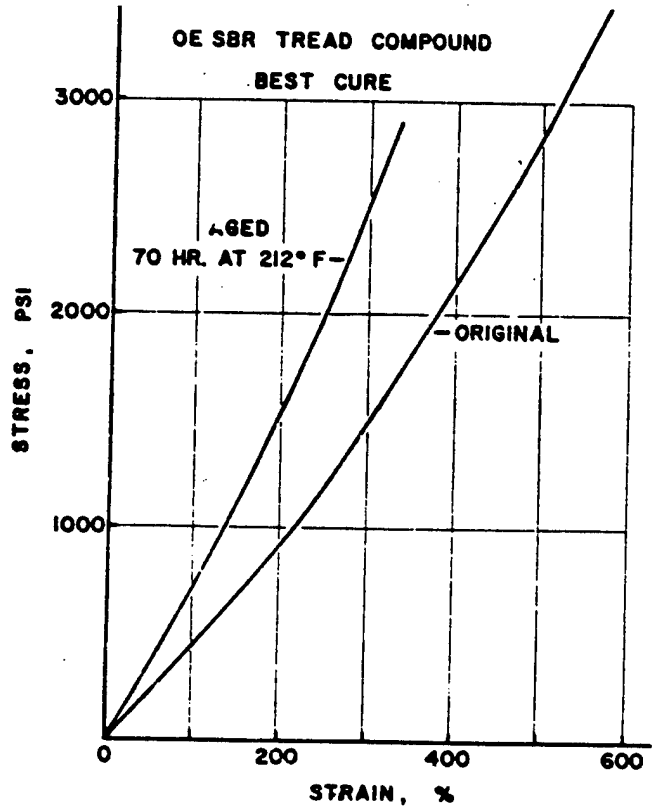

Figure 2.4 Effect of air-oven aging on stress-strain curve of the rubber compound of figure1.1.

I couldn't find Fig 1.1.

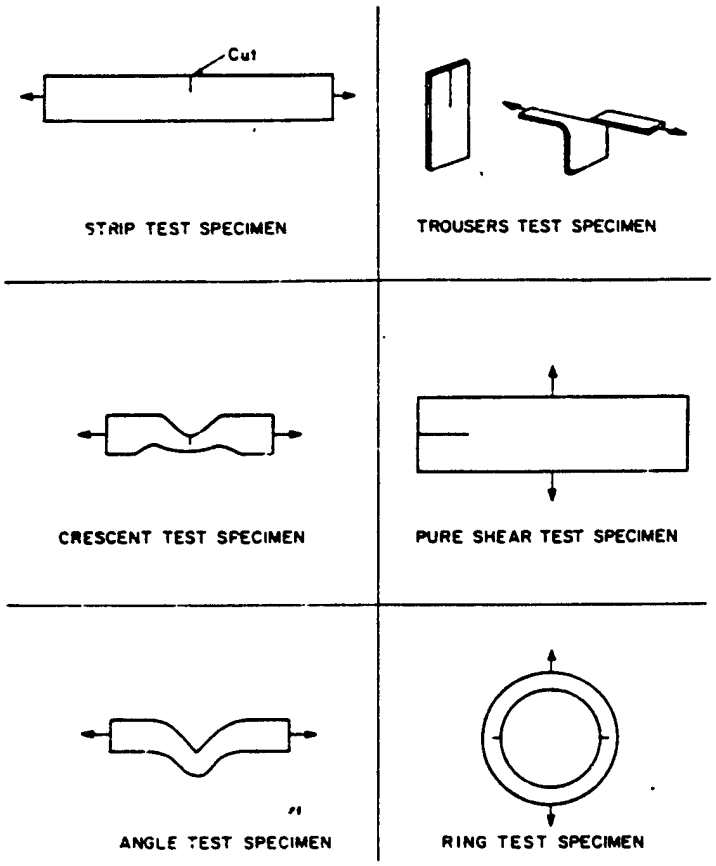

Figure 2.5 Tear test specimens.

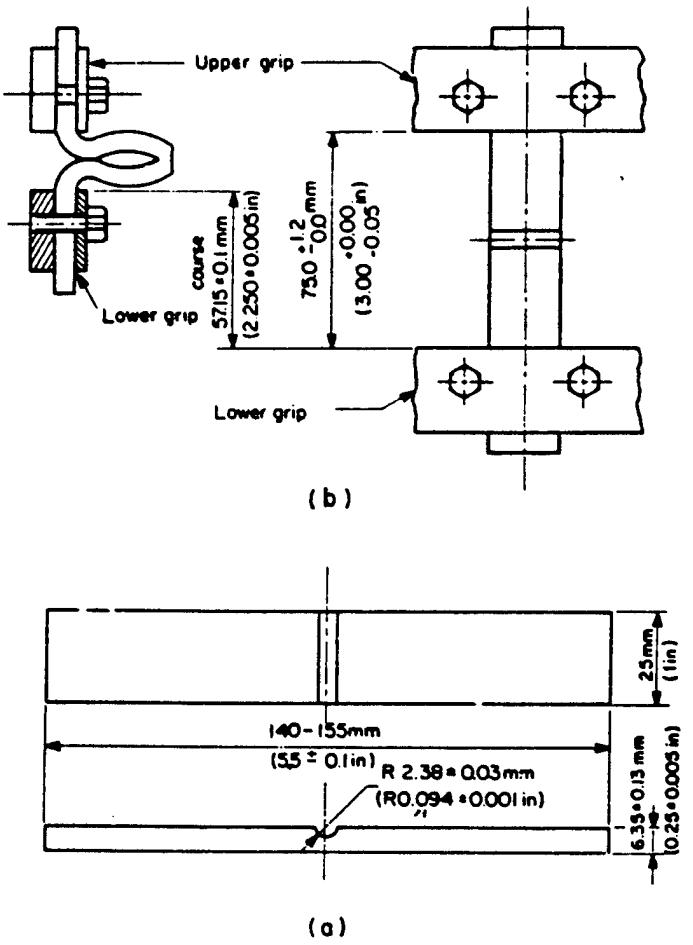

Figure 2.6 (a) De Mattia testpiece (b) Mounting of De Mattia testpiece.

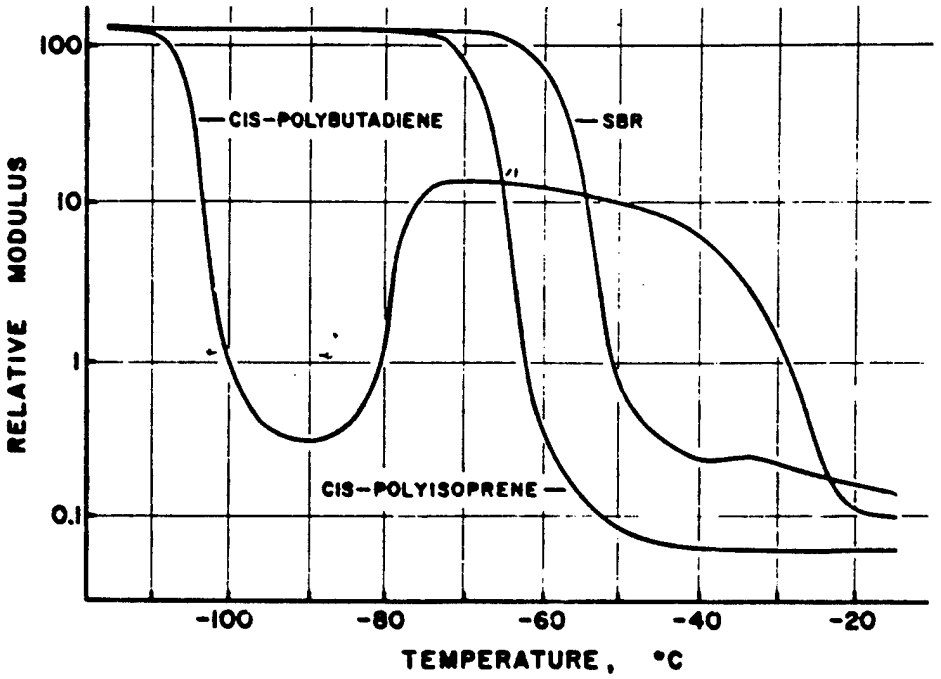

Figure 2.7 Effect of low temperatures on rubber moduls; data by ASTM method 1053-65.

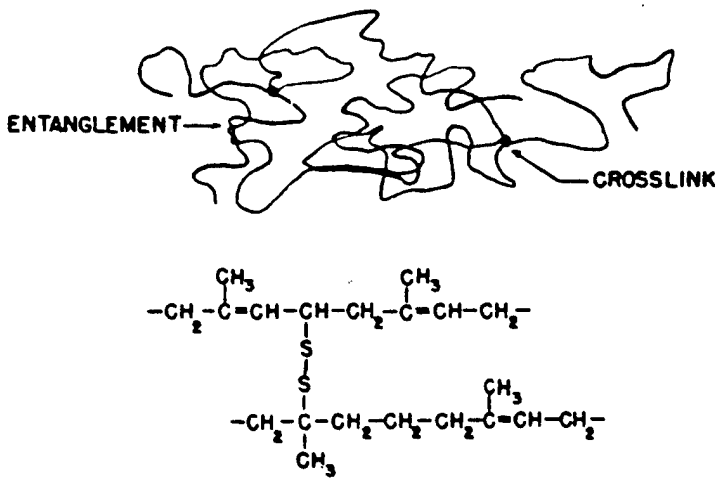

Figure 2.8 Diagram to illustrate concept of molecular structure of rubber.

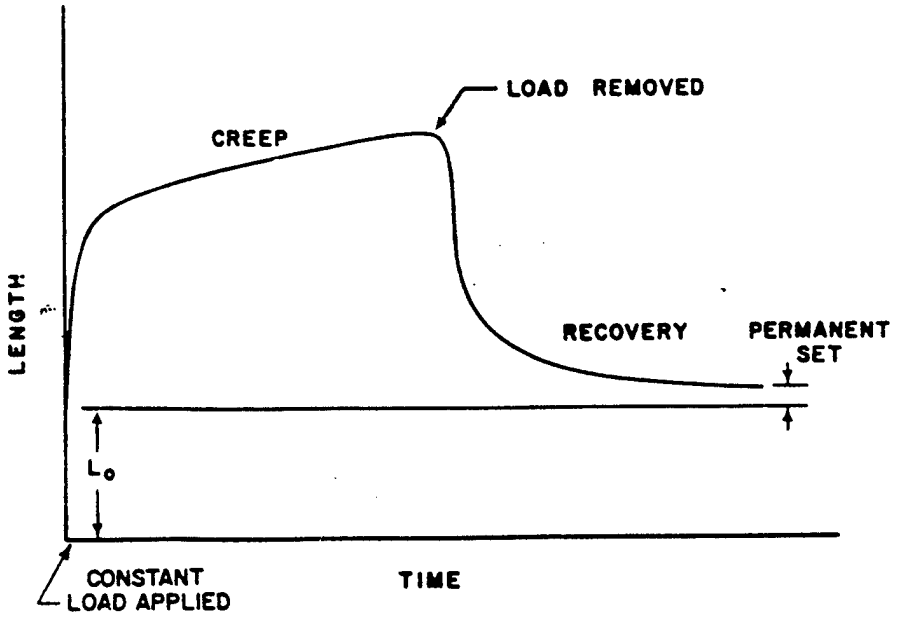

Figure 2.9 Typical deformation in creep, recovery, and permanent set.

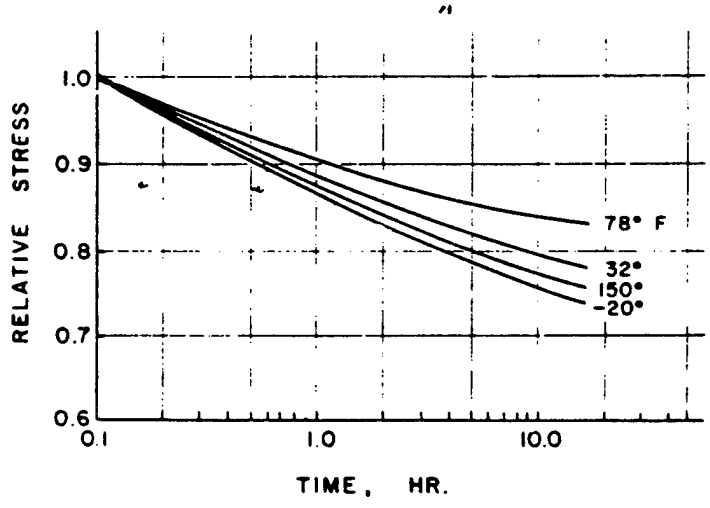

Figure 2.10 Compressive stress relaxation for an SBR tread compund under 30% compression.

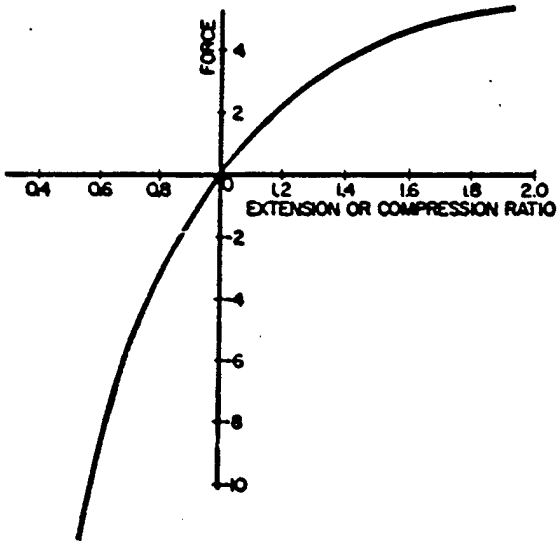

Figure 2.11 Force-extension ratio for a typical rubber.

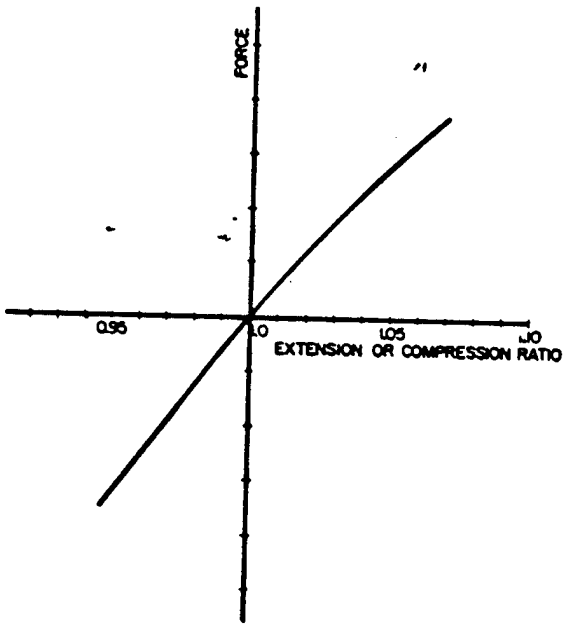

Figure 2.12 Region near origin of force-extension ratio curve for rubber.

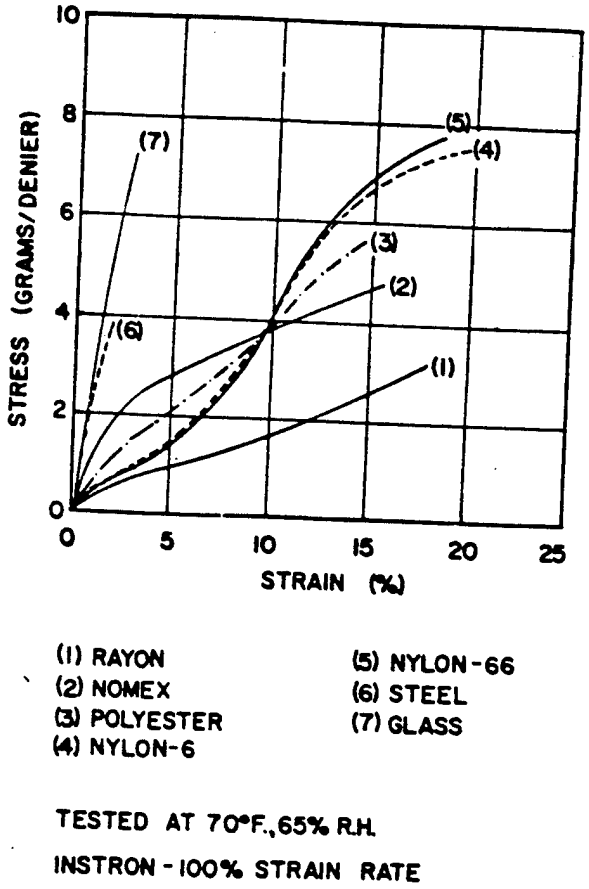

Figure 2.13 Stress-strain characteristics of typical tire cords.

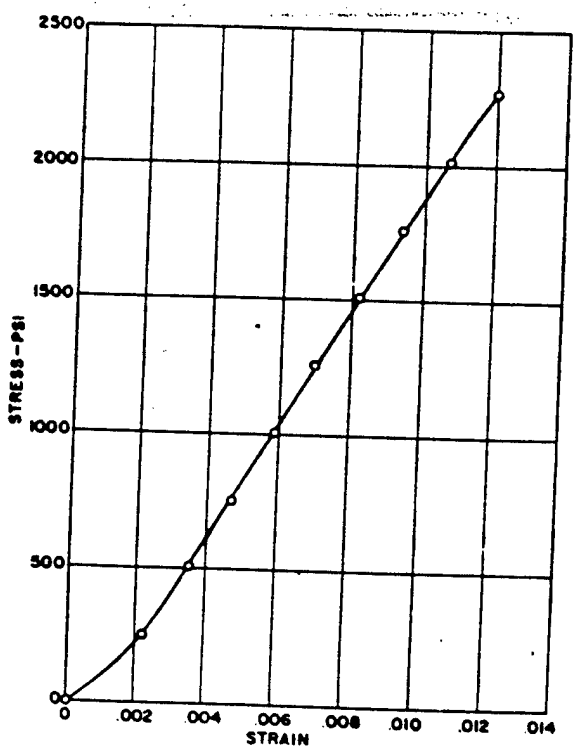

Figure 2.14 Stress-strain curve in tension of rayon cords embedded in rubber, where stress is based on total cross-section area of specimen.

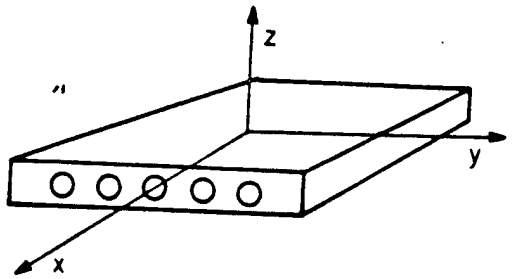

Figure 2.15 End view of a series of parallel textile cords embedded in rubber.

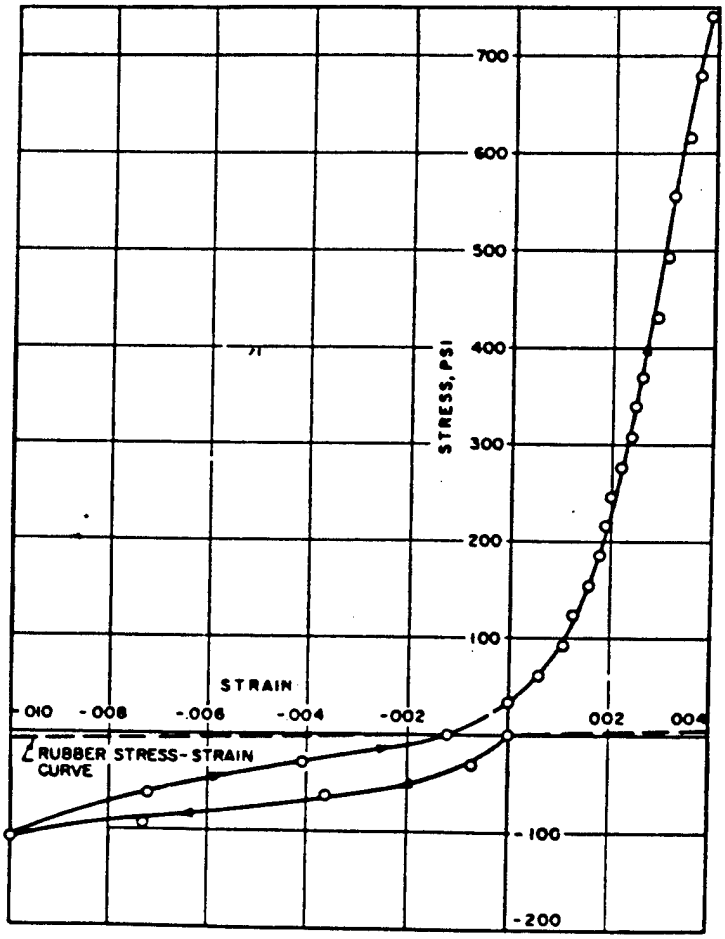

Figure 2.16 Continuous stress-strain curve through compression and into tension for rayon cords embedded in rubber.

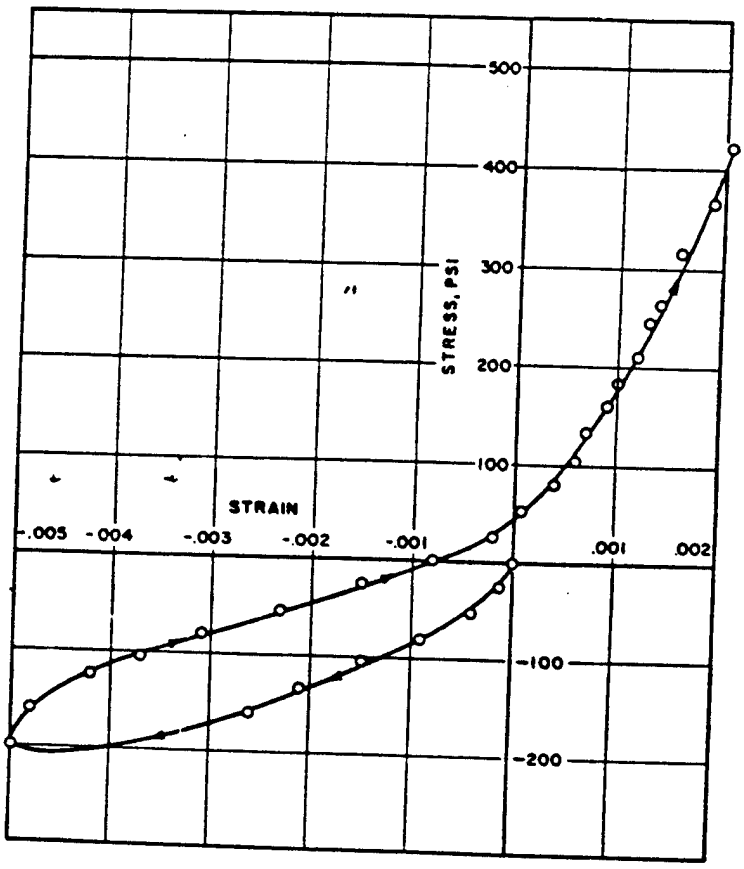

Figure 2.17 Continuous stress-strain curve through compression and into tension for nylon cords embedded in rubber.

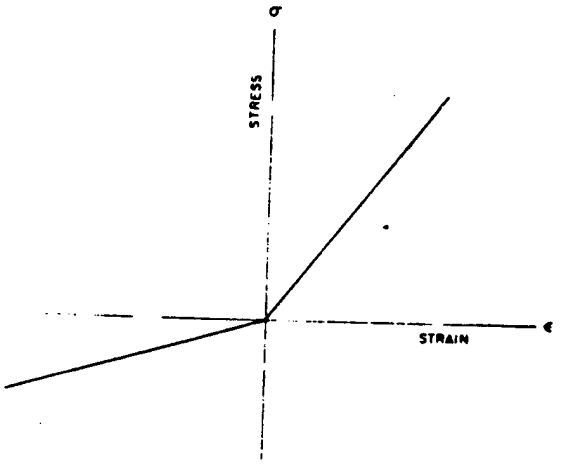

Figure 2.18 Idealized bilinear stress-strain curve.

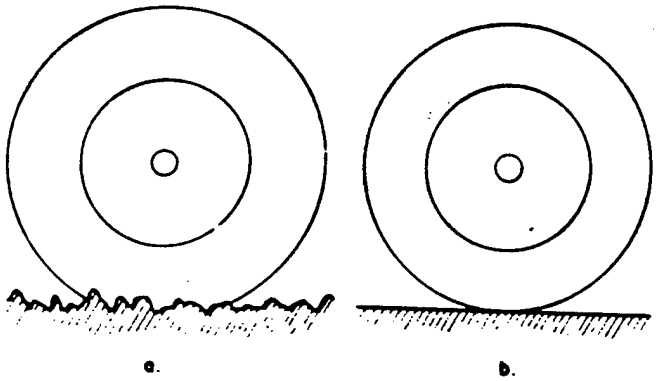

Figure 2.19 Conflicting requirements which a tire has to meet.

(a) ability to absorb surface irregularities - this requires flexibility.

(b) constant axle height and effective rolling radius on smooth roads - this requires uniformity, and is most easily obtained with a rigid wheel.

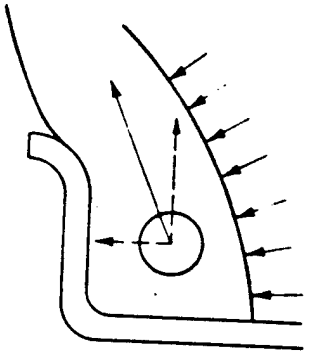

Figure 2.20 Forces pressing bead against rim flange on the wheel to obtain driving and braking reactions.

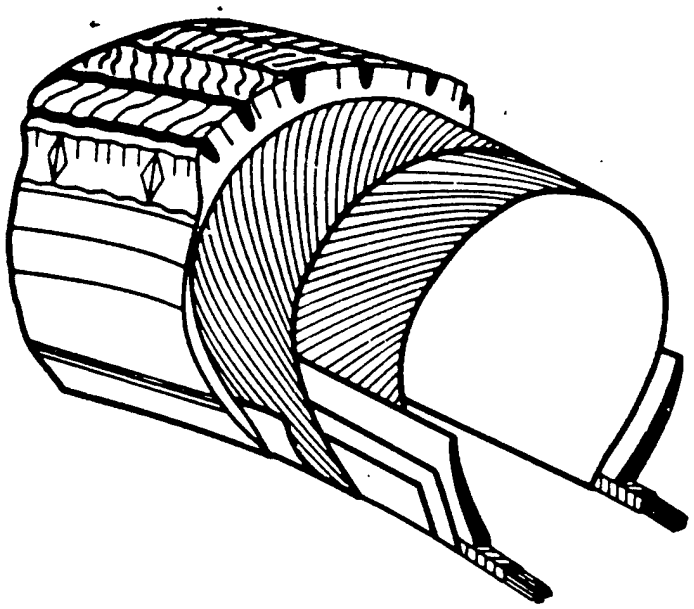

Figure 2.21 Conventional cross-bias tire.

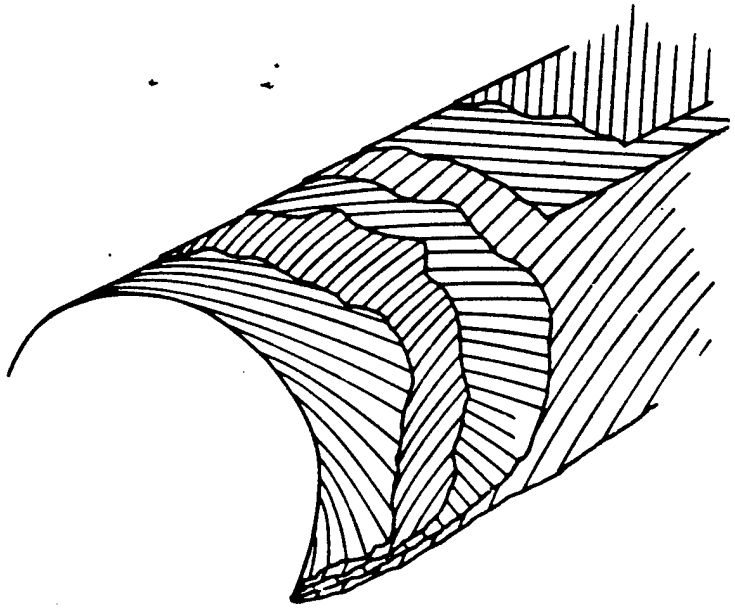

Figure 2.22 Breaker layers in conventional cross-bias tire.

I didn't see any reference to many of these figures.

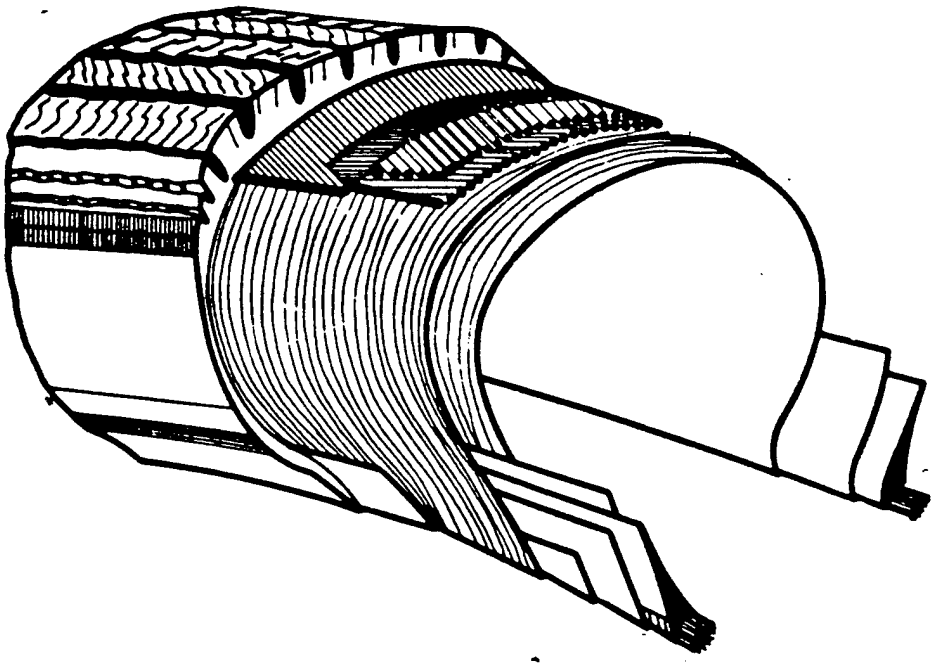

Figure 2.23 Radial ply rigid breaker tire.

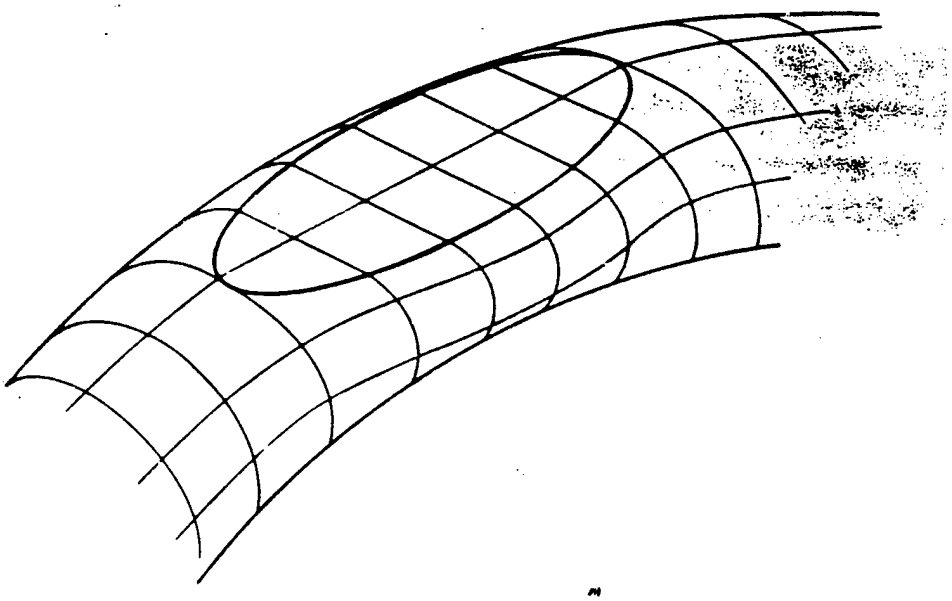

Figure 2.24 Perspective sketch of toroidal shell contact.

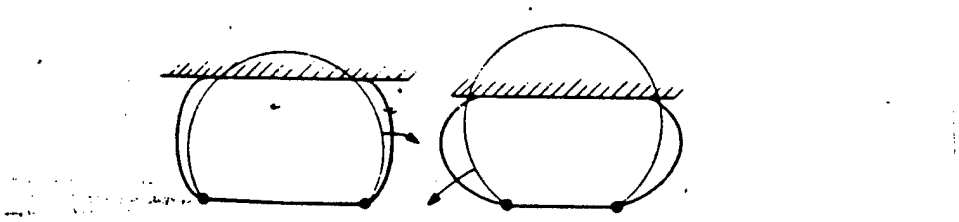

Figure 2.25 Cross-sections of figure 2.24 showing deflections of sidewalls which reduce the tension component radially outward at the inner cylinder edge.

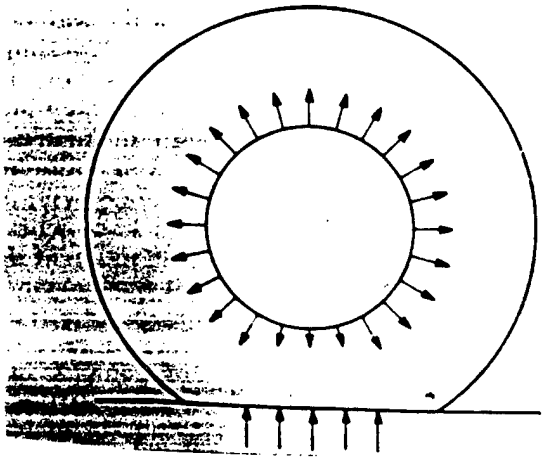

Figure 2.26 Polar plot of radially outward component of wall tension of membrane toroid on inner cylinder.

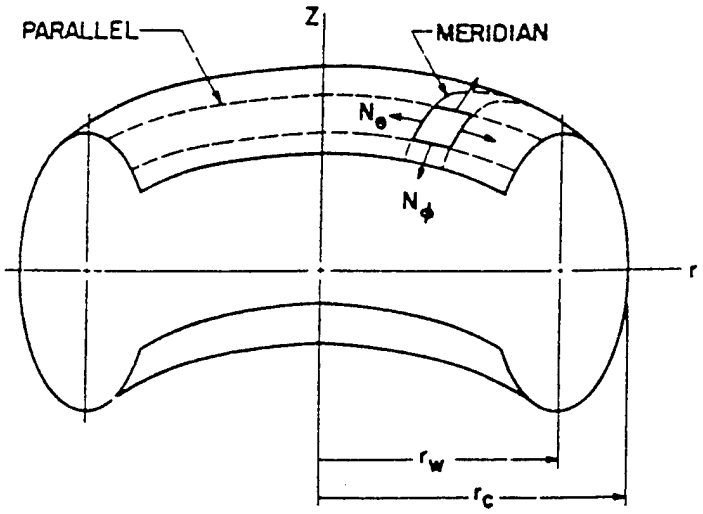

Figure 3.1 Portion of a pressurized toriodal shell.

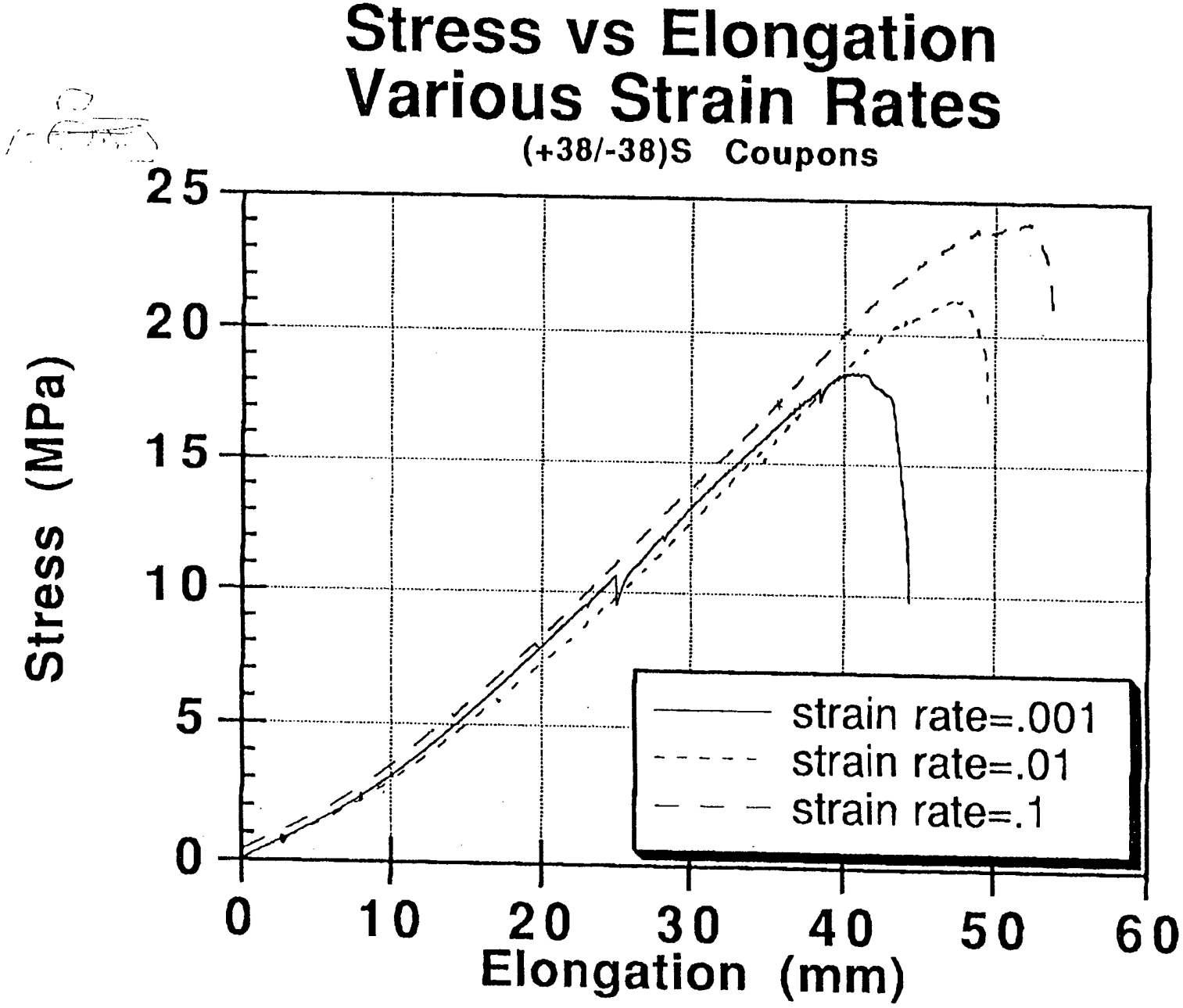

Figure 3.2 Stress vs Elongation (+38/-38) S Coupons - Experimental

Stress vs Strain

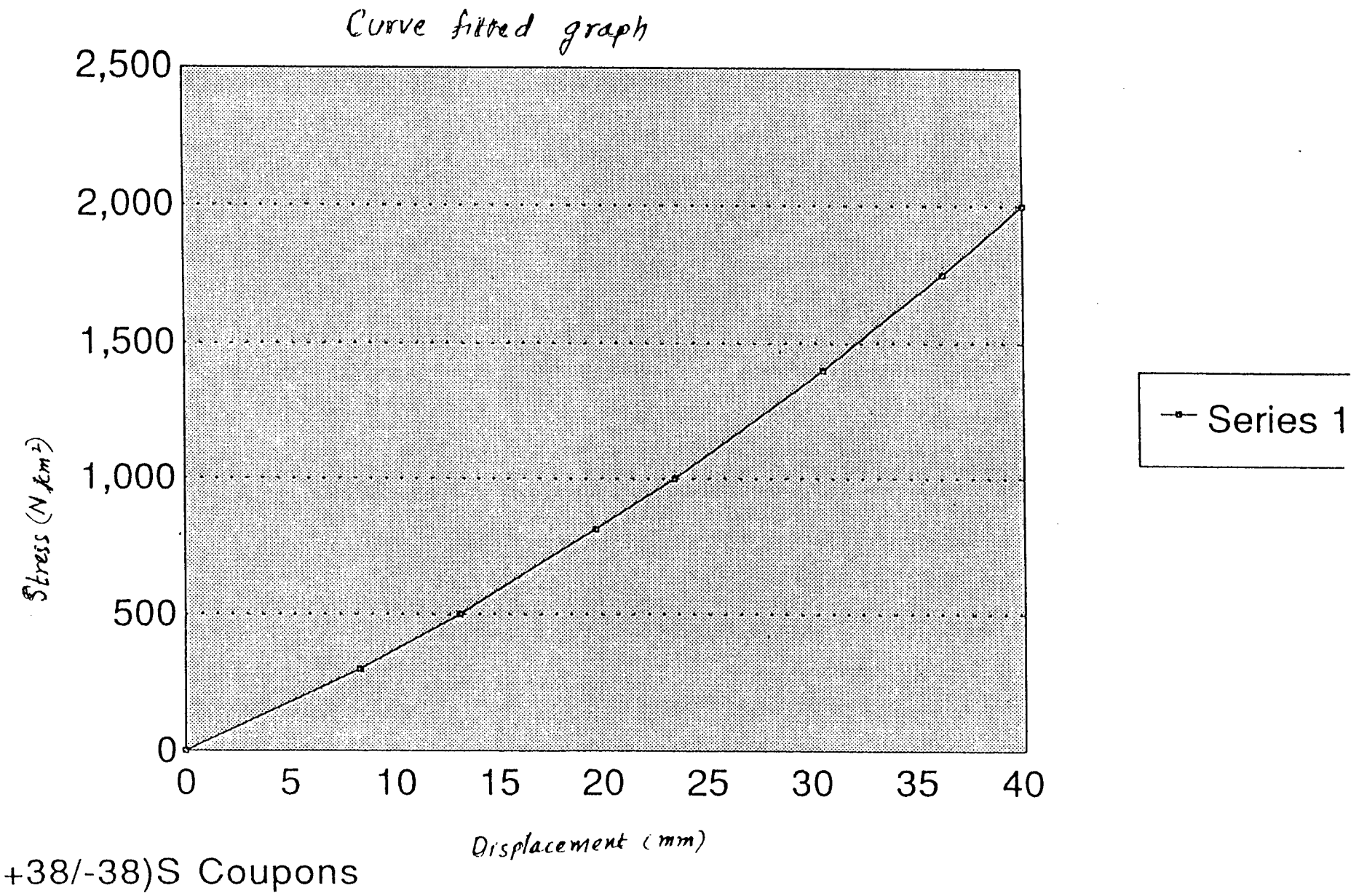

Figure 3.3 Stress vs Elongation (+38/-38) S Coupons - Numerical

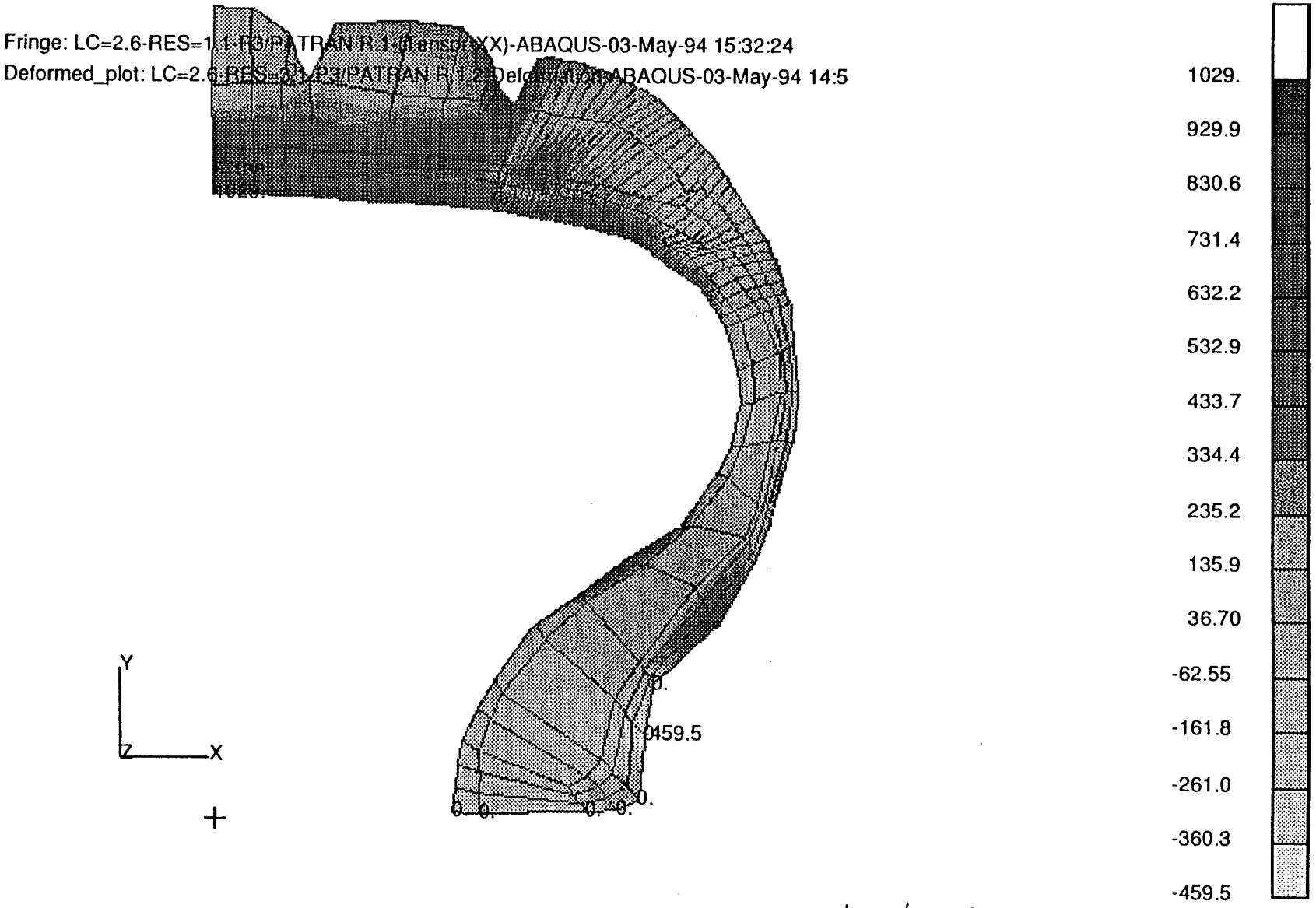

Figure 6.1.1 Stress vs Strain - Radial Direction - CAX4RH Elements

What % of Sidewall Deflection?

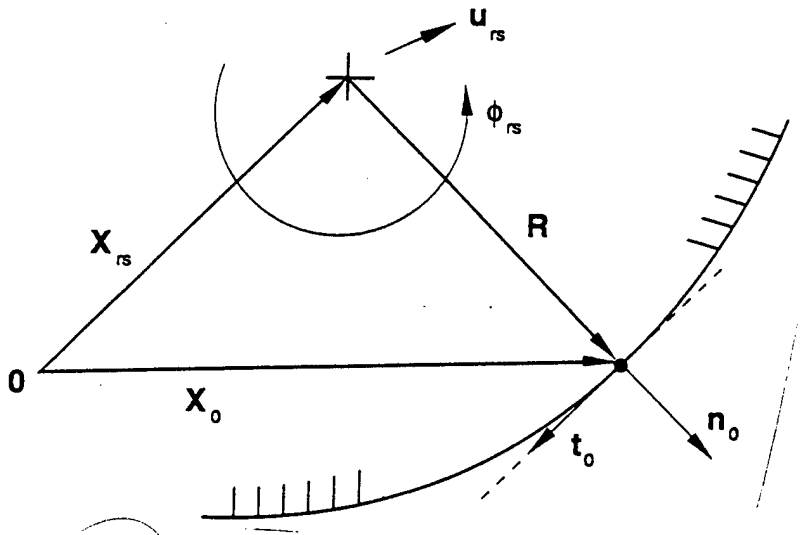

Figure 3.4 Rigid body reference geometry

after Fig 6?

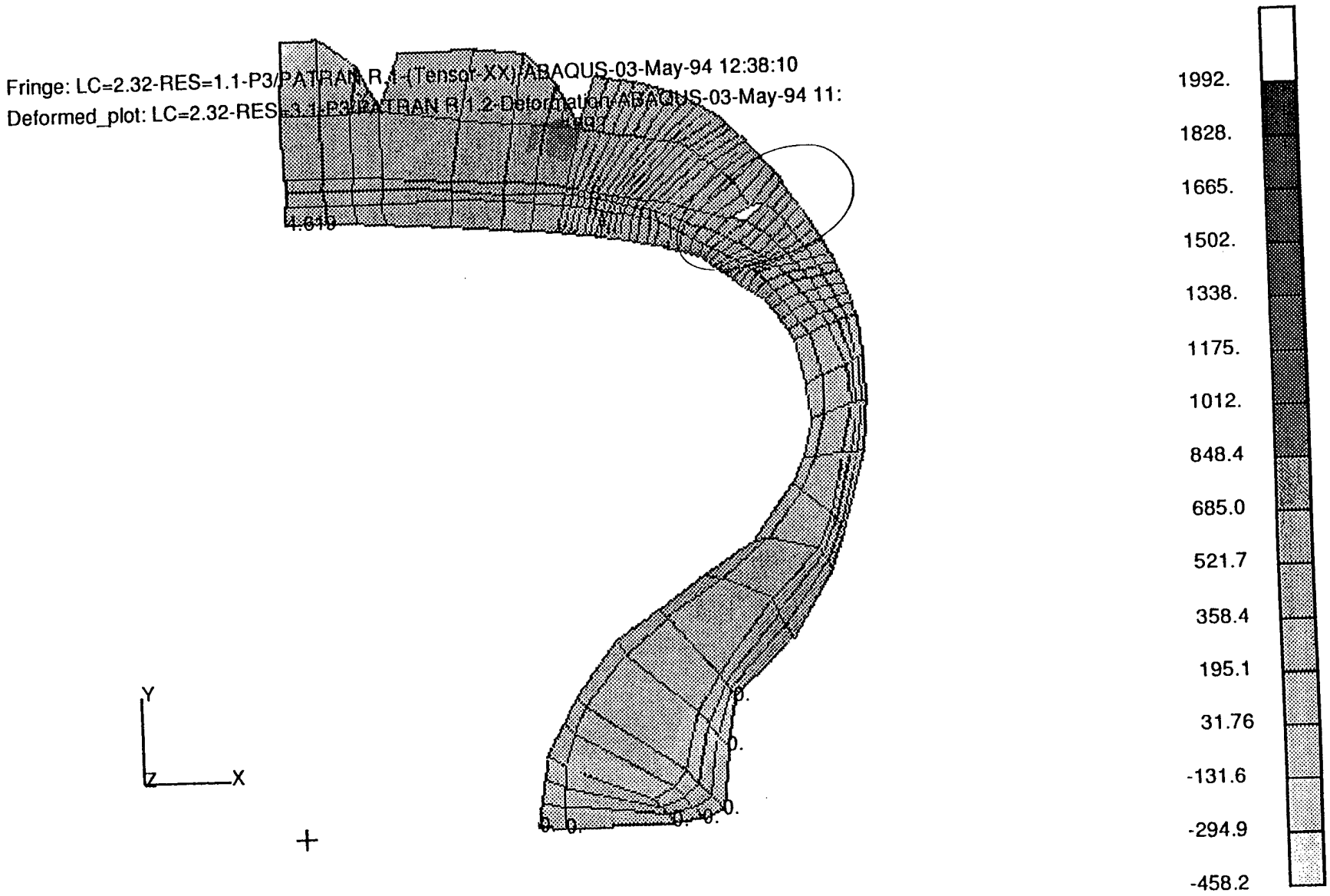

Figure 6.1.2 Stress vs Strain - Radial Direction - CAX4IH Elements

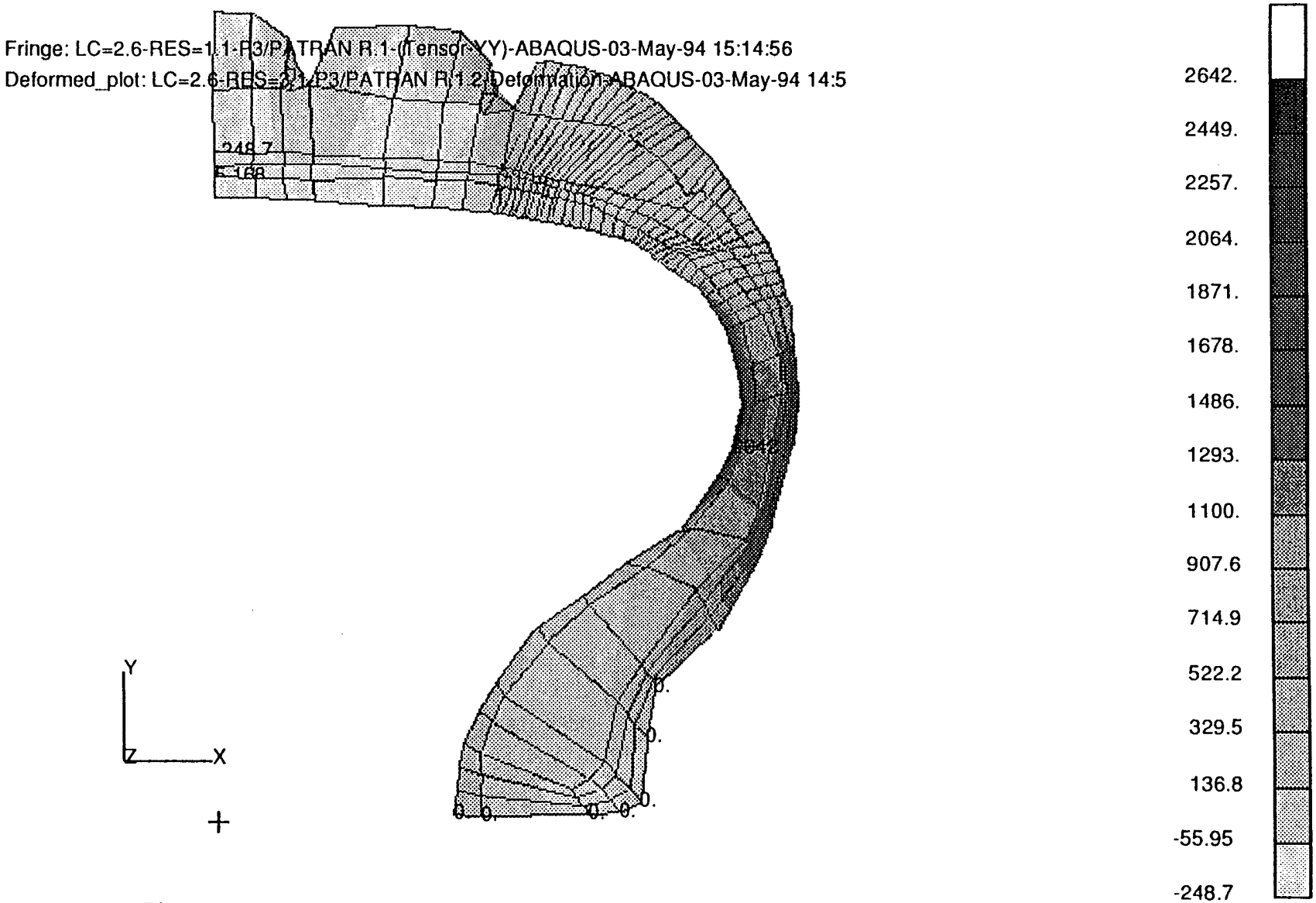

Figure 6.1.3 Stress vs Strain - Angular Direction - CAX4RH Elements

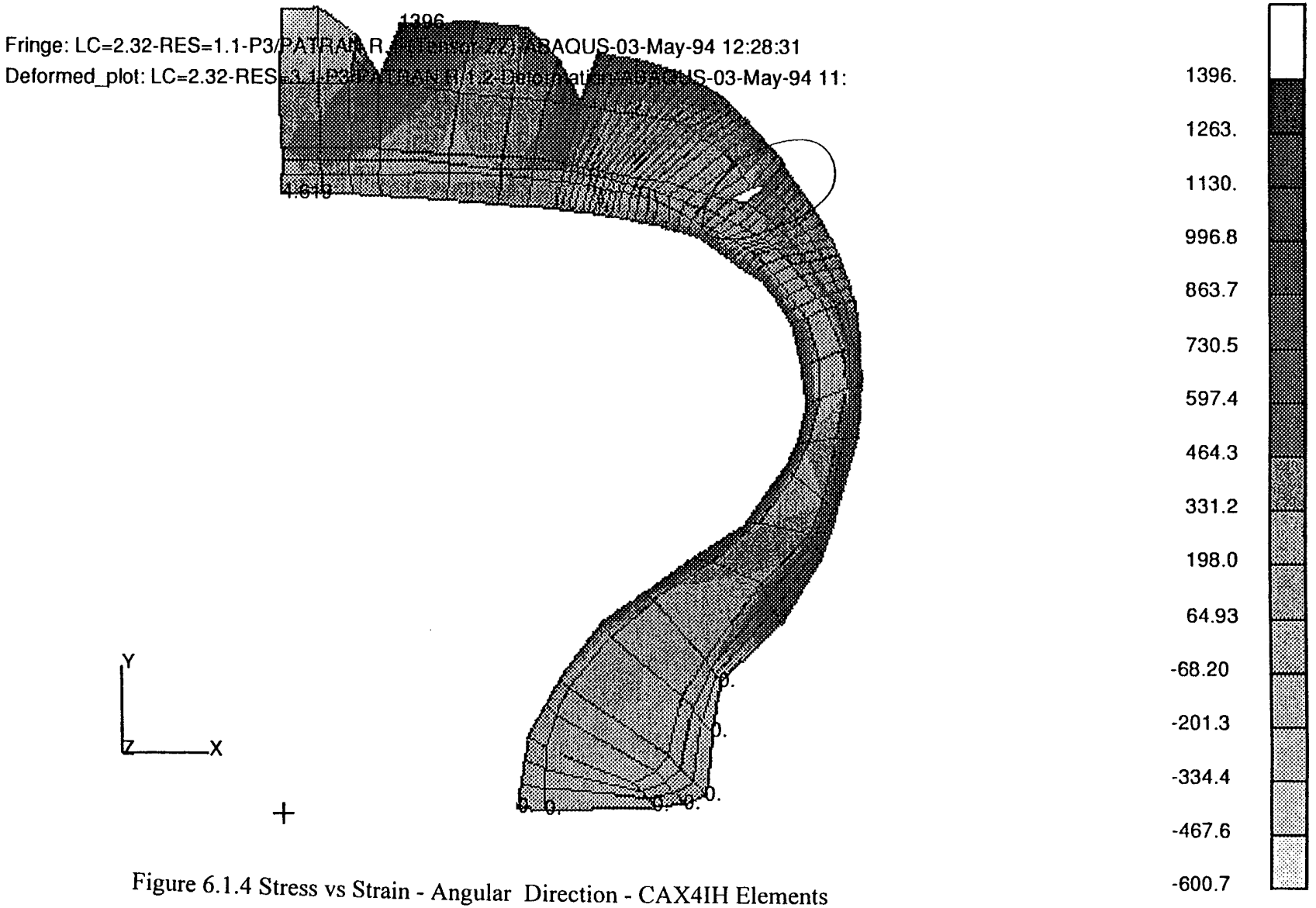

Figure 6.1.4 Stress vs Strain - Angular Direction - CAX4IH Elements

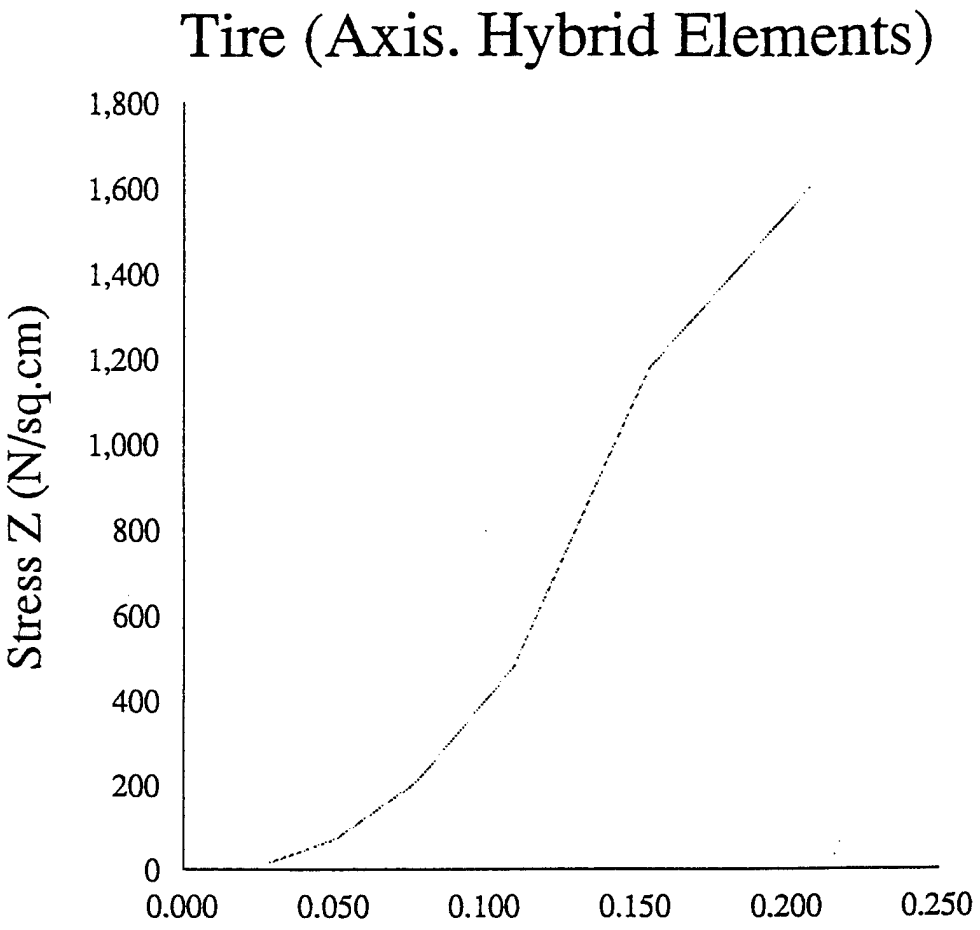

Figure 6.1.5 Stress vs Strain - Thickness Direction - CAX4RH Elements

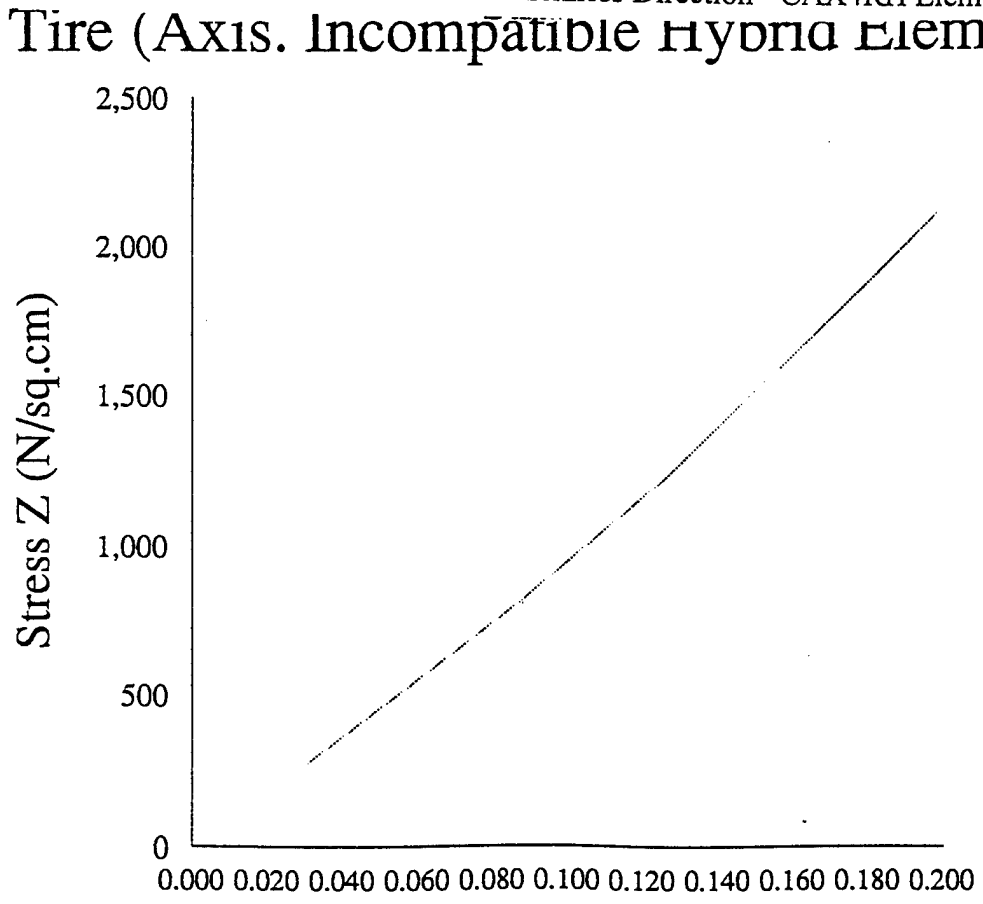

Figure 6.1.6 Stress vs Strain - Thickness Direction - CAX4IH Elements

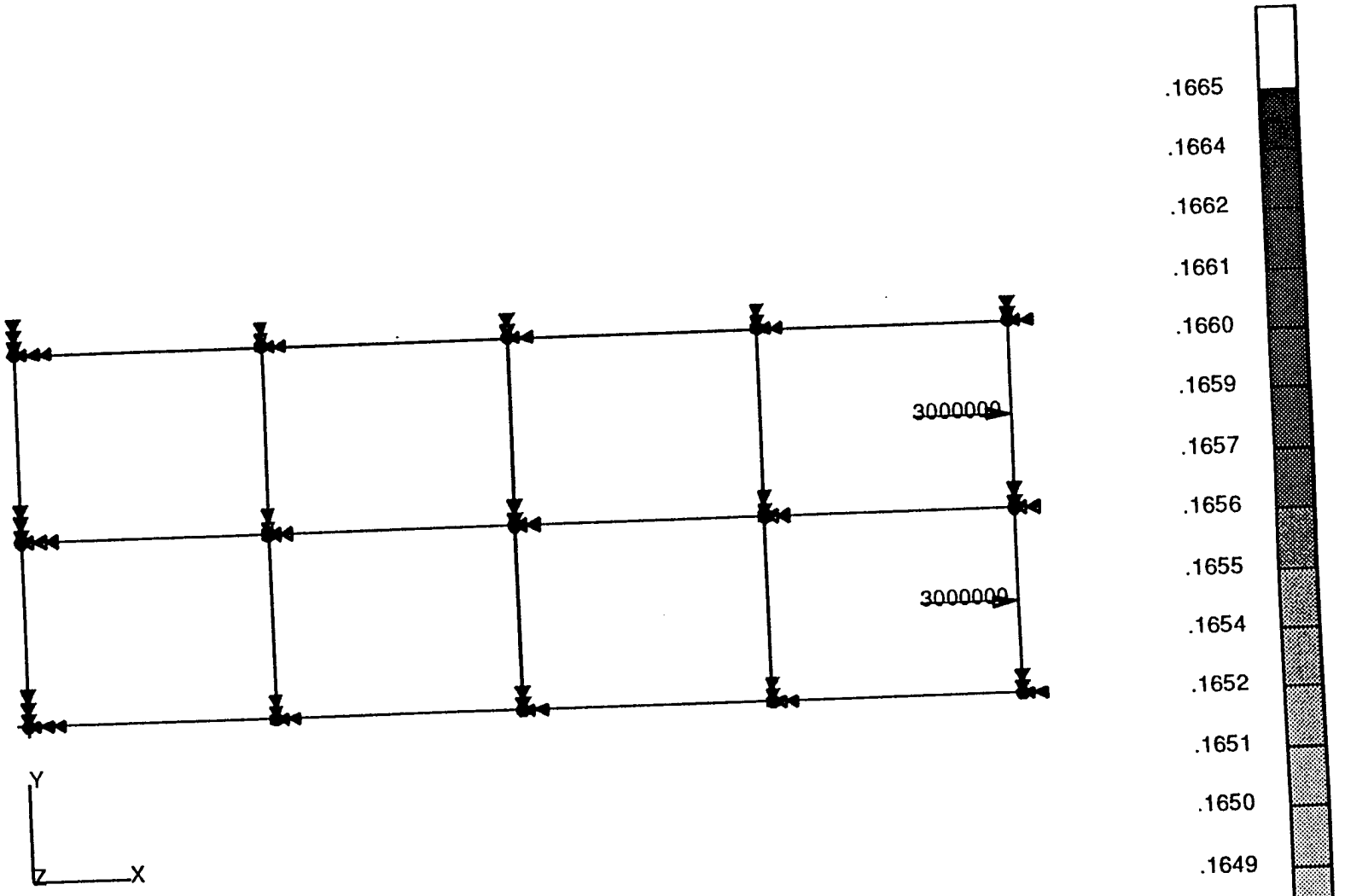

Figure 6.1.8 (+/-38) S Nylon-Rubber Coupon - Load & Boundary Condition Applied

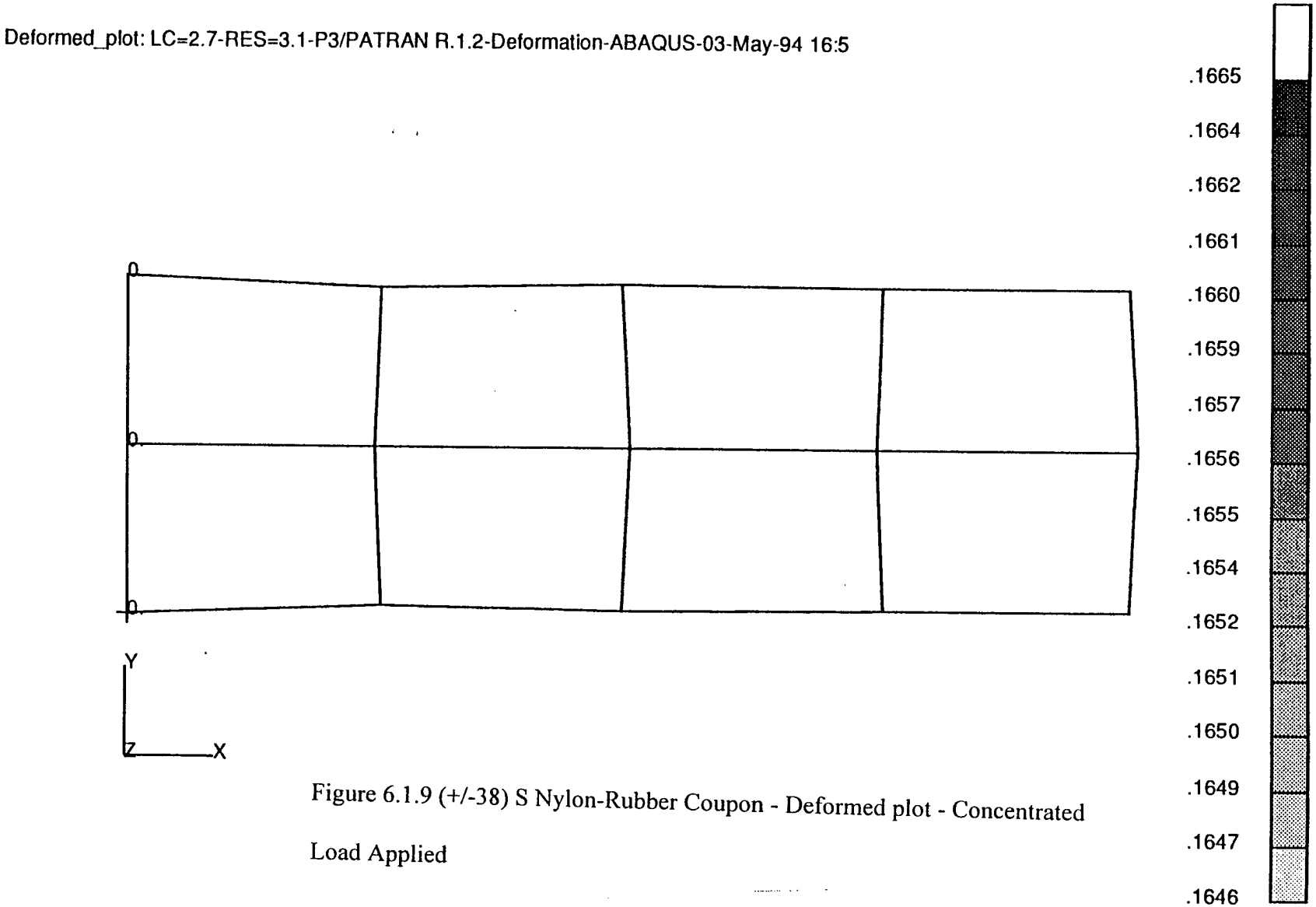

Figure 6.1.9 (+/-38) S Nylon-Rubber Coupon - Deformed plot - Concentrated Load Applied

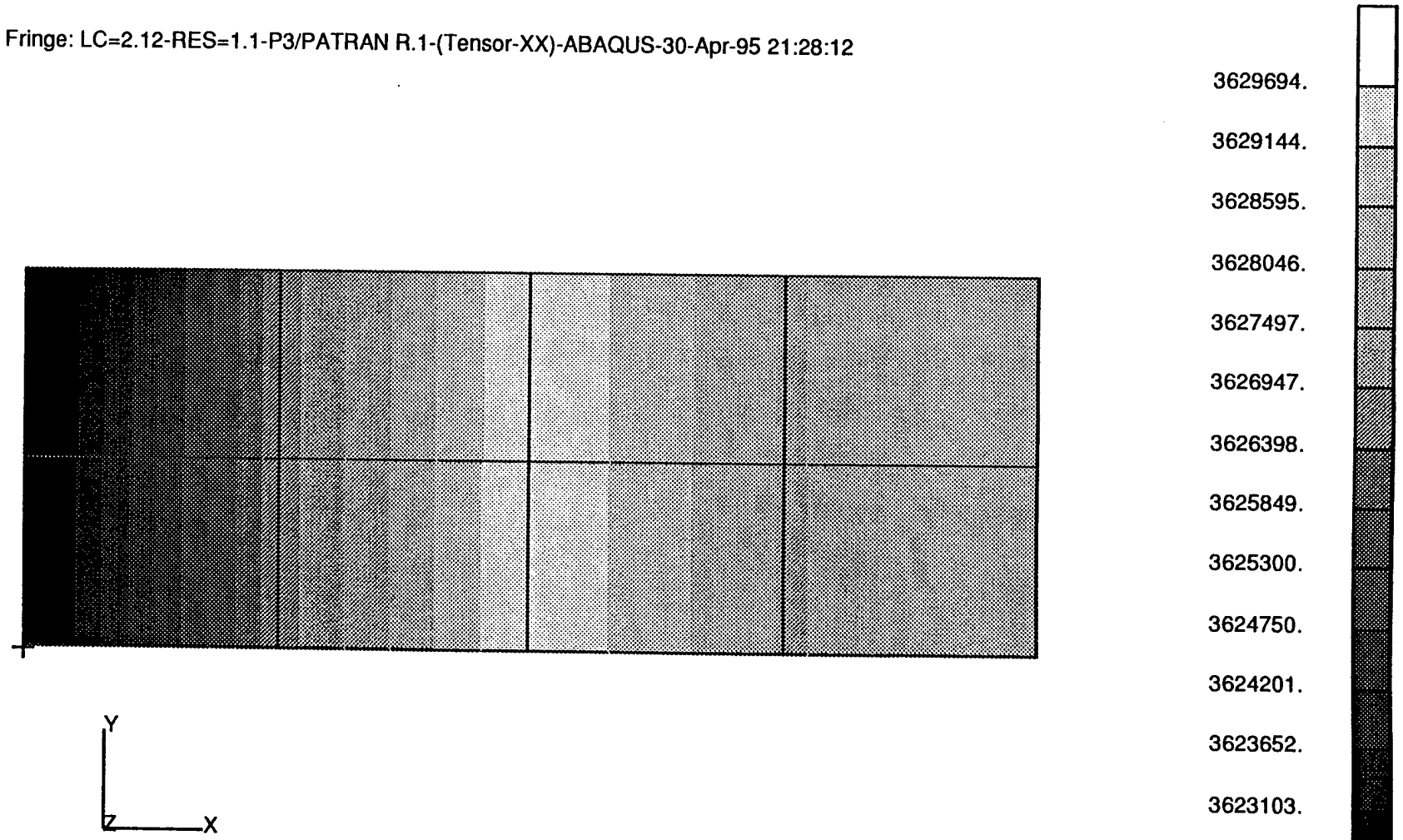

Figure 6.1.10 (+/-38) S Nylon-Rubber Coupon - Stress plot - Concentrated Load Applied

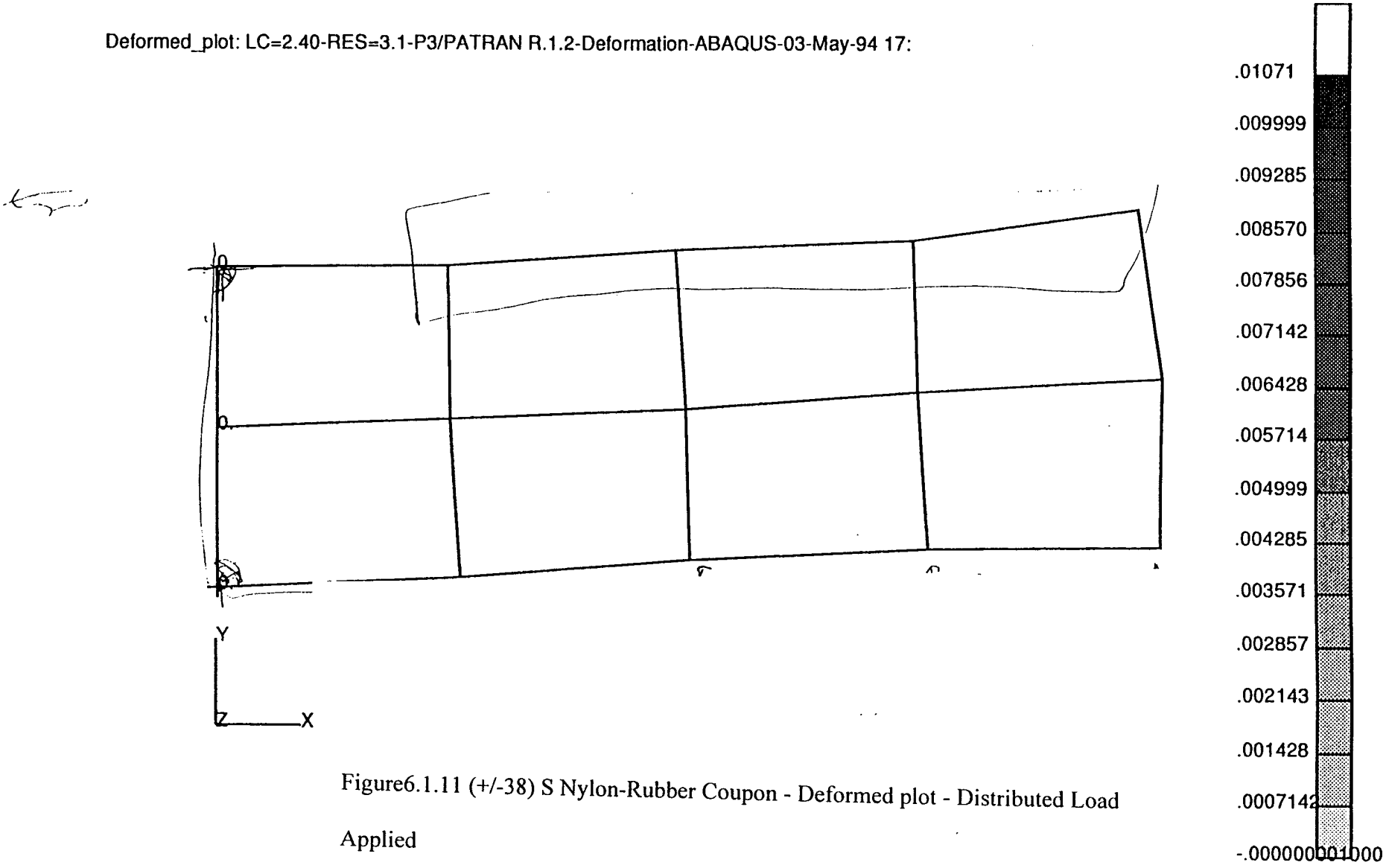

Figure6.1.11 (+/-38) S Nylon-Rubber Coupon - Deformed plot - Distributed Load Applied

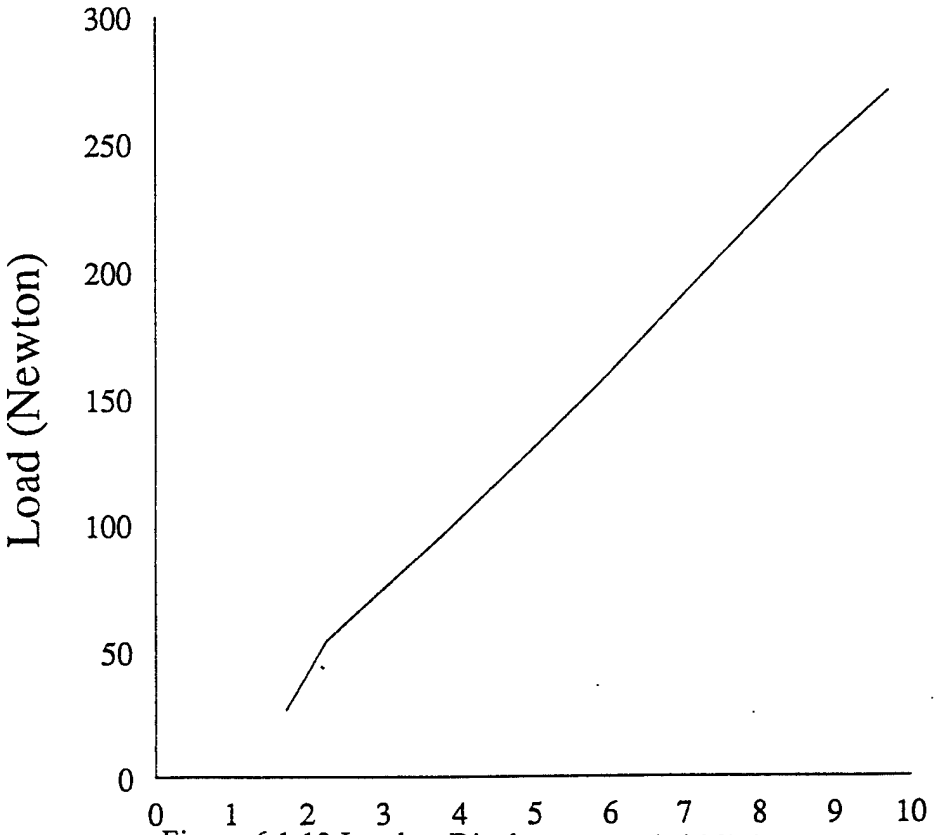

Figure 6.1.13 Load vs Displacement - (+/-38) S Nylon-Rubber Coupon - Concentrated Load

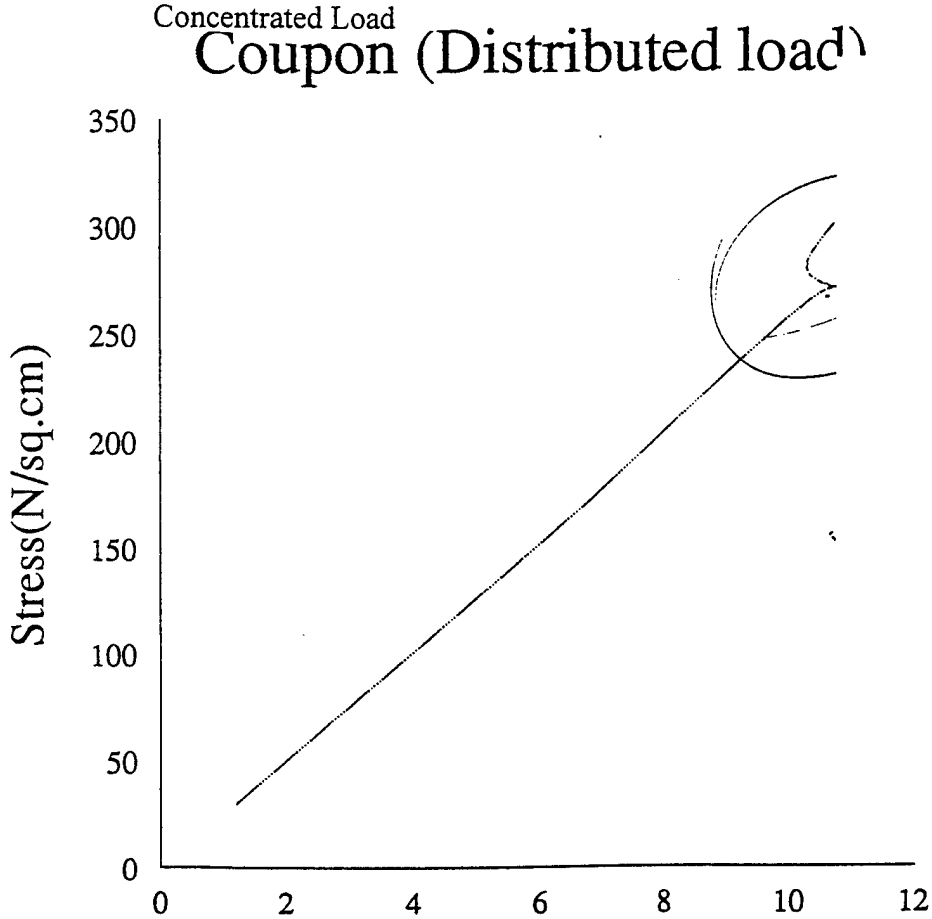

Figure 6.1.14 Load vs Displacement - (+/-38) S Nylon-Rubber Coupon - Distributed Load

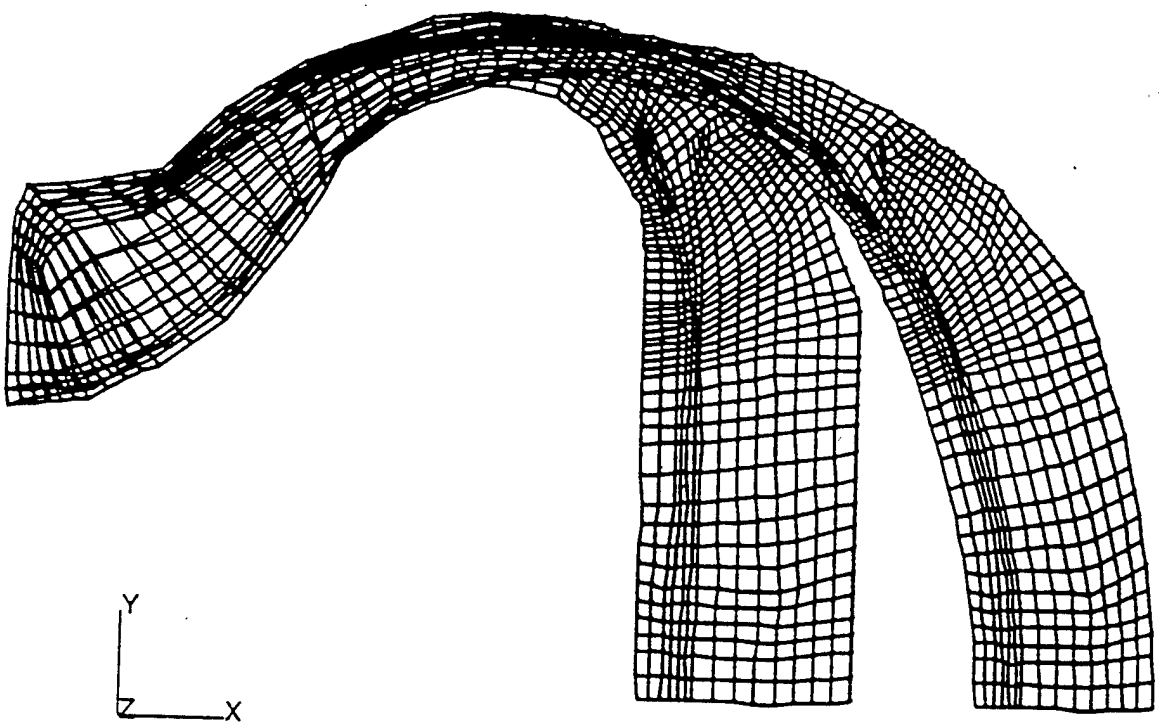

Figure 6.2.1 Finite - Element Model of The Tire Cross-section Under Inflation

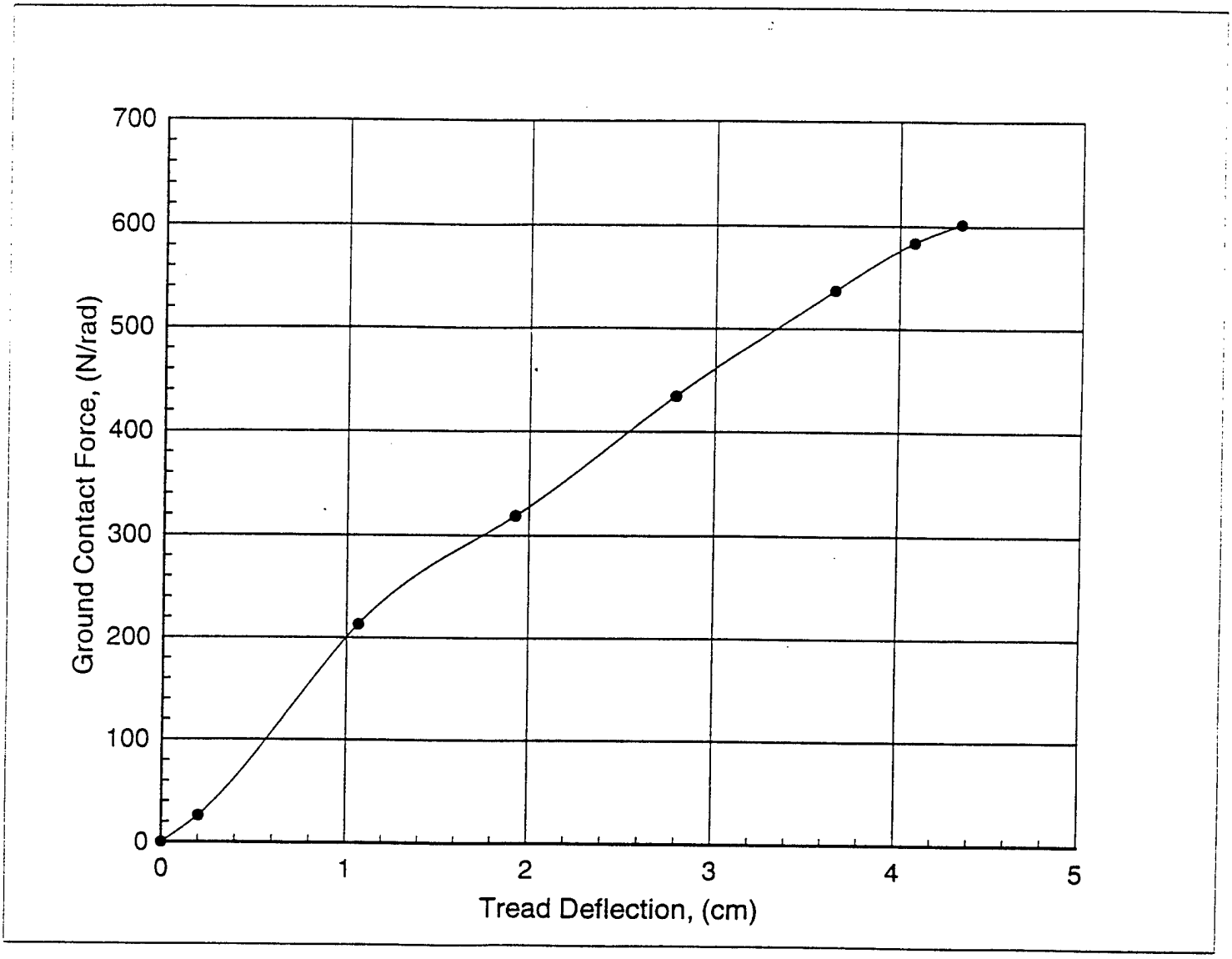

Figure 6.2.2 Ground Contact Force Versus Cross-Section Tread Deflection

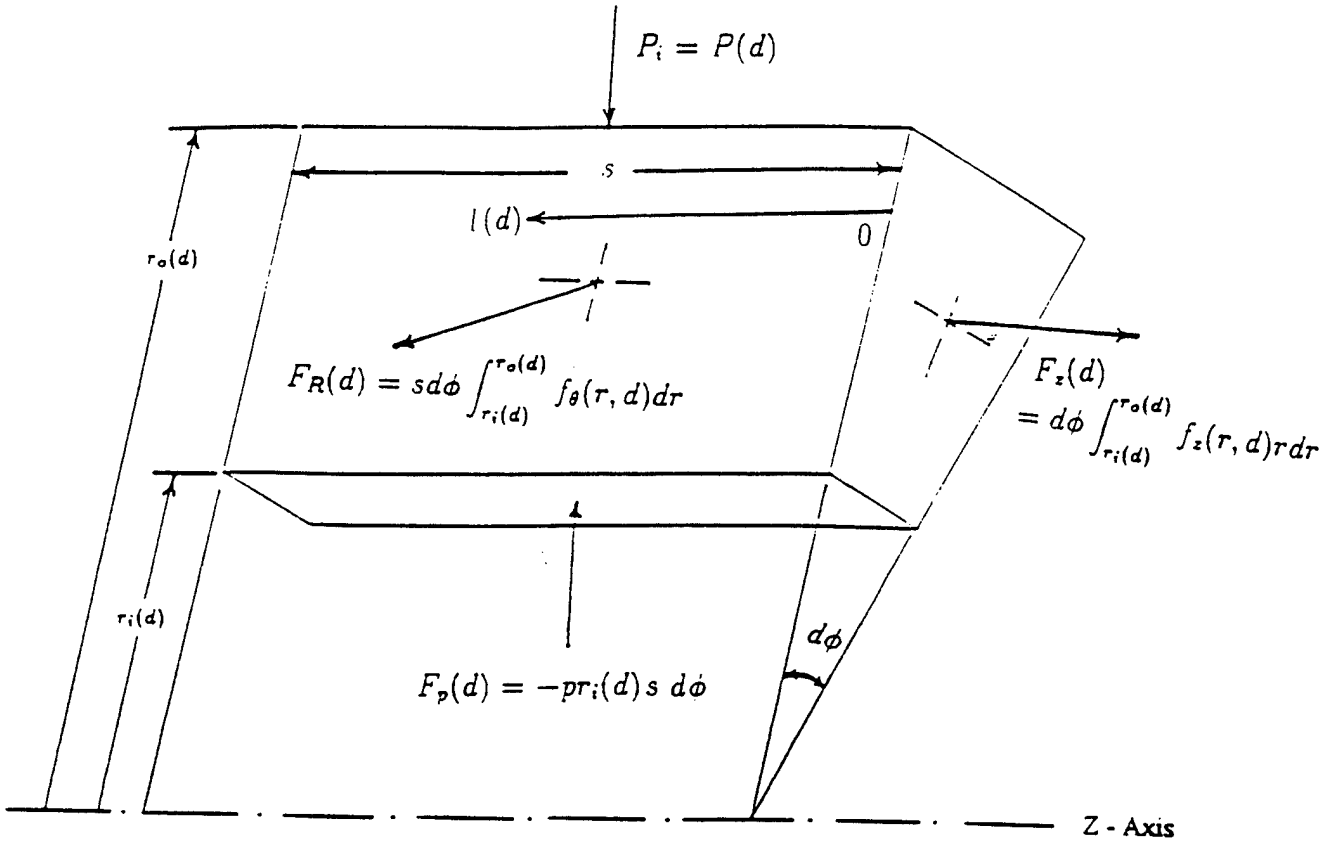

Figure 6.2.3 Tread Band Idealized Element And Forces on Faces

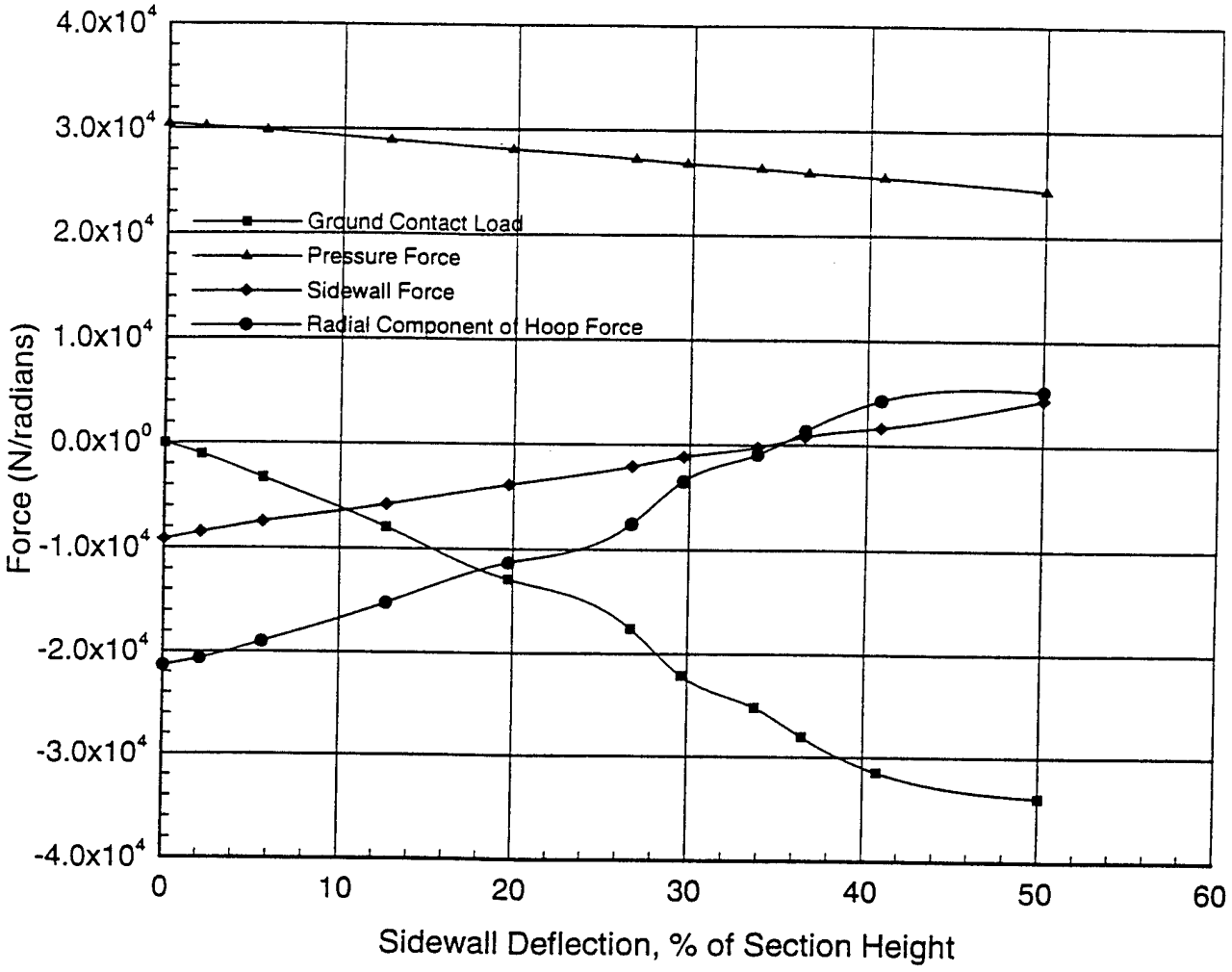

Figure 6.2.4 Various Forces Acting on the Axisymmetric Model of the Tire

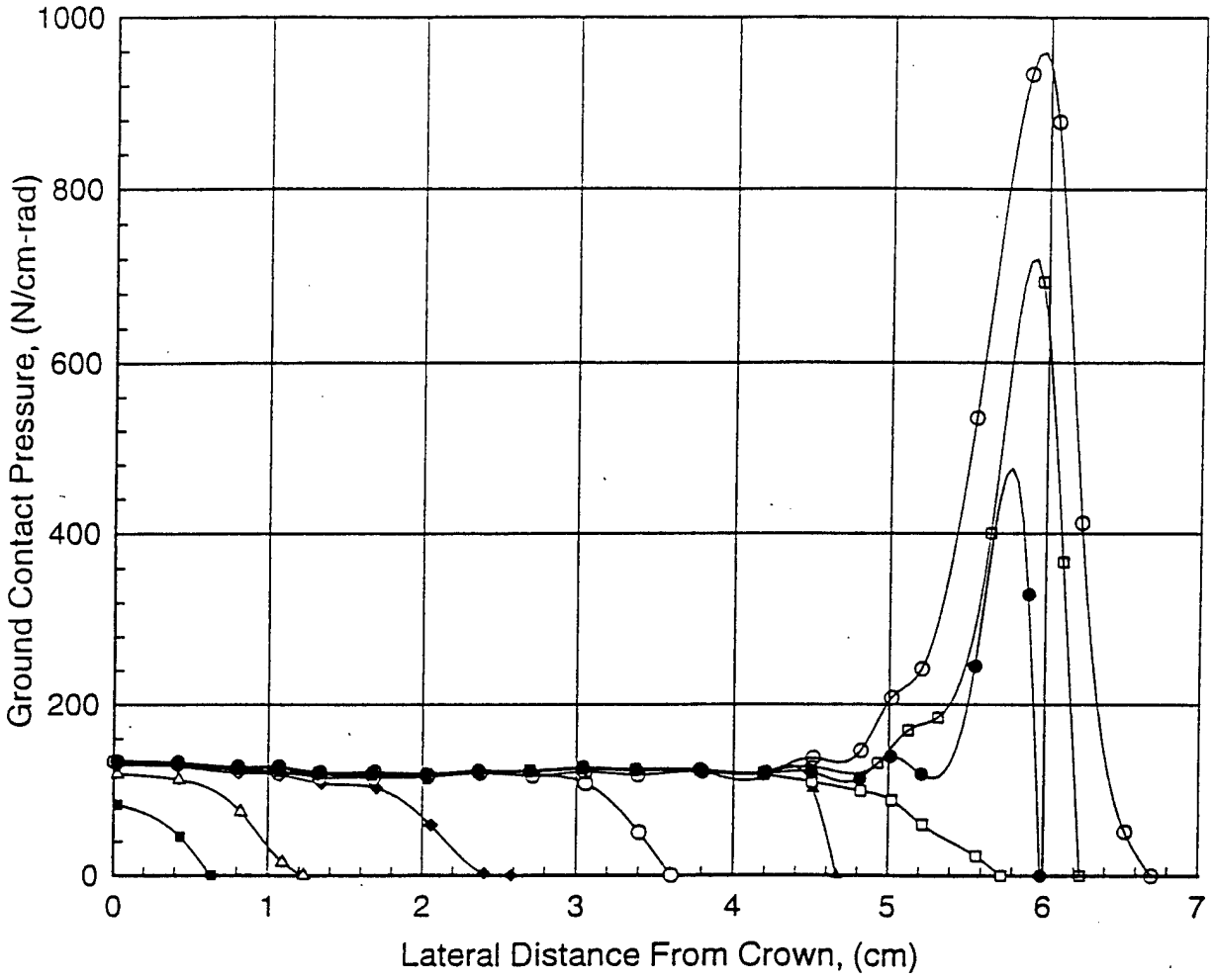

Figure 6.2.5 Lateral Ground Contact Pressure Variation Over Tread Band of Cross-Section at Various Percent Sidewall Deflection.

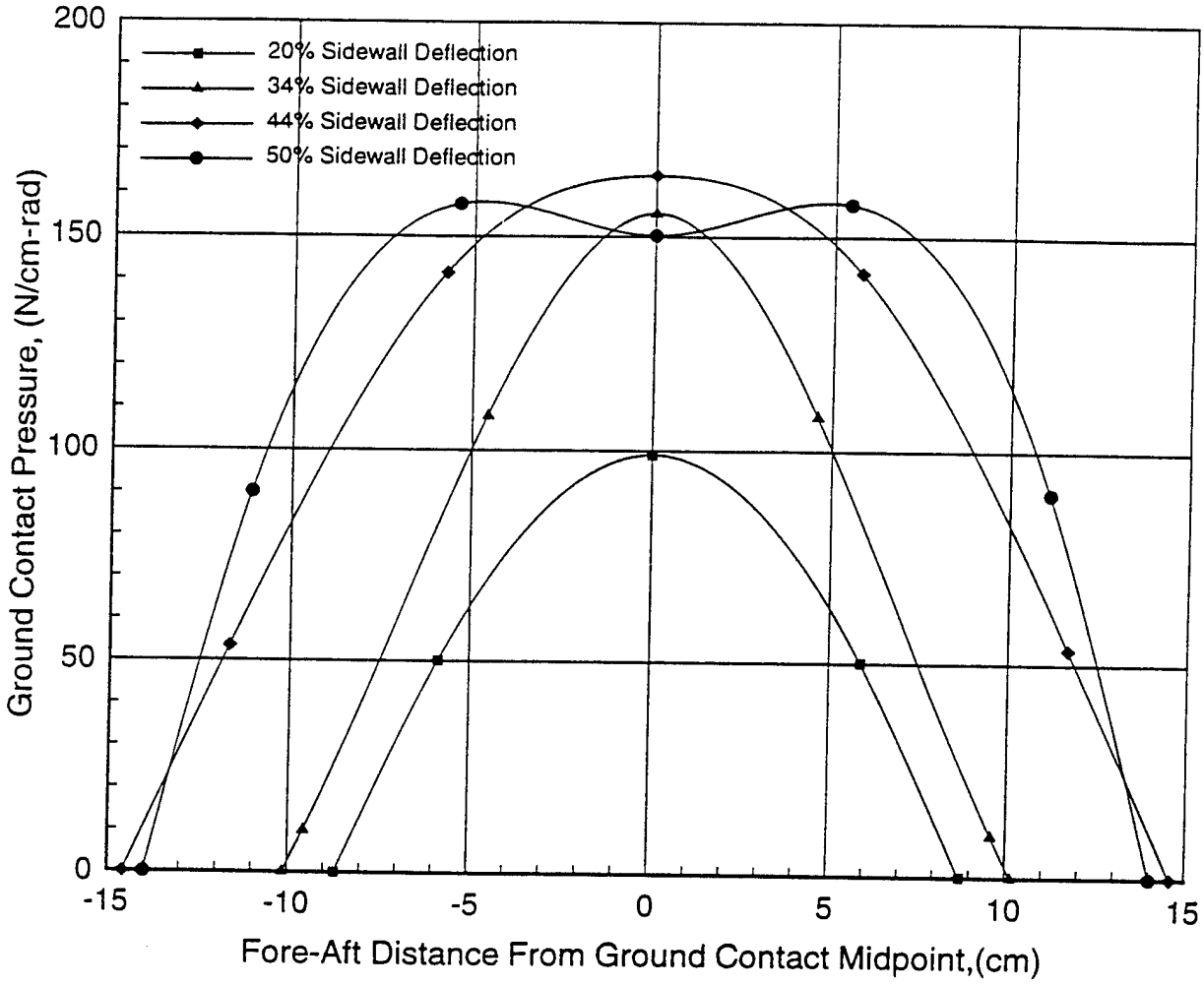

Figure 6.2.6 Ground Contact Pressure Distribution In the Rolling Direction.

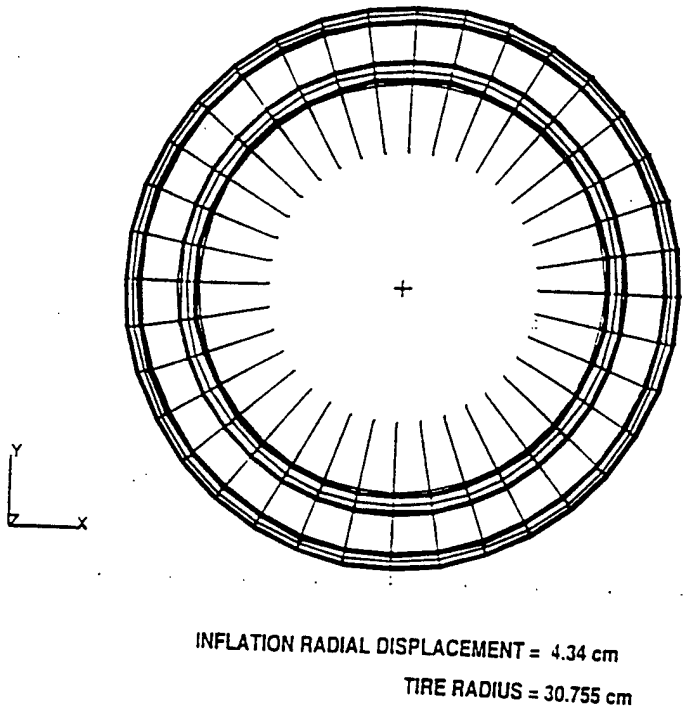

Figure 6.2.7 The Ring Model In Inflated And Uninflated State

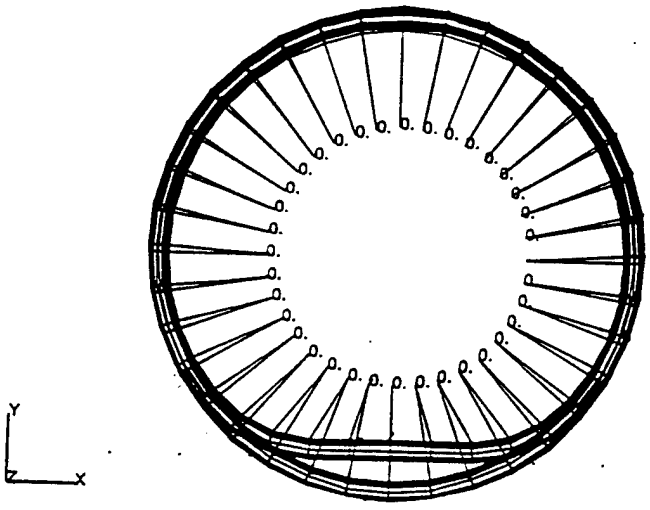

Figure 6.2.8 Deformation of The Ring Model Due to Ground Contact

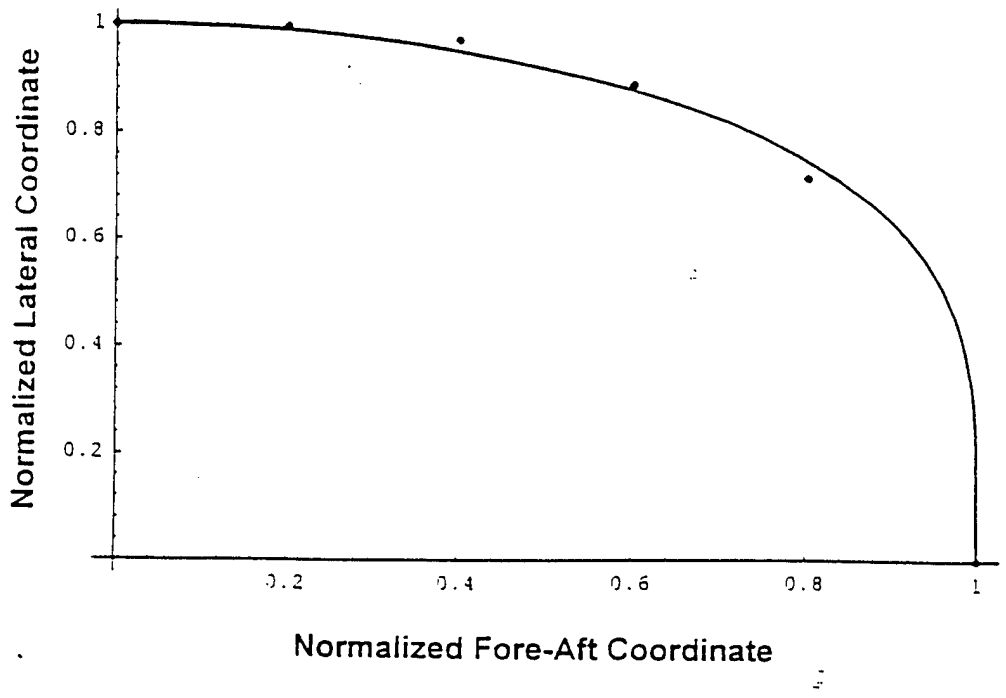

Figure 6.2.9 Foot Print Shape For 20 percent Sidewall Deflection

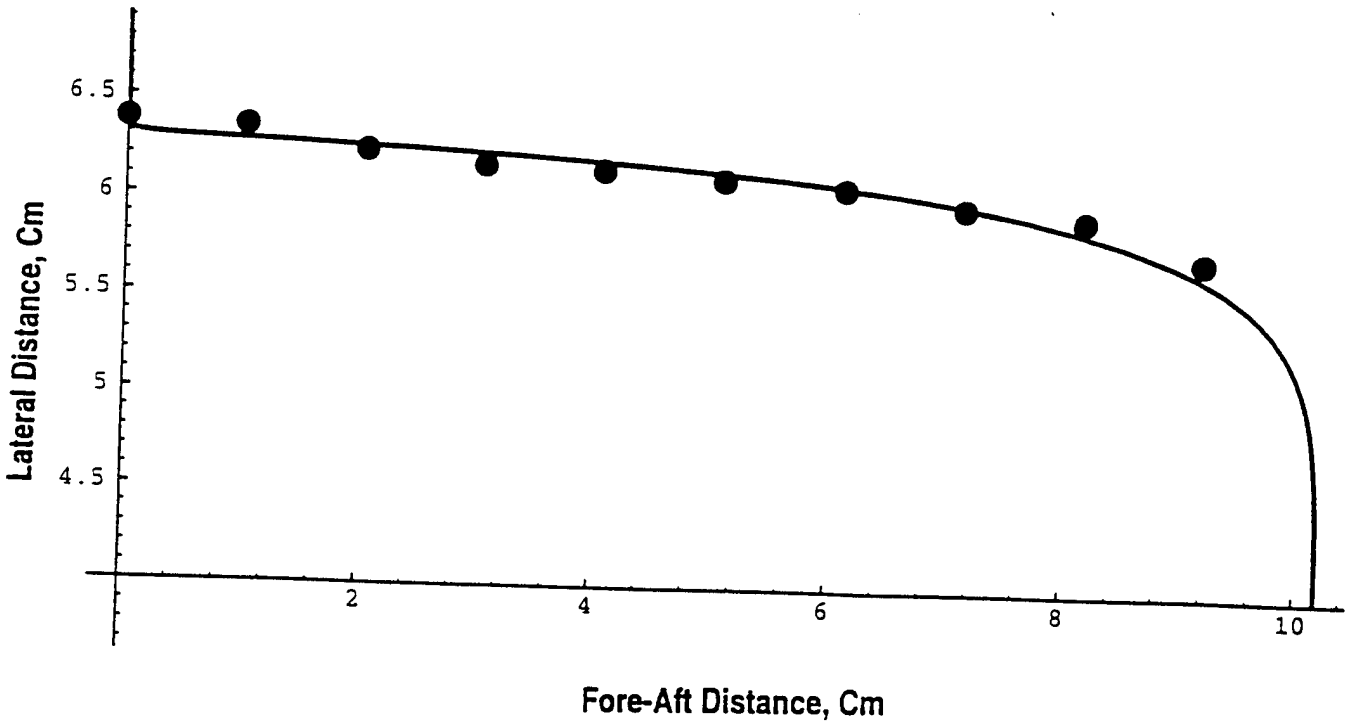

Figure 6.2.10 Foot Print Shape For 34 percent Sidewall Deflection

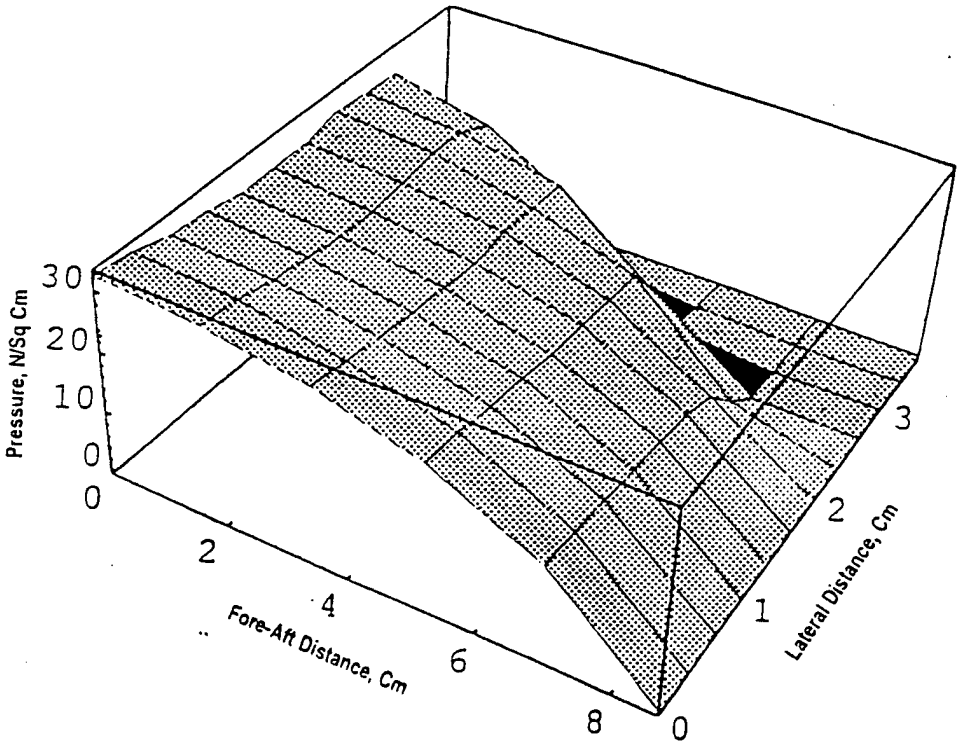

Figure 6.2.11 Ground Pressure Distribution For 20 percent Sidewall Deflection

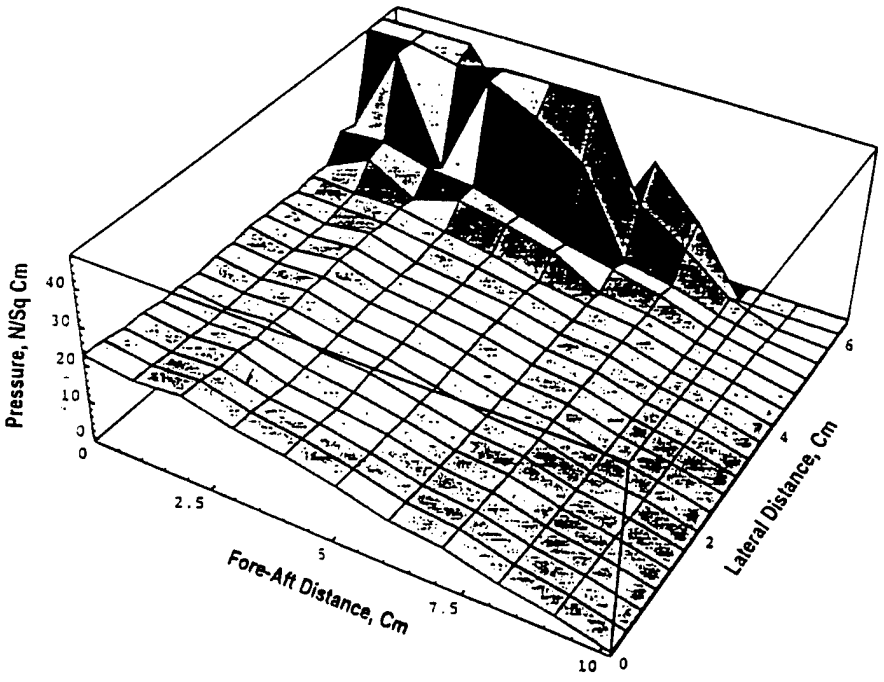

Figure 6.2.12 Ground Pressure Distribution For 34 percent Sidewall Deflection

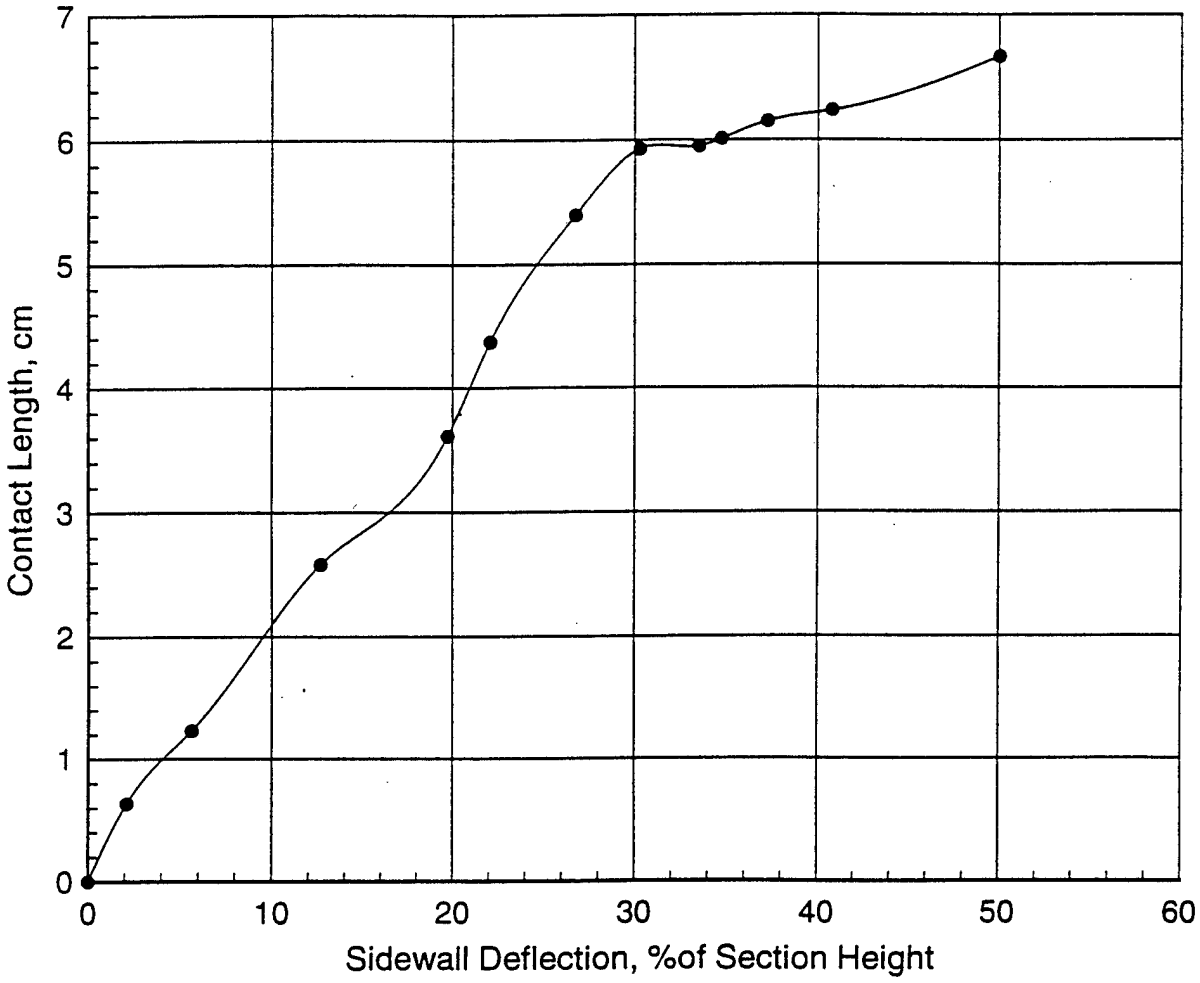

Figure 6.2.13 Variation of Ground Contact Length With Sidewall Deflections

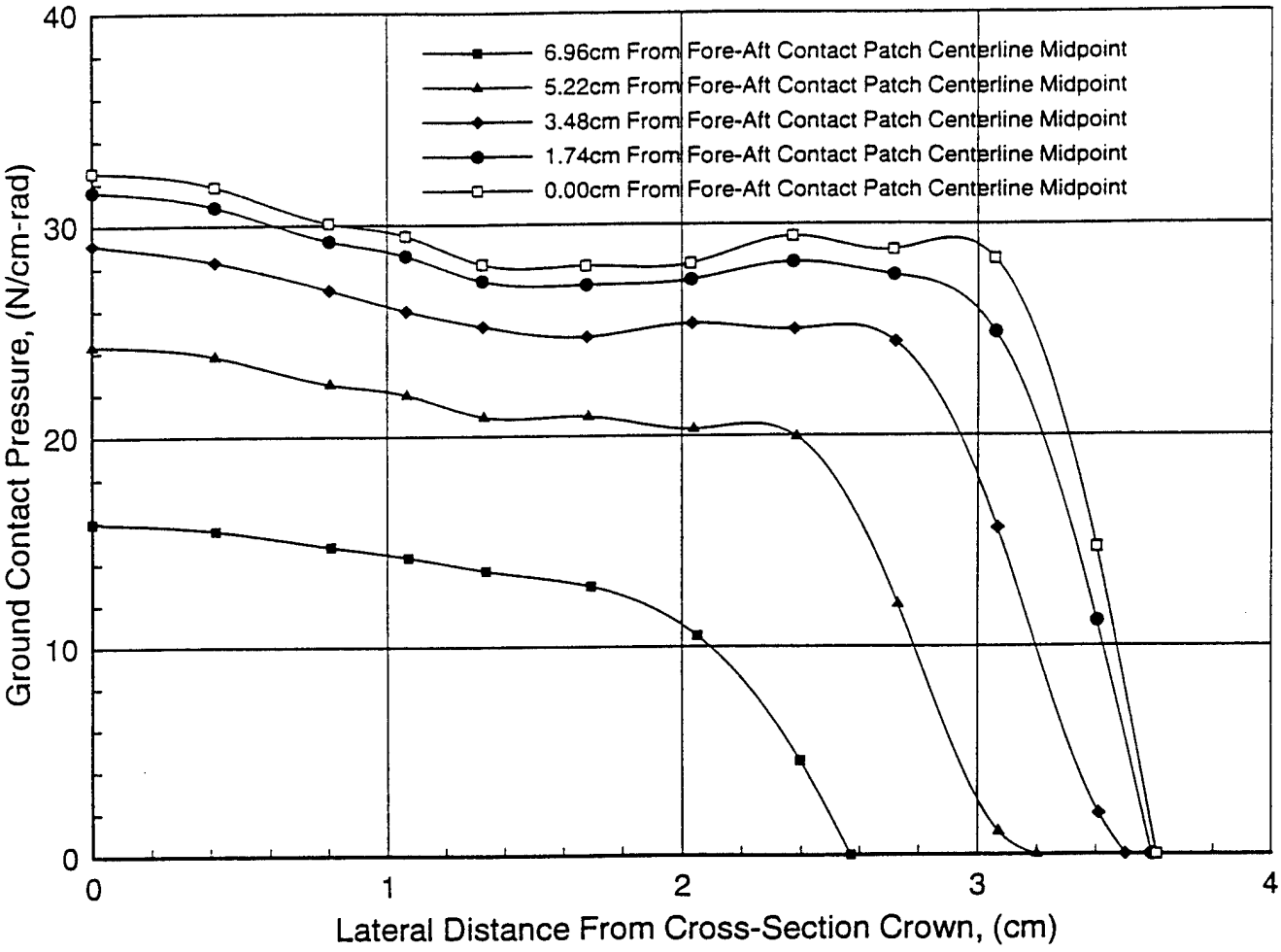

Figure 6.2.14 The Contact Pressure Distribution Variation With Fore-Aft Distance

From Midpoint of Contact Patch Centerline for 20 percent sidewall deflections

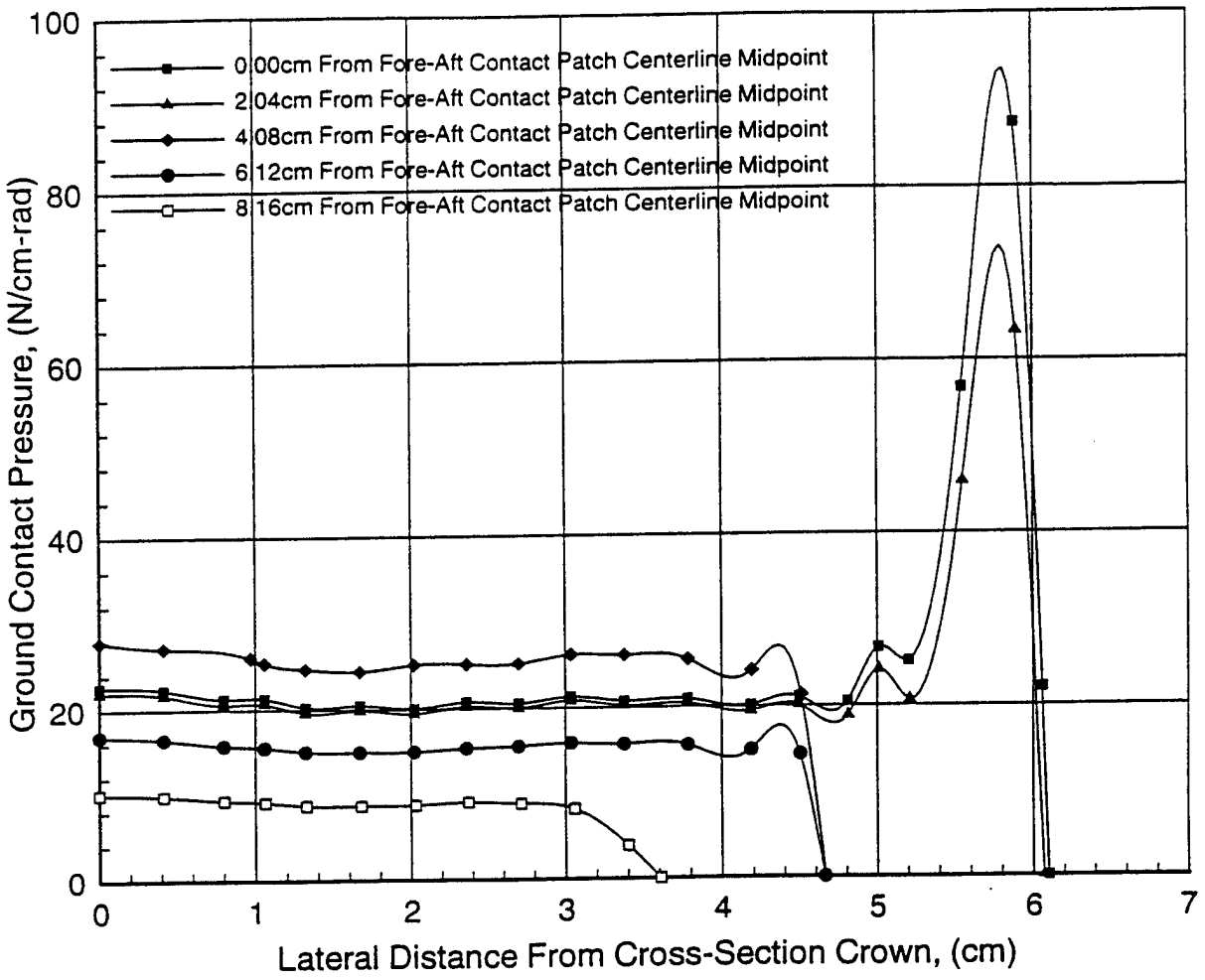

Figure 6.2.15 The Contact Pressure Distribution Variation With Fore-Aft Distance From From Midpoint of Contact Patch Centerline for 34 percent sidewall deflections.